The Role of the E3 Ubiquitin Ligases Nedd4-1 and Nedd4-2 in Synaptic Transmission and Plasticity

PhD Thesis

in partial fulfillment of the requirements

for the degree "Doctor of Philosophy (PhD)"

at the Georg-August-University Göttingen,

Faculty of Biology

Submitted by

Michiko Takeda

Born in

Kitakyushu, Japan

May 2012

Referent:	Prof. Dr. Nils Brose
Korreferent:	Prof. Dr. Andreas Stumpner
Prüfungsdatum:	12th June 2012

Declaration

I hereby declare that this thesis “The Role of the E3 Ubiquitin Ligases Nedd4-1 and Nedd4-2 in Synaptic Transmission and Plasticity” has been written independently, with no other aids than those cited.

Michiko Takeda
Goettingen, May 2012

Acknowledgments

I owe a great many thanks to many people who supported and encouraged me throughout the completion of this thesis. At first, I would like to express my sincere gratitude towards Dr. Hiroshi Kawabe for giving me the opportunity to achieve my PhD in his group, for his support, his encouragement, and his training in experimental skills. I am also grateful for his skillful advice on my presentation and writing. I am indebted to Prof. Dr. Nils Brose, head of the Molecular Neurobiology Department and my thesis committee. I would like to thank him for giving me the opportunity to achieve my PhD in his department and providing constant support, guidance, and critical input.

I am also deeply grateful to Prof. Dr. Andreas Stumpner, the other core member of my thesis committee, for his guidance and suggestions during the course of this study.

This project would have been markedly poorer without the collaborations with Dr. Jeong Seop Rhee and Dr. Oliver Schlueter. I truly appreciate their instructions, technical support, and valuable discussions in my electrophysiological study. I am also grateful to Dr. SangYong Jung, Plino, and Ania for their kind and helpful support. I would also like to thank Dr. Olaf Jahn and Dr. Kalina Dimova for their support in mass spectrometric analyses.

I am eternally grateful to Bernd, Anja, Ines, Martin, Fritz, Dayana, and Ivonne for their excellent technical support and to our institute driver Herr Treger and all the staff of the animal facility at the Max-Planck Institute of Experimental Medicine.

It has been my honor to work with Mika, Hung-En, Bekir, and Mateusz as a member of Dr. Kawabe's group, and I would like to acknowledge all my friends and colleagues in the Molecular Neurobiology Department for their support, discussions, and sharing great moments, especially Sonja, Mimi, Christoph, Ramya, Tolga, Ben, Thea, Klaus, Christine, and Birgit. I also appreciate Liam for proofreading of this thesis. I also would like to thank to all members of the Schlueter lab for their kind help and warm welcome.

Last, but not the least, I am indebted to my family, who have been always there for me, for their invaluable encouragements and support throughout the whole time.

Abstract

Neurons are highly specialized cells that are connected at synapses to allow for the transfer of neuronal information. The development of synapses and the information processing and memory storage in mature synapses require dynamic remodeling of synaptic networks, including synapse formation and elimination, synaptic protein turnover, and alteration in synaptic transmission. Ubiquitination, a regulatory posttranslational modification, has been proposed as one of the critical processes required for such complex synaptic remodeling.

Nedd4-1, a HECT type E3 ubiquitin ligase, positively regulates neurite development through ubiquitinating Rap2. In order to investigate the roles of Nedd4-dependent ubiquitination in the mature brain, neuron specific KO mice lacking *Nedd4-1* and its closest homolog *Nedd4-2* were generated and analyzed. I found that Nedd4-1 and Nedd4-2 are critical regulators of neuronal morphogenesis and synaptic plasticity, especially in the maintenance of LTP. Furthermore, I found that synaptopodin (SYNPO), a proline-rich actin associated protein, is ubiquitinated by Nedd4-1 and Nedd4-2 *in vitro*, indicating the involvement of SYNPO in the mechanism by which Nedd4-1 and Nedd4-2 maintain LTP. Thus, the present study sheds new light on the functional role of Nedd4-dependent ubiquitination in higher functions of the mammalian brain as well as in neuronal development.

Table of Contents

List of Figures

Abbreviations

ACSF	Artificial cerebrospinal fluid
AMPAR	α-amino-3-hydroxy-5-methyl-4-isoxazolepropionic acid receptor
APS	Ammoniumpersulfate
AZ	Active zone
CA1	Cornu Ammonis area 1
CA3	Cornu Ammonis area 3
DAT	Dopamine transporter
ddH_2O	Double distillation water
DEPC	Diethylpyrocarbonate
DG	Dentate gyrus
DIG	Digoxigenin
DIV	Days in vitro
DMEM	Dulbecco's modified Eagle's medium
DNA	Deoxyribonucleic acid
E. *coli*	Escherichia coli
E1	Ubiquitin activating enzyme
E2	Ubiquitin conjugating enzyme
E3	Ubiquitin ligase
EGFP	Enhanced green fluorescent protein
E-LTP	Early-phase LTP
ENaC	Epithelial sodium channel
EPSC	Excitatory postsynaptic current
EPSP	Excitatory postsynaptic potential
fEPSP	field excitatory postsynaptic potential
FV	Fiber volley
HECT	Homologous to E6-AP carboxyl-terminus
HFS	High frequency stimulation
Hz	Hertz
IEG	Immediate early gene
IP	Immunoprecipitation
IR	Input resistance
KD	Knockdown
KO	Knockout
LFS	Low frequency stimulation
L-LTP	Late-phase LTP
LTD	Long-term depression
LTP	Long-term potentiation
M	Molar
MEF	Mouse embryonic fibroblast
mEPSC	miniature EPSC
mM	Mili molar
mOsm	miliosmole
mTOR	Mammalian target of rapamycin
MΩ	Mega Ohm

Nedd4	Neuronal precursor cell-expressed developmentally down-regulated 4
Nedd4 cDKO	excitatory neuron-specific *Nedd4-1* and *Nedd4-2* conditional double KO
NMDAR	*N*-methyl-D-aspartate receptor
OD	Optical density
P …	Postnatal … day
PBS	Phosphate buffered saline
PCR	Polymerase chain reaction
PFA	Paraformaldehyde
PPR	Paired pulse ratio
PSD	Postsynaptic density
PSD95	Postsynaptic density 95
PTEN	Phosphatase and tensin homolog deleted on chromosome 10
PTX	Picrotoxin
RING	Really interesting new gene
RT	Room temperature
RyR	Ryanodine receptor
SC	Schaffer collateral
SDS-PAGE	Sodium dodecyl sulfate-polyacrylamide gel electrophoresis
SR	Series resistance
SYNPO	Synaptopodin
TNIK	TRAF2 and NCK-interacting protein kinase
TTX	Tetrodotoxin
UV	Ultraviolet
VDCC	Voltage-dependent-calcium-channel
YTH	Yeast two-hybrid

1 Introduction

1.1.1 The Brain and Its Cellular Components

The brain as the center of the nervous system is the most complex mammalian organ. It receives complex information from the sensory organs, processes it, and stores it or generates an appropriate output. Four crucial areas of the brain are usually distinguished, although they are interconnected: the cerebrum, the cerebellum, the limbic system, and the brain stem. The cerebrum occupies the largest part of the brain and performs higher brain functions, including thoughts and perceptions. The cerebellum is located at the lower back of the brain, coordinating movements, posture, and balance. The limbic system, including the hippocampus (see 1.1.3), lies buried within the cerebrum and is responsible for consciousness and creating emotions or memories. The brain stem is located underneath the limbic system and governs vital survival functions.

The main functional unit of the brain in each of these areas is the brain cell. Brain cells are of two main types, neurons and non-neuronal cells such as glia. Neurons are specialized cells that primarily mediate information transfer in the brain while the non-neuronal cells are in most cases supporting, facilitating, or modulating this process. It is often stated that a single human brain contains approximately 100 billions neurons and potentially many times more glial cells, however a recent paper states that the neuronal number may be closer to 86 billion, with approximately the same number of non-neuronal cells (Azevedo et al., 2009).

Typical neurons have a highly specialized structure to process the signal transfer through two types of protrusions, dendrites and axons (Fig. 1-1). Individual neurons project multiple dendrites with numerous branches, covering a local field of the brain to receive inputs from hundreds of different neurons. In addition, individual neurons project a single long extended axon, which transmits signals to other neurons or non-neuronal target cells. The present study is mainly focused on neurons as the main information-processing units of the brain.

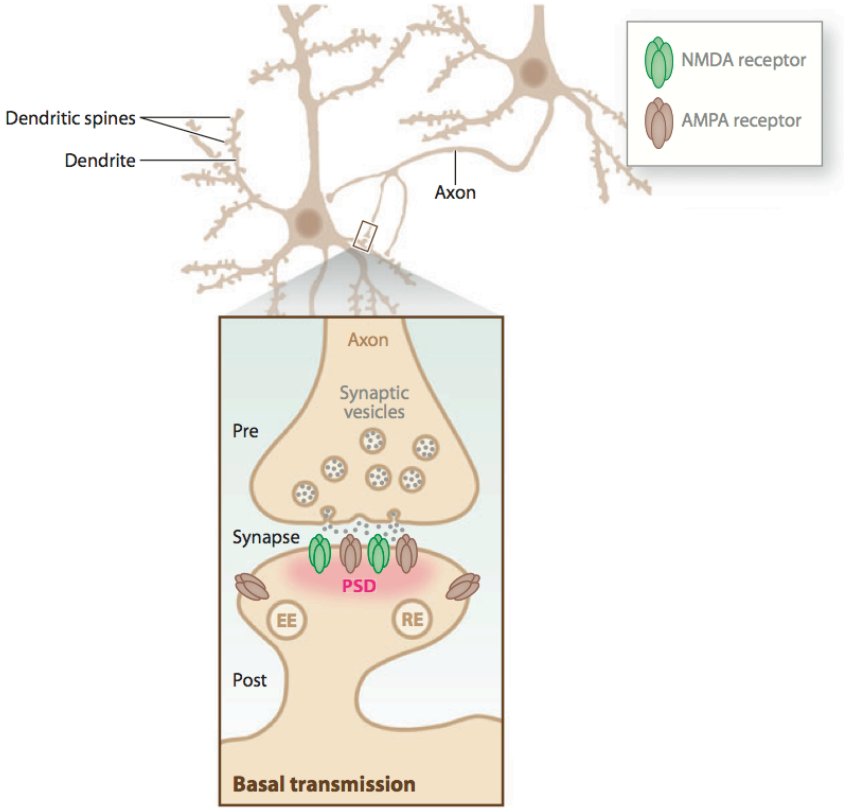

Figure 1-1 The structure of an excitatory synapse

A single neuron is composed of a soma, multiple dendrites, and typically a single axon. Dendrites usually arborize with a highly complex pattern and are covered by a large number of dendritic spines. An axonal terminal projects on a dendritic spine of another neuron, forming a synapse where neural information is transferred through neurotransmitters. The neurotransmitters are packaged in synaptic vesicles, released at the axon terminal, and received by postsynaptic receptors, mainly AMPA and NMDA receptors, at the PSD. Postsynapses contain recycling endosomes (REs) and early endosomes (EEs) for recycling of the receptors. (Modified from Mabb and Ehlers, 2010)

1.1.2 Synaptic Transmission - Transfer of Information in the Brain

Neurochemical signaling molecules known as neurotransmitters are released from one neuron and received by another with the resultant transfer of information (Fig. 1-1). Uni-directional synaptic signaling originates from a presynaptic terminal (or bouton), where neurotransmitters are released into the synaptic cleft, a small ~20 nm space between the pre- and postsynaptic plasma membranes (Montgomery et al., 2004). The neurotransmitters diffuse across the cleft and bind to postsynaptic receptors on the recipient neuron. Such neurotransmission is tightly regulated by deactivation of neurotransmitter inputs, e.g. by enzymatic cleavage and/or reuptake by neurotransmitter transporters in the periphery of the presynapse (Masson et al., 1999).

Glial cells also uptake and metabolize neurotransmitters to terminate neurotransmission (Schousboe et al., 1977).

The neurotransmitters are synthesized in the cytosol of presynaptic neurons and loaded into synaptic vesicles. Depolarization of the neuron at its dendrites and soma is converted into an action potential at the axon initial segment, which propagates to the axon terminal. Upon arrival of an action potential at the presynaptic terminal release site, voltage gated calcium channels (VGCCs) are activated, leading to local calcium ion influx. This transient elevation of calcium ions triggers the fusion of synaptic vesicles with the membrane and completes neurotransmitter release (Sudhof, 2004).

In the brain there are two main types of neurotransmitters, excitatory and inhibitory. Glutamate is the major excitatory neurotransmitter and depolarizes or increases the firing rate of recipient neurons, whereas γ-aminobutyric acid (GABA) and glycine are inhibitory neurotransmitters and hyperpolarize and thus decrease the firing rate of the postsynaptic neuron. The balance of excitatory and inhibitory inputs is key to the systematic control of neuronal networks.

Excitatory synapses are characterized by a highly specialized, asymmetric structure. Active zones (AZs) are electron-dense protein meshworks that are localized adjacent to the presynaptic plasma membrane. These multimeric protein complexes are involved in the organization of docking, priming, and fusion of synaptic vesicles at the neurotransmitter release site (Rosenmund et al., 2003). AZs are found in most presynaptic terminals and vary in shape and size depending on the neuron type.

Excitatory postsynapses form unique structures called dendritic spines, small protrusions arising from dendritic shafts. Spines are highly dynamic structures enriched in actin filaments (F-actin) and exhibit a wide range of sizes and shapes. Membranes of dendritic spines contain the postsynaptic density (PSD), a dense matrix organized in an array of scaffolding proteins, tethering neurotransmitter receptors at a high density to coordinate postsynaptic function (Montgomery et al., 2004).

Glutamate receptors fall into two main classes; the ionotropic receptors including a-amino-3-hydroxy-5-methyl-4-isoxazole propionic acid receptors (AMPARs), kainate receptors (KAs), and *N*-methyl-D-aspartate receptors (NMDARs), and the large group of G-protein coupled metabotropic glutamate receptors (mGluRs) (Collingridge et al., 2004). The present study has not focused on the functions of mGluRs, and therefore the properties of those receptors are not

described here. Ionotropic receptors form ion pores in the membrane allowing the flux of specific ions when activated. The role of postsynaptic kainate in synaptic transmission is currently not very well understood and so the present study primarily focused on AMPARs and NMDARs.

AMPARs are tetramers formed through dimerization of homodimers of GluR1, 2, 3, and 4 subunits. AMPAR-mediated currents dominantly contribute to the fast component of excitatory responses in the central nervous system (CNS), owing to their rapid activation and fast desensitization (Spruston et al., 1995). Activated AMPARs are generally permeable to sodium, potassium, and calcium ions and depolarize the postsynaptic membrane. However, the permeability of calcium ions depends on incorporation of GluR2 in the AMPARs, because GluR2 causes calcium impermeability (Hollmann et al., 1991).

The majority of NMDAR subunits in the forebrain are NR1, NR2A, and NR2B. NMDARs are tetramers containing two essential NR1 subunits assembled with variable NR2 subunits (Collingridge and Bliss, 1995; Sprengel et al., 1998). Although NMDARs are permeable to sodium, potassium, and calcium ions, NMDARs are blocked at resting conditions by magnesium ions bound to the extracellular pore domain. The removal of this magnesium-ion block requires depolarization of the postsynaptic membrane (Spruston et al., 1995). Thus, NMDARs act like a coincidence detector of simultaneous pre- and postsynaptic activation, because simultaneous glutamatergic inputs and depolarization of postsynaptic membrane are required for their activation. NMDAR-mediated currents contribute to the slow component of excitatory responses (Spruston et al., 1995). In addition, NMDARs unusually require co-binding of glycine along with glutamate for their activation.

The major inhibitory neurotransmitter GABA acts on two types of receptors, ionotropic type A receptors ($GABA_A$Rs) and metabotropic type B receptors ($GABA_B$Rs) (Collingridge et al., 2004). The activation of $GABA_A$ receptors allows for the passage of chloride ions, leading to hyperpolarization of the postsynaptic membrane at resting conditions. $GABA_B$ receptors are distributed in a large part of the brain, are localized to pre- and postsynaptic sites, and mediate complex regulation of neural activity.

1.1.3 Learning and Memory Formation in the Hippocampus

In addition to controlling basic body functions, the brain is the organ responsible for thoughts and wills – what we call the mind. Numerous neural processes generate thinking, feeling, perceiving, learning and memory, curiosity, behavior, and consciousness (Okano et al., 2000). Learning and memory formation is an elemental and essential mental process that allows an individual to be capable of more than simple reflexes and stereotyped behaviors (Okano et al., 2000), and that are deeply associated with functions of the limbic system that forms the inner border of the cerebral cortex.

The hippocampus, a small sea-horse shaped structure and a part of the limbic system, exhibits a well-organized laminar structure with principal neurons and neuropil layers (Fig. 1-2A). The mouse hippocampus comprises of three distinct sub-regions; the dentate gyrus (DG), the hippocampus proper [consisting of *Cornu Ammonis* area 3 (CA3), CA2, and CA1], and the subiculum (Sb) (Andersen et al., 1971). The major information flow in the hippocampus is mediated through the "trisynaptic loop" (Jones, 1993). The granule cells in the DG give rise to the mossy fiber pathway projecting to the CA3. In turn axons of the CA3, named Schaffer collaterals (SCs), project to the CA1. Lastly axons of the CA1 project to the subiculum (Fig. 1-2A). The hippocampus mainly receives neural inputs from the entorhinal cortex (Jones, 1993), cholinergic inputs from the medial septal area (Givens and Olton, 1990), and dopaminergic inputs from the ventral tegmental area (Swanson, 1982).

The hippocampus plays a critical role in learning and memory formation. Significant insights into this function were obtained from the case of an epileptic patient known as H.M. (Scoville and Milner, 1957). To reduce bouts of epilepsy, his bilateral medial temporal lobes, including a large part of hippocampus, entorhinal cortex, and amygdala, were surgically removed, which led to continuous memory deficits, and anterograde and partial retrograde amnesia (Corkin et al., 1997). This patient had become incapable of forming new episodic memories after this surgery and of recalling any events that had occurred just before the surgery, but kept memories for earlier events, such as memories of his childhood. The implication of the case of H. M. is that the hippocampus participates in memory acquisition, but not in storing memory, and that it is a determinant of establishing memory and retrieving memory from other structures.

Additionally, the hippocampus is especially vulnerable to epileptic seizures (Miles et al., 1988) and very sensitive to ischemic damage (Barth and Mody, 2011; Nikonenko et al., 2009) and has been implicated in Alzheimer's disease (Hyman et al., 1984). As a result, significant research efforts have focused on the hippocampus to decipher the fundamental and physiological and pathological mechanisms underlying memory formation and psychiatric disorders, respectively.

1.1.4 Synaptic Plasticity, a Candidate Model for Learning and Memory

Synaptic plasticity, the ability of neurons to change their connectivity and synaptic strength in an activity (experience) dependent manner, is thought to be a key molecular and cellular process during learning and memory formation. Neurons are thought to encode, store, and retrieve sequential tracks of neural activity through synaptic plasticity.

There are two major opposing forms of synaptic plasticity: long-term potentiation (LTP) and long-term depression (LTD). LTP and LTD are experimental phenomena, involving various activity-dependent alterations in synaptic strength, and are often examined in rodent hippocampus or amygdala (Malenka and Bear, 2004). The types, robustnesses, and mechanisms of LTP/LTD largely depend on the type of specific synapses in a certain brain region, on the developmental time point, and on the induction protocol (Raymond, 2007). Although it is a daunting task to prove the link between experimental synaptic plasticity and a given functional output, such as behavior (Malenka and Bear, 2004), the connection between synaptic plasticity and memory formation is supported by common properties. For example, both can be short-term or long-term and protein synthesis dependent or independent, and a number of genetic and other manipulations affect both in a similar manner (Lu et al., 2008).

As shown in Fig. 1-2C, a brief period of coordinated neuronal activity causes a long-term increase in the synaptic strength, LTP. LTP is characterized by two phases, an induction phase of triggering the potentiation and a maintenance phase of enduring potentiation over time (Sacktor, 2008). LTP can be reversed to the basal level (the state before LTP induction) by a process called depotentiation, elicited by additional distinct patterns of neural activity during LTP (Barrionuevo et al., 1980). The same pattern of neural activity that is required for depotentiation was shown to be capable

of de novo LTD induction (Dudek and Bear, 1992).

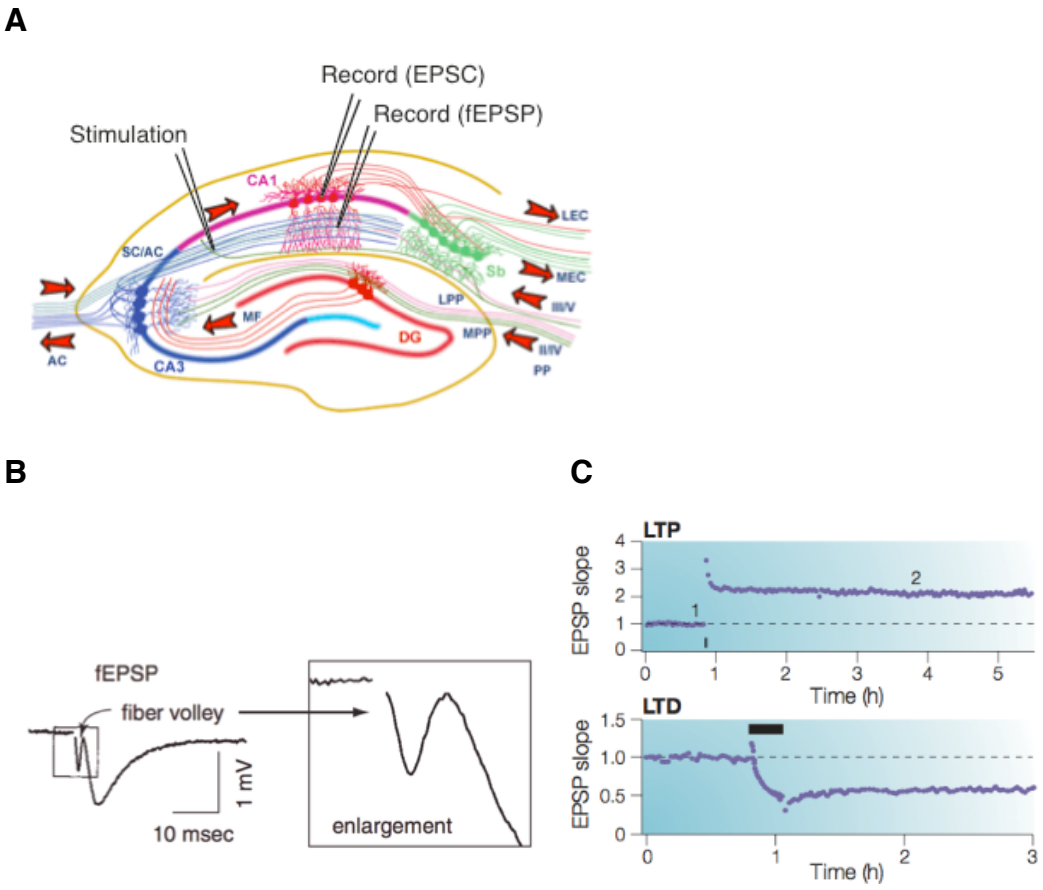

Figure 1-2 Synaptic plasticity in the hippocampus

(A) Schematic diagram of the rodent hippocampal formation with the hippocampus network. The major information flow is indicated by the red arrows. (II/IV and III/V; entorhinal cortex layers II/IV and III/V; MPP and LPP, medial and lateral perforant path; DG, dentate gyrus; MF, mossy fiber; AC, associational/commissural; SC, Schaffer collateral; Sb, subiculum; MEC and LEC, medial and lateral entorhinal cortex). Typical placements of electrodes to stimulate and record activities of the SC/CA1 synapses (extracellular field recording, fEPSP; whole cell patch clamp recording, EPSC) are indicated.
(B) Representative trace of fEPSP showing a fiber volley and an EPSP, measured in the CA1 stratum radiatum. (Adapted from Bortolotto et. al., 2011)
(C) Examples of time-course plots showing changes in the synaptic responses (slopes of EPSPs, normalized to baseline) against time during LTP (upper) and LTD (lower). Black bars indicate the time of stimulus to induce LTP or LTD. (Adapted from Collingridge et. al., 2004)

1.1.5 Initiation of Synaptic Plasticity

Postsynaptic calcium influx is essential for LTP induction, and NMDA receptors play a central role in synaptic plasticity (Raymond, 2007). It has been hypothesized that the magnitude of NMDAR activation determines the polarity of the synaptic modifications by specifying the following calcium signal cascade to be activated (Collingridge et al., 2004; Zucker, 1999). High frequency stimulations (HFSs, e.g. at 100 Hz) and theta burst stimulations (TBSs, including 5 Hz pulses) of the presynaptic fibers leads to a large depolarization of the postsynaptic membrane and glutamatergic inputs simultaneously, leading to activation of NMDARs, followed by calcium influx into the postsynapses (Raymond, 2007). This NMDAR dependent calcium influx is essential for induction of NMDAR-dependent LTP at mature SC/CA1 synapses.

Alternatively, other calcium sources are also capable of inducing LTP. More intensive stimulations (e.g. higher frequency in a train or increased train length) than those of NMDAR-dependent LTP activate the voltage-gated calcium channels (VGCC) additionally, producing more robust LTP (Swant and Wagner, 2006). Certain stimulations can induce compound LTP comprising NMDAR- and VDCC-dependent LTPs (Grover and Teyler, 1990). Another important calcium source for LTP induction is the intracellular calcium released from the endoplasmic reticulum (ER) through ryanodine receptors (RyRs) and inositol (1,4,5)-trisphosphate [Ins(1,4,5)P_3] receptors. RyRs sense increased cytoplasmic calcium ions to release the stored calcium ions, which are required for LTP induced by a weak stimulation (Balschun et al., 1999; Behnisch and Reymann, 1995). Ins(1,4,5)P_3 receptors are activated and opened by the activation of metabotropic receptors (e.g. mGluR1) (Raymond, 2007) to release calcium ions. Among the intracellular singling cascades activated by calcium ions, CaMKII activation is required to generate all types of LTP. Although PKA, PKC, IP3K, and Src play important roles in NMDAR-dependent LTP, it is still unclear whether and how each of them acts as a mediator or modulator of LTP (Malenka and Bear, 2004).

In contrast, generally a prolonged low frequency stimulation (LFS), typically at 1 Hz of 900 pulses at hippocampal SC/CA1 synapses, effectively induces LTD. Like HFS, LFS also activates NMDARs, but triggers only a modest elevation of intracellular calcium levels, leading to the activation of several phosphatases,

including phosphatase1 (PP1) and calcineurin. Those enzymes likely dephosphorylate proteins that have been pre-phosphorylated by PKA (Malenka and Bear, 2004). LTD induced by LFS is age dependent, as LTD is hardly induced in mature mice (Milner et al., 2004). Nevertheless, mGluR activation is also inducible of LTD (mGluR-dependent LTD) by stimulating intracellular calcium release (Malenka and Bear, 2004).

1.1.6 Expression of Synaptic Plasticity

Since Bliss and his colleagues discovered the phenomenon of LTP (Bliss and Lomo, 1973), the question of whether the increased synaptic strength in LTP is caused by pre- or postsynaptic alterations, or both, has been unsolved or at least is still under debate. However, the discovery of 'silent synapses' (Durand and Konnerth, 1996; Isaac et al., 1995) provided a compelling insight into the mechanisms underlying LTP that dominantly rely on postsynaptic alterations, and this notion has been generally agreed since (Collingridge et al., 2004; Malenka and Bear, 2004). Among the excitatory synapses, there are silent synapses that contain only NMDARs, but little or no AMPARs, and that remain irresponsive to glutamatergic inputs at rest. Following an LTP induction, AMPARs are rapidly inserted into these silent synapses to arouse them, concurrent with an increase of the synaptic responses. Thus, the number of synaptic AMPARs is tightly regulated in an activity-dependent manner, which is a key mechanism underlying LTP and LTD.

In addition, direct phosphorylation of AMPARs is involved in the expression of synaptic plasticity. GluR1 is phosphorylated at two sites during LTP, at Ser831 by CaMKII and at Ser845 by PKA. Phosphorylation of GluR1-Ser831 increases the conductance of GluR1 (Derkach et al., 1999; Soderling and Derkach, 2000), and phosphorylation of Ser845 is required for delivery of GluR1 to the activated synapses (Ehlers, 2000; Shi et al., 2001).

In NMDAR-dependent LTD, GluR1 Ser845 is selectively dephosphorylated, leading to a reduced open channel probability (Banke et al., 2000; Lee et al., 2003), a possible acceleration of receptor endocytosis (Ehlers, 2000), and thereby a reduced AMPAR-mediated response. Removal of GluR2 from synapses is accelerated through phosphorylation of Ser880 by PKC (Chung et al., 2000; Matsuda et al., 2000), which is also critical for LTD expression.

Thus, postsynaptic alterations, especially of synaptic trafficking and characteristic modifications of AMPARs, are critical factors for the expression of synaptic plasticity at the SC/CA1 synapse, although the contribution of presynaptic alterations may be also involved as observed in another type of hipocampal LTP that occurs at the mossy fiber/CA3 synapse and depends on presynaptic strengthening.

1.1.7 Trafficking of AMPA Receptors

AMPARs are highly mobile due to lateral diffusion and endo/exocytosis, and tightly organized by protein interactions (Collingridge et al., 2004; Malenka and Bear, 2004). All subunits of AMPARs are similar in one large extracellular and four membrane-associated domains, but differ somewhat in their cytoplasmic tails of the C-terminus (C-tails), which are critical determinants for their protein interactions. GluR1 and GluR4 contain longer C-tails, while GluR2 and GluR3 contain homologous shorter C-tails (Malinow and Malenka, 2002). The interaction with PSD-95 and other discs large, zona occludens 1 (PDZ) domain containing proteins is generally important for postsynaptic receptors to organize their cellular localization and protein complex formation. GluR1s contain group I PDZ ligands interacting with synapse-associated protein 97 (SAP97), and GluR2s and GluR3s contain group II PDZ ligands interacting with glutamate receptor-interacting protein (GRIP), AMPAR binding protein (ABP), and protein interacting with C-kinase (PICK1) (Malinow and Malenka, 2002).

GluR1/2 and GluR2/3 are dominantly expressed in the mature hippocampus (Wenthold et al., 1996), and their trafficking is regulated differently. The trafficking of GluR1/2 is governed by a regulated pathway, where GluR1/2 receptors are incorporated into synapses in an activity-dependent process that operates during synaptic plasticity. In contrast, the trafficking of GluR2/3 is governed by a constitutive pathway, where GluR2/3 is continuously inserted into and removed from synapses, thus maintaining basal synaptic transmission and contributing to LTD expression (Malinow and Malenka, 2002; Shepherd and Huganirl, 2007).

N-ethylmaleimide-sensitive factor (NSF) and adaptor protein 2 (AP2) directly target the same cytoplasmic region of GluR2 (Lee et al., 2002; Nishimune et al., 1998). The interaction of NSF with GluR2 leads to insertion and stabilization of GluR2 at synapses, while replacement of NSF by AP2 causes internalization of

GluR2 through clathrin- and dynamin-dependent endocytosis (Lee et al., 2002). NSF/AP2-dependent endo/exocytosis of GluR2 is significantly involved in basal synaptic transmission and LTD (Luscher et al., 1999; Luthi et al., 1999). Another region of GluR2 short C-tail associates with GRIP/ABP and PICK1. GRIP/ABP interaction with GluR2 stabilizes and anchors GluR2 in synapses and intracellular pools through protein interactions mediated by their multiple PDZ domains (DeSouza et al., 2002; Setou et al., 2002). PICK1 interacts with PKC to promote GluR2-Ser880 phosphorylation, allowing PICK1 to interfere with APB/GRIP1 binding to GluR2. Thus interaction of PICK1 with GluR2 leads to destabilization of synaptic GluR2 and subsequent internalization of GluR2 (Chung et al., 2000; Matsuda et al., 1999).

Whereas GluR2 trafficking is involved in basal transmission and LTD, it is evident that incorporation/removal of GluR1 into/from the synaptic plasma membrane plays a critical role in LTP and LTD (Hayashi et al., 2000). GluR1 interacts with SAP97, and CaMKII-dependent phosphorylation of SAP97 leads to incorporation of SAP97/GluR1 into the synaptic plasma membrane (Mauceri et al., 2004). GluR1 is delivered to the surface of synapses through actin-based trafficking by SAP97-dependent interaction with Myosin-VI (Wu et al., 2002).

Mammalian AMPARs functionally require the interaction with transmembrane AMPA receptor regulatory proteins (TARPs) as auxiliary subunits (Nicoll et al., 2006). In one model, GluR1 is incorporated into synapses by indirect interaction with a postsynaptic scaffold protein PSD95 through stargazin, a TARP protein (Chen et al., 2000; Ehrlich and Malinow, 2004).

Thus, AMPAR trafficking is strictly regulated under basal conditions and during synaptic plasticity. Complex protein interactions of AMPARs drive exocytotic entry into the plasma membrane, lateral diffusion into synapses, tethering at synapses, and recycling from endosome into synapses during LTP. On the other hand, the removal of the receptors from the plasma membrane via multiple endocytotic processes is required for LTD induction (Collingridge et al., 2004; Kessels and Malinow, 2009; Opazo and Choquet, 2011; Wang et al., 2008).

1.1.8 Late-Phase LTP

Like memory, NMDAR-dependent LTP occurs in two temporally and mechanistically distinct phases, early-phase LTP (E-LTP) that lasts 1-2 h, and late-phase LTP (L-LTP) that lasts 2-3 h or even longer. E-LTP requires protein

modification and synaptic trafficking of existing proteins (Bliss and Collingridge, 1993; Malenka and Bear, 2004), while L-LTP further requires gene transcription and new protein synthesis for maintenance (Frey et al., 1988).

Signaling pathways that link the synapse to the nucleus in L-LTP involve PKA, CaMKII, and MAPK, which in turn lead to simultaneous activation of adenosine 3', 5'-monophosphate (cAMP) response element-binding protein (CREB), a key transcription factor for L-LTP, and immediate early genes (IEGs) such as zif268 and activity-regulated cytoskeleton-associated protein (Arc) (Malenka and Bear, 2004). One of the important targets for CREB dependent transcription is the brain-derived neurotrophic factor (BDNF) gene, which encodes the BDNF ligand of TrkB receptors. L-LTP also relies on local protein translation at the dendrite, regulated by the protein kinase mTOR, which phosphorylates and inactivates a translation repressor 4E-BP, initiating protein translation of specific target proteins (Tang et al., 2002).

According to current hypotheses, a process termed ‘synaptic tagging and capture’ accounts for the maintenance of L-LTP. In order to generate L-LTP, i.e. to transform E-LTP into L-LTP, ‘tagged synapses’ generated by a weak or strong stimulation ‘capture’ plasticity related proteins (PRPs) that are induced by a strong stimulation. These steps are required for homo- and heterosynaptic L-LTP (Frey and Morris, 1997; Redondo and Morris, 2011). Arc and PKMζ have been identified as PRPs (Redondo and Morris, 2011). Further, it was shown that induction of LTP leads to increased spine size and new spine formation (Maletic-Savatic et al., 1999; Okamoto et al., 2004), and inhibition of actin polymerization impairs L-LTP (Kim and Lisman, 1999; Krucker et al., 2000). This structural remodeling could in principle take place independently of L-LTP (Kopec et al., 2007; Yang et al., 2008), but likely plays a critical role in the ‘tag’ setting at synapses (Fonseca, 2012; Redondo and Morris, 2011). Dopaminergic inputs also significantly contribute to L-LTP through a synergistic interaction with NMDA-receptor activation (Frey et al., 1990; Lisman and Otmakhova, 2001). Dopamine activates the cAMP/PKA pathway, leading to generation of PRPs including PKMζ (Navakkode et al., 2010).

1.2 Ubiquitination

1.2.1 Ubiquitination

Ubiquitination is a post-translational protein modification that regulates a variety of basic cellular functions upon various stimuli. This biological process operates by the covalent conjugation of ubiquitin moieties to substrate proteins, mediated by the sequential action of three enzymes: E1 ubiquitin activating enzymes (E1s), E2 ubiquitin conjugating enzymes (E2s), and E3 ubiquitin ligases (E3s) (Fig. 1-3A). Ubiquitin moieties are first activated by E1s through formation of high-energy intermediates using ATP and then transferred to E2s that directly interact with E3s. E3 ligases interact with specific substrate proteins via protein-protein interactions, and thus ubiquitination processes are completed by the protein complex of E2, E3, and substrate.

E3 ligases fall into two major groups: Really Interesting New Gene type ligases (RING finger type E3 ligases) and Homologous to E6-AP Carboxyl-Terminus type ligases (HECT type E3 ligases). RING-finger type E3 ligases catalyze direct transfer of the ubiquitin moieties from the E2s to the substrates, while HECT type E3 ligases receive the ubiquitin moieties to form covalent E3-ubiquitin intermediates and subsequently transfer the ubiquitin moieties to the substrate proteins. In contrast to E1 and E2 enzymes, E3s have diversified in higher vertebrates. Approximately 600 genes encode E3s in the human genome (Li et al., 2008b). Owing to their diversity and their capability of interacting with specific substrates, E3 ligases are thought to be the main determinants of the substrate specificity of ubiquitination processes. Ubiqutination is a reversible process, similar to phosphorylation, and deubiquitination is catalyzed by deubiquitination enzymes (DUBs) to regulate the process and to recycle ubiquitin moieties. Thus ubiqitination, like phosphorylation, governs posttranslational protein modification.

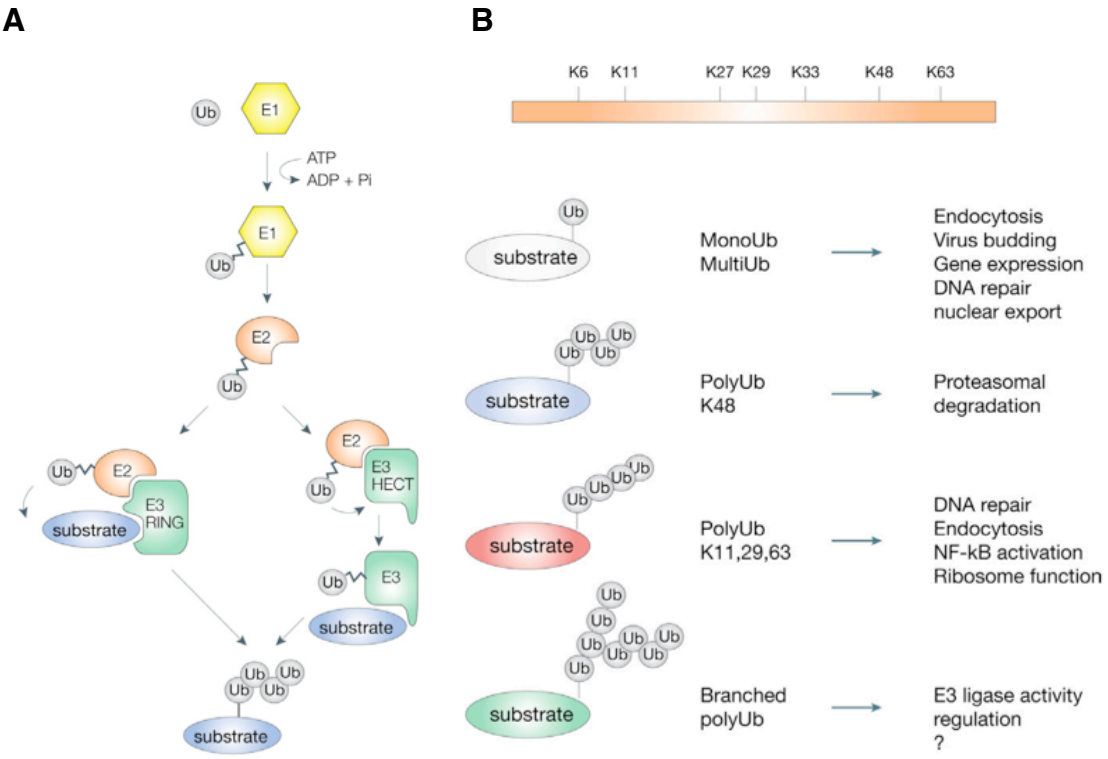

Figure 1-3 Ubiquitination pathways

(A) Protein ubiquitination is mediated by the sequential action of three enzymes. An E1 ubiquitin-activating enzyme (E1) initiates activation of an ubiquitin moiety through thioester linkage using ATP. The ubiquitin moiety is then transferred to an E2 ubiquitin-conjugating enzyme (E2). The E2 with ubiquitin in turn forms a protein complex with an E3 ubiquitin ligase (E3) that recognizes a substrate protein. RING-finger type E3 ligases transfer the ubiqutin moiety directly from the E2 to the substrate protein. While HECT type E3 ligases receive the ubiquitin moiety from the E2, forming a covalent bond via a cysteine residue in the HECT domain, and subsequently transfer the ubiquitin to the substrate protein. The human genome encodes two E1, approximately 30 E2, and more than 600 E3 enzymes (Li et al., 2008b).
(B) Top: Scheme of a ubiquitin moiety highlighting the seven lysine residues. Bottom: Functional consequences of ubiquitination. Monoubiquitination or multi-monoubiquitination regulate endocytosis and protein functions. K48-linked polyubiquitination leads to proteasomal degradation. K11, K29, and K63-linked polyubiquitinations regulate substrate proteins in many distinct ways. The consequences of branched polyubiquitin structures are unknown. (Adapted from Woelk et. al., 2007)

In the ubiquitination process, the C-terminal of an ubiquitin moiety is conjugated onto a lysine residue of a substrate. Ubiquitin-dependent signaling is very dynamic and versatile, because ubiquitin moieties can be conjugated in many different ways (Fig. 1-3B). Monoubiquitination is the conjugation of a single ubiqutin moiety to a substrate protein, and can occur at several lysine residues of the substrate simultaneously (multi-monoubiquitiantion). Monoubiquitination and multi-

monoubiquitination, often found in transmembrane proteins, mainly lead to endocytosis but also control other cellular events including virus budding and gene expression. Furthermore free ubiquitin moieties can be conjugated to an acceptor lysine residue of the first ubiquitin on a substrate, leading to formation of a polyubiquitin chain (polyubiquitination). A ubiqitin moiety possesses seven lysine residues (K6, 11, 27, 29, 33, 48, or 63; Fig. 1-3B), and recent studies have shown that all lysine residues can be used for polyubiquitination (Peng et al., 2003). K48-linked polyubiquitin chains, which were first discovered and are well-characterized, are recognized by the proteasome, leading to substrate degradation. Instead, non-K48-linked (atypical K11-, K29-, or K63-linked) polyubiquitin chains have been found more recently and are as abundant as K48-linked polyubiquitin chains in cells (Xu et al., 2009b). Functional consequences of non-48K-linked polyubiquitin chains have been poorly characterized to date, but recent data indicate that they play roles in DNA repair, endocytosis, or kinase activation (Yang and Kumar, 2010). The chain specificities are determined by E3s in HECT-type E3 ligase mediated ubiquitinaion, while E2s are dominant determinants of the chain specificity in RING-finger-type E3 ligase mediated polyubiqutination (Kim and Huibregtse, 2009). Thus, ubiqutination is versatile and essential for basic and common cellular functions. Furthermore its involvement in neural-specific functions has also been proposed (Mabb and Ehlers, 2010).

1.2.2 The Involvement of Ubiquitination in Memory Formation and Synaptic Plasticity

In addition to protein synthesis, mechanisms underlying learning and memory formation require protein degradation, which is mediated by ubiquitination. This is also true in experimental models of synaptic plasticity. Inhibition of the proteasome affects an animal's behavior and other higher brain functions. For example, bilateral infusion of a proteasome inhibitor into rat CA1 hippocampus results in retrograde amnesia as examined by inhibitory avoidance learning (Lopez-Salon et al., 2001). Conversely, behavioral training, e.g. inhibitory avoidance memory and fear memory training, likely activates ubiquitination-dependent signaling (Lee et al., 2008; Lopez-Salon et al., 2001).

Synaptic plasticity requires the remodeling of synaptic proteins. Therefore, posttranslational protein modifications, including ubiquitination appear to be essential

and favorable processes to regulate long-lasting changes in synaptic strength. One piece of important evidence for the involvement of ubiquitination in synaptic plasticity has emerged from studies by Bingol and colleagues, who showed that synaptic activity promotes the redistribution of proteasomes from dendritic shafts into synaptic spines for local protein degradation (Bingol and Schuman, 2006). In addition to the individual requirement of protein synthesis and degradation for L-LTP, proteasome inhibition rescues impaired L-LTP caused by protein synthesis inhibition, indicating a tight coupling of synthesis and degradation of plasticity-associated proteins, the identity of which remains to be determined (Fonseca et al., 2006; Mabb and Ehlers, 2010).

In mammals, concrete molecular evidence for the importance of the UPS in synaptic plasticity was first obtained in the analysis of *Ube3a* mutant mice lacking the HECT type E3 ligase E6-AP (Jiang et al., 1998). These mice display motor dysfunction, inducible seizures, a context-dependent learning deficit, and impaired hippocampal LTP (Jiang et al., 1998). These characteristics are analogous to those of Angelman syndrome, a hereditary neurodevelopmental disorder where maternal deficiency in the *Ube3a* gene leads to severe cognitive impairment, absent speech, tremor, ataxia, seizures, dysmorphic facial features, sleep disturbance, and inappropriate laughter (Robb et al., 1989). The second piece of evidence for a link between the UPS and synaptic plasticity was provided by studies on APC^{cdh1} mutant mice. The heterozygous mutants, lacking one allele encoding the Cdh1 adaptor subunit of the APC/C complex, which is a RING-finger type E3 ligase, exhibit an impaired L-LTP in the hippocampus and altered contextual fear conditioning (Li et al., 2008a).

1.3 HECT type E3 ligases – Nedd4-1 and Nedd4-2

1.3.1 Nedd4-1 and Nedd4-2 Form a Subfamily in the Nedd4 Family of HECT Type Ubiquitin E3 Ligases

HECT type E3 ligases are characterized by a HECT domain and form a subfamily of ~30 proteins within the approximately 600 E3 ligases found in human. HECT type E3 ligases fall into two groups based on their domain structures, the neuronal precursor cell-expressed developmentally down-regulated 4 (Nedd4) family and the HECT and RCC1-like (HERC) family (Yang and Kumar, 2010).

Nedd4 family members are highly conserved among eukaryotic organisms, sharing a characteristic domain structure with a C2 domain at the N-terminus, several WW domains in the center, and a HECT domain at the C-terminus (Fig. 1-4). The C2 domains determine the cellular localization of the enzymes by binding to phospholipids in a calcium dependent manner and partially determine substrate specificity through their potential to interact with various other proteins. The WW domains dominantly determine the substrate specificities through binding to proline-rich motifs of other proteins. The HECT domains are catalytic domains for ubiquitination and carry one catalytic cysteine residue. Nedd4-1, the prototypical member of this family, was originally identified in a genetic screen for developmentally downregulated genes in mouse neuronal precursor cells (Kumar et al., 1992), and subsequently, other members of this family were identified, including its closest isoform Nedd4-2. The *Nedd4-2* gene generates two splice variants with or without the N-terminal C2-domain (Fig. 1-4) (Dunn et al., 2002). The *S. cerevisiae* gene contains only one member of the Nedd4 family, Rsp5, which is closely related to Nedd4-1. The Nedd4 family has evolutionarily expanded, with eight and nine members in the mouse and the human Nedd4 family, respectively (Fig. 1-4), and all vertebrates appear to possess both Nedd4-1 and Nedd4-2. In spite of similar domain structures, individual members of Nedd4 family appear to play distinct as well as overlapping roles (Yang and Kumar, 2010).

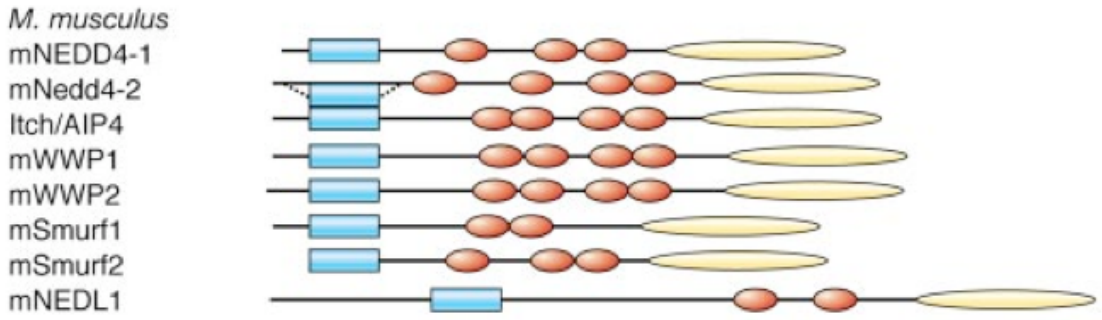

Figure 1-4 Nedd4 superfamily of E3 ubiquitin ligases in *M. musculus*

All members share similar domain structures; a C2 domain (blue boxes, dashed lines indicate a case spliced out), several WW domains (red ellipses), and a HECT domain (yellow ellipses). C2 domains are calcium-dependent lipid binding domains and interact with other proteins. WW domains mainly determine the substrate specificity by recognizing PPxY(x represents any amino acids), LPxY, PPLP, or PxxP motifs (Pirozzi et al., 1997). HECT domains catalyze ubiquitination. (Adapted from Stub and Rotin, 2006)

1.3.2 Functions of Nedd4-1 and Nedd4-2 in Non-Neuronal Cells

Studies on *Nedd4-1* and *Nedd4-2* deficient mice demonstrated that Nedd4-1 and Nedd4-2 are essential for several basic cellular functions. *Nedd4-1* deficient mice exhibit severe growth retardation from an early embryonic stage onwards and die during late gestation probably, because of impaired vasculogenesis or angiogenesis (Kawabe et al., 2010), while *Nedd4-2* deficient mice exhibit collapsed lungs and die perinatally of respiratory distress (Boase et al., 2011). As mentioned, a prominent physiological role of Nedd4-1 is in cell growth, and an analysis of *Nedd4-1* deficient mouse embryonic fibroblasts (MEFs) revealed that Nedd4-1 positively regulates the surface levels of the type 1 insulin-like growth factor receptor (IGF-1R) and the insulin receptor (IR), and consequently activates Akt, a kinase operating downstream of these growth factor receptors (Cao et al., 2008). Grb10 is known as an adaptor protein, linking IGF-1R and Nedd4-1 to induce IGF-1R endocytosis (Vecchione et al., 2003). However, the expression level of Grb10 increases in *Nedd4-1* deficient MEFs, and simultaneous *Grb10* and *Nedd4-1* deficiency restores the surface expression level of IGF-1Rs (Cao et al., 2008). Therefore, it remains unknown how Nedd4-1 regulates the stability and endocytosis of IGF-1R through Grb10.

A well-known target of Nedd4-2 is the epithelial sodium channel (ENaC). Nedd4-2 controls the surface expression level of ENaC through ubiquitination-mediated endocytosis, which is an important component of the physiological processes that regulate fluid and electrolyte homeostasis, e.g. in the lung (Garty and Palmer, 1997). Nedd4-2 dysfunction is thought to be causative for Liddle's syndrome, a genetic hypertensive disorder with autosomal-dominant mutations in PY motifs of the C-terminal tail of ENaC (Kimura et al., 2011; Pradervand et al., 2003).

1.3.3 Nedd4-1 Plays Critical Roles in Developing Neurons

Nedd4-1 is one of the most abundant E3 ligases in the developing brain, and previous studies showed that Nedd4-1 positively regulates neurite development *in vitro* and *in vivo* by monoubiquitinating Rap2, a small GTPase (Kawabe et al., 2010). Nedd4-1 forms a protein complex with Rap2 through TRAF2 and NCK-interacting protein kinase (TNIK), leading to monoubiqutination or K63-linked diubiquitination of Rap2. The inhibition of Rap2 activity via ubiquitination is required for proper neurite development, because active Rap2 promotes activation of TNIK, which leads to slow-down of dendritic growth. Moreover, the analysis of glutamatergic neuron

specific conditional *Nedd4-1* KO mice revealed that Nedd4-1 also determines the mass size of certain brain regions (Figs. 1-5A and B) and the morphology of mature neurons, which exhibit shorter dendrites and less arborization in *Nedd4-1* KO mice than in control mice (Fig. 1-5C) *in vivo* (Kawabe et al., 2010).

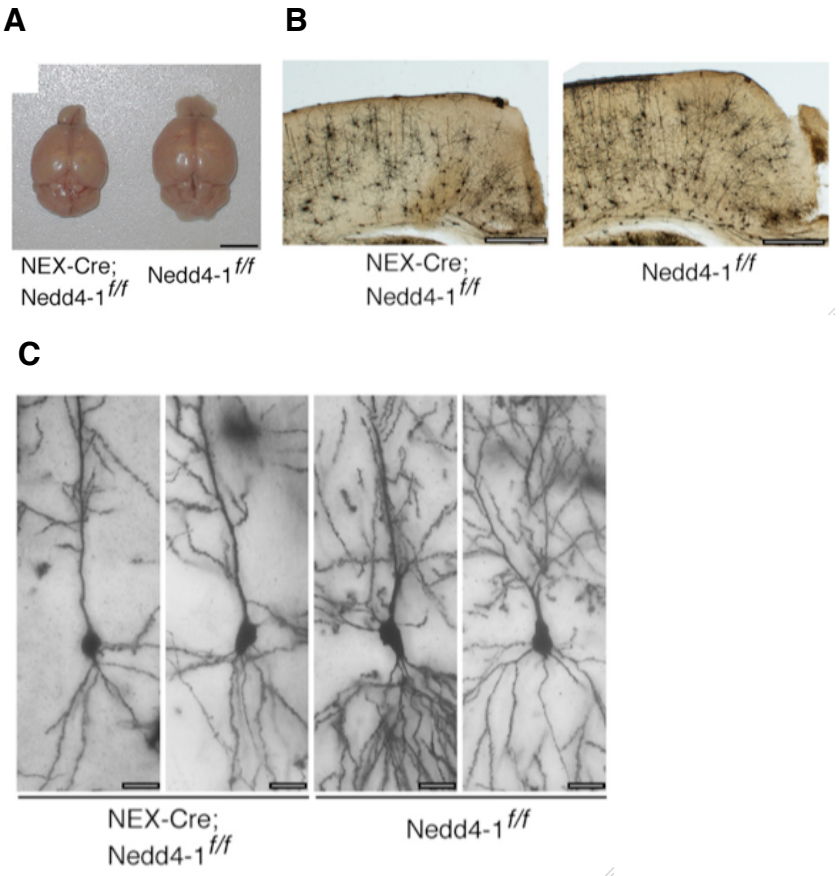

Figure 1-5 The excitatory neuron-specific loss of *Nedd4-1* leads to defective dendrite development *in vivo*

(A) The NEX-Cre; Nedd4-1$^{flox/flox}$ (left) mouse displays smaller cerebrum than the control Nedd4-1$^{flox/flox}$ mouse (right) at postnatal month 8. Scale bars, 5 mm.
(B) Overviews of Golgi-impregnated samples of NEX-Cre; Nedd4-1$^{flox/flox}$ and Nedd4-1$^{flox/flox}$ cerebra. Sections were from 2-month-old littermates. Scale bars, 0.5 mm.
(C) Golgi-impregnated CA1 pyramidal neurons in NEX-Cre; Nedd4-1$^{flox/flox}$ (left two panels) and control (right two panels) mice at 3 months of age. The tops of the images are the apical sides. Scale bars, 20 µm. (Adapted from Kawabe et. al., 2010)

In a complementary study, Nedd4-1 was shown to be responsible for the regulation of axonal branching in developing Xenopus neurons (Drinjakovic et al., 2010). In this process, Nedd4-1 appears to target phosphatase and tensin homolog deleted on chromosome 10 (PTEN). Nedd4-1 knockdown (KD) and PTEN

overexpression lead to a reduction in axonal branching without affecting long-range axon navigation. Nedd4-1 promotes the proteasomal degradation of PTEN, and PTEN KD rescues the impaired axon branching caused by Nedd4-1 KD.

Thus, Nedd4-1 may simultaneously, but locally, control axonal and dendritic development by targeting distinct molecules, Rap2 and PTEN, respectively. However it has been still debated whether PTEN is a target of Nedd4-1. Several studies using *Nedd4-1* KO cells have shown that Nedd4-1 is dispensable for ubiquitination-dependent stabilization of PTEN (Fouladkou et al., 2008). Others showed mono- and polyuniquitination of PTEN by Nedd4-1, which leads to nuclear translocation and proteasomal degradation of PTEN, respectively (Howitt et al., 2012; Wang et al., 2007). Thus, PTEN regulation by Nedd4-1 appears to depend on the cell type and on the developmental stage.

1.3.4 Putative Roles of Nedd4-1 and Nedd4-2 in Mature Neurons

1.3.4.1 Nedd4-1 Accelerates GluR1 Endocytosis

Three studies showed that GluR1 is a direct target of Nedd4-1 in mature neurons. Upon application of AMPA, but not of NMDA (Schwarz et al., 2010), and upon application of glutamate to neurons (Lin et al., 2011), Nedd4-1 ubiquitinates GluR1 to accelerate its endocytosis and lysosomal degradation. Indeed, single synaptic activation causes rapid endocytotic removal of AMPARs, accompanied by accumulation of Nedd4-1 and polyubiquitinated proteins at the activated synapse. This process is NMDAR-activation dependent, and the degradation of the AMPARs depends on proteasomal activity (Hou et al., 2011).

Although the type of glutamate receptors triggered and the degradation pathways detected are different between these studies, they support the notion that Nedd4-1 accelerates endocytosis of AMPA receptors through direct ubiquitination in a synaptic-activation dependent manner.

1.3.4.2 Nedd4-2 Accelerates Endocytosis of Dopamine Transporter (DAT)

Nedd4-2, but not Nedd4-1, has been identified as an E3 ligase responsible for PKC-dependent endocytosis of DAT in an RNA interference (RNAi) screen (Sorkina et al., 2006). The interaction between Nedd4-2, DAT, and epsin has been shown in naive adult rat striatal slices. Nedd4-2 interacts with DAT through the WW3 and WW4 domains, and DAT is ubiquitinated by Nedd4-2 via K63-polyubiquitin chains (Vina-Vilaseca and Sorkin, 2010).

1.3.4.3 Nedd4-2 Accelerates Endocytosis of Voltage-Gated Sodium Channels

A potential involvement of Nedd4-2 in the regulation of neural ion channels was proposed based on *in vitro* experiments. Nedd4-2 may target voltage-gated sodium channels, such as $Na_v1.2$, $Na_v1.3$, $Na_v1.6$, $Na_v1.7$, and $Na_v1.8$ (Fotia et al., 2004; Rougier et al., 2005), indicating that Nedd4-2 may regulate synaptic excitability. However, physiological data are required to prove a role of Nedd4-2 in the regulation of neuronal excitability.

1.4 Aim of the Present Study

Ubiquitination is one of the most important regulatory processes in neuronal functions as well as basic cellular functions. My previous study demonstrated that Nedd4-1, a HECT-type E3 ubiquitin ligase abundantly expressed in the mammalian brain, acts as an essential positive regulator of neurite arborization *in vitro* (Kawabe et al., 2010). Because the loss of *Nedd4-1* cause embryonic lethality, in parallel with the present study, I have generated and analyzed the glutamatergic-neuron specific conditional *Nedd4-1* KO mouse with my supervisors and confirmed the critical role of Nedd4-1 in neurite development and arborization *in vivo* (Kawabe et al., 2010).

The present study focused on deciphering the functions of Nedd4-1 and its closest homolog Nedd4-2 in the mature neuron, especially in synaptic plasticity because of still enigmatic involvement of ubiquitination process in it. For this purpose, we planned to study as the following;

1. Analysis of the expression profiles of Nedd4-1 and Nedd4-2 in the rodent brain.
2. Generation of excitatory neuron specific conditional *Nedd4-1* and *Nedd4-2* double KO mouse lines.
3. Analysis of the excitatory neuron specific conditional *Nedd4-1* and *Nedd4-2* double KO mouse by morphological and electrophysiological methods.
4. Identification of interacting proteins of Nedd4-1 and Nedd4-2.

2 Materials and Methods

2.1 Animals

My host laboratory generated the Nedd4-1$^{flox/flox}$ and the Nedd4-2$^{flox/flox}$ mouse lines (Fig. 3-2A). PCR primers for the genotyping of genomic DNA extracted from mouse tail biopsies were designed to distinguish the floxed mice from wild type mice. The Nex-Cre mouse line was generously provided by Dr. Goebbles and Prof. Dr. Nave (Goebbels et al., 2006), and the Nex-Cre ERT2 mouse line was provided by Dr. Agarwal and Prof. Dr. Nave (Agarwal et. al., 2011). All animal experiments were performed in compliance with the guidelines for the welfare of experimental animals issued by the State Government of Lower Saxony (comparable to NIH guidelines).

2.1.1 Tamoxifen Application

Tamoxifen freebase (10 mg/ml) was freshly mixed in corn oil and vigorously vortexed for 45 min at RT. This solution was stored at 4ºC in the dark for 10 days. The animals were administered a dose of 80 mg/kg body weight for 10 consecutive days.

2.2 Reagents

2.2.1 Chemicals and Reagents

Acrylamide/*N,N'*-Methylene-bis-Acrylamide (29:1)	BioRad
Adenosine 5'-triphosphate disodium salt hydrate (Na_2-ATP)	BioRad
Agarose (UltraPure agarose)	Invitrogen
Alkaline phosphatase	Roche
Amid acids: adenine, uracil, L-tryptophan, L-histidine HCl, L-arginine, L-methionine, L-tyrosine, L-isoleucine, L-lysine HCl, L-phenylalanine, and L-leucine	Sigma-Aldrich
Ammonium persulfate (APS)	Sigma-Aldrich
Ampicillin	Invitrogen
Anti-DIG antibody conjugated with alkali phosphate	Roche
Aprotinin	Roche
Bacto-agar	DIFCO, BD
Bacto-casamino acids	DIFCO, BD
Bacto-peptone	DIFCO, BD

Bacto-yeast extract	DIFCO, BD
BM Purple	Roche
Boric acid (H_3BO_3)	Sigma-Aldrich
Bovine serum albumin (BSA), Fraction V	Pierce, Thermo
Caesium chloride (CsCl)	Pierce, Thermo
Caesium hydroxide (CsOH)	Sigma-Aldrich
Corn oil	Sigma-Aldrich
Darbecco modified eagle's medium (D'MEM)	Gibco, Invitrogen
Denhardts solution (100x)	Sigma-Aldrich
Dextran sulfate	Sigma-Aldrich
DIG RNA labeling mix	Roche
Dimethyl sulfoxide (DMSO)	Sigma-Aldrich
Dionized formamide	Sigma-Aldrich
Dithiothreitol (DTT)	Sigma-Aldrich
DNA ladder mix sample, GeneRuler	Fermentas
DNaseI (RNase free)	Roche
dNTPs	GE Healthcare
ECL reagent	Amersham
Ethanol	Sigma-Aldrich
Ethidium bromide (1% solution)	Carl Roth
Ethylene glycol tetraacetic acid (EGTA)	Sigma-Aldrich
Ethylenediaminetetraacetic acid (EDTA)	Sigma-Aldrich
Glucose	Sigma-Aldrich
Glycerol	Sigma-Aldrich
Glycine	Sigma-Aldrich
Goat serum	Gibco, Invitrogen
Guanosine 5'-triphosphate sodium salt hydrate (Na-GTP) hydrate(29:1)	BioRad
HEPES	Sigma-Aldrich
Hydrochloric acid (HCl)	Sigma-Aldrich
IPTG	BioMol Feinchemikalien
Kanamycin	Invitrogen
Leupeptin	Roche
Luria Broth (LB)	Sigma-Aldrich
Magnesium chloride ($MgCl_2$ $6H_2O$)	Sigma-Aldrich

Magnesium sulfate ($MgSO_4$ $7H_2O$)	Merck
Methanesulfonic acid ($MeSO_3H$)	Fluka
Methanol	Sigma-Aldrich
N-Ethylmaleimide ($C_6H_7NO_2$, NEM)	Sigma-Aldrich
N'N'N'-tetramethylethyl enediamine (TEMED)	BioRad
Nonidet P40 (NP40)	Invitrogen
Opti-MEM I	Invitrogen
Phosphate buffered saline (PBS)	PAA Laboratories
PEG (3350)	Sigma-Aldrich
Pfu polymerase	Stratagene
Phenol	Carl Roth
Phenylmethylsulfonyl fluoride (PMSF)	Roche
Picrotoxin	Tocris
Potassium acetate (CH_3CO_2K)	Sigma-Aldrich
Potassium chloride (KCl)	Sigma-Aldrich
Protein molecular weight standards	Invitrogen
QX-314	Tocris
Restriction endonucleases	NewEngland Biolabs (NEB)
Salmon sperm DNA	Sigma-Aldrich
Skim milk	Nestle
Sodium bicarbonate ($NaHCO_3$)	Sigma-Aldrich
Sodium butyrate	Merck
Sodium chloride	Sigma-Aldrich
Sodium deoxycholate	Sigma-Aldrich
Sodium dodecyl sulfate (SDS)	Roche
Sodium phosphate (NaH_2PO_4)	Roche
Sucrose	Sigma-Aldrich
Tetraethylammonium chloride (TEA-Cl)	Fluka
Tetrodotoxin	Tocris
T4 DNA Ligase	Invitrogen
Tamoxifen freebase	Sigma-Aldrich
Taq-Polymerase (REDTaq)	Sigma-Aldrich
Tri-sodium citrate dihydrate	Sigma-Aldrich
Trichloromethane (Chloroform)	Sigma-Aldrich

Tris Base	Sigma-Aldrich
Triton X-100	Roche
Tween 20	Sigma-Aldrich
X-Gal	BioMol
Z-Leu-Leu-Leu-CHO (MG-132)	Boston Biochem

2.2.2 Kits

PureLink Quick Plasmid Miniprep Kit	Invitrogen
PureLink Quick Plasmid Midiprep Kit	Invitrogen
PureLink Quick Plasmid Maxiprep Kit	Invitrogen
PureLink Gel Extraction Kit	Invitrogen
QuickChangeII Site-Directed Mutagenesis Kit	Stratagene
TOPO TA cloning Kit	Invitrogen
MEGAscript (SP6, T7) transcription Kit	Ambion
BCA protein Assay Kit	Thermo, Piece
FD Rapid GolgiStain^{TM} Kit	MTR Scientific

2.2.3 Bacteria and Yeast Strains

E. coli XL-1 Blue competent cells	Stratagene
E. coli. Electro 10-Blue competent cells	Stratagene
E. coli JM109 competent cells	Promega
E. coli TOP10 competent cells	Invitrogen
E. coli BL21DE3 competent cells	Stratagene
E. coli HB101 competent cells	Promega
S.cerevisiae PJ69-4A strain (James et al. 1996)	Invitrogen

2.2.4 cDNA Libraries

Mouse Brain Qiock-clone cDNA	Clontech (Cat. #637301)
Mouse Brain Prey library (constructed in pGAD-GL vector)	Provided by Dr. Hiroshi Kawabe
Rat Brain Prey library (constructed in pVP16-3 vector)	Provided by Prof. Dr. Nils Brose

2.2.5 Vector Plasmids

pCR2.1 TOPO	Invitrogen
pCR2.1-Nedd4-1	Provided by Dr. Hiroshi Kawabe
pCR2.1-Nedd4-2 (WT, -C2 domain)	Generated in this study

pCR2.1-Nedd4-2 (WT, +C2 domain)	Generated in this study
pEGFPC2	Clontech
pEGFPC2-Nedd4-1 (WT)	Provided by Dr. Hiroshi Kawabe
pEGFPC2-Nedd4-1 (CS)	Provided by Dr. Hiroshi Kawabe
pEGFPC2-Nedd4-2 (WT, +C2 domain)	Generated in this study
pEGFPC2-Nedd4-2 (WT, -C2 domain)	Provided by Dr. Hiroshi Kawabe
pEGFPC2-Nedd4-2 (CS, +C2 domain)	Generated in this study
pEGFPC2-Nedd4-2 (CS ,-C2 domain)	Generated in this study
pEGFPC2-Nedd4-2 (WT, +C2 domain) +oligo	Generated in this study
pEGFPC2-Nedd4-2 (WT, -C2 domain) +oligo	Provided by Dr. Hiroshi Kawabe
pEGFPC2-Nedd4-2 (CS, +C2 domain) +oligo	Generated in this study
pEGFPC2-Nedd4-2 (CS, -C2 domain) +oligo	Generated in this study
pF(syn)W-RBN	Provided by Dr. Hiroshi Kawabe
pF(syn)W-RBN-Nedd4-1	Provided by Dr. Hiroshi Kawabe
pF(syn)W-RBN-Nedd4-2 (WT, +C2 domain)	Generated in this study
pF(syn)W-RBN-Nedd4-2 (WT, -C2 domain)	Generated in this study
pClneo Myc	Provided by Dr. Hiroshi Kawabe
pCRII-Synaptopodin	Provided from Dr. Joachim Kremerskothen
pClneo Myc-Synaptopodin (short)	Generated in this study
pCR2.1-Mena	Generated in this study
pFLAG2b-Mena	Generated in this study
L21	Provided by Prof. Dr. Pavel Osten
PACK	Provided by Prof. Dr. Pavel Osten
ENV	Provided by Prof. Dr. Pavel Osten
pGAG424-HA	Clontech
pGBD-C2	Provided by Dr. Philip James
pVP16-3	Provided by Prof. Dr. Nils Brose
pRK5-HA-Ubiquitin	Provided by Dr. Hans-Juergen Kreienkamp

2.2.6 Oligonucleotides

Oligonucleotide primers used in this study are listed below. They were synthesized in the MPI-EM DNA Core Facility on an ABI 5000 DNA/RNA synthesizer. Restriction sites used for molecular cloning are underlined where applicable.

Primer #	Sequence	Rest. site
12287	5'-GGGAATTCTCCATGGAGAGACCCTATACAT -3	EcoRI
12288	5'-TCCTCTAGATTAATCCACACCTTCGAAGC -3'	XbaI

12344	5'-GTCCAAGTTGTGGTTCGATTG -3'	-
12432	5'-CCAGAGCTCATACAAGTTTTAATCGCCTTGATTTACCTCC-3'	-
12433	5'-GGAGGTAAATCAAGGCGATTAAAACTTGTATGAGCTCTGG -3'	-
12687	5'-GGGAATTCTCCATGGCGACCGGGCTTG -3'	EcoRI
89	5'-TGTAAAACGACGGCCAGT -3'	-
91	5'-AACAGCTATGACCATGATTACG -3'	-
14740	5'-CCATACGTGAAGCTGTCCTTG -3'	-
14741	5'-GGTCTCTCCATGGTTGGATC -3'	-
12911	5'-GGGAATTCTCCCGAGTCAAGGGGTTTTTGAGG -3'	EcoRI
12913	5'-GGGAATTCTCCACCCTTTCCAATCCACAGTCC -3'	EcoRI
12914	5'-GGGAATTCTCCAAGCCTGCTGATATTCCAAACAGG -3'	EcoRI
12915	5'-GAAGATCTTACTGTTCCCCGTTGGAGTCC -3'	BglII
12916	5'-GAAGATCTTAAAGGGTATCTTTCACGGCACG -3'	BglII
12917	5'-GAAGATCTTAGGAGTACGGAACAGCCGGAC -3'	BglII
12918	5'-GAAGATCTTAATCCACACCTTCGAAGC -3'	BglII
12945	5'-GGGAATTCTCCCCCGGAAGTGATGTCACAGATAC -3'	EcoRI
12946	5'-GGGAATTCTCCGCCACCCATTTGCAGCATC -3'	EcoRI
12947	5'-GGGAATTCTCCACCAGCCAGCCAGTCACCAG -3'	EcoRI
12948	5'-GGGAATTCTCCCATCTGAGAGGAAAGACACCAGTC -3'	EcoRI
12949	5'-GGGAATTCTCCCATCTGAGAGGAAAGACACCAGTC -3'	EcoRI
12950	5'-GAAGATCTTATGACGGAGGCGACTGAACAG -3'	BglII
12951	5'-GAAGATCTTAGTCATTGGAGTCGACTGGTGTC -3'	BglII
12952	5'-GAAGATCTTAAATGTTTGCACGGCGAAGTTTC -3'	BglII
12953	5'-GAAGATCTTAATCAACCCCATCAAAGCCCTG -3'	BglII
12966	5'-GGGAATTCTCCGACTCCAACGGGGAACAG -3'	EcoRI
12302	5'-GGGAATTCTCCATGAGTGAACAGAGTATCTGTCAGG -3'	EcoRI

12303	5'-ACGTCGACTTATGCAGTGTTCGACTTGCTCAG - 3'	SalI

2.2.7 Antibodies

Primary antibodies used for immunoblotting in this study.

	Host Species	Origin	WB
α-Actin	Rabbit	Sigma	1:5000
α-GFP	Mouse	Roche	1:1000
α-Myc	Mouse	Sigma	1:1000
α-PSD95	Mouse	BD	1:500
α-Synaptophysin	Mouse	SYSY	1:1000
α-βTubilin	Mouse	Sigma	1:6000
α-Synaptopodin	Rabbit	Sigma	1:1000
α-Ubiquitin (P4D1)	Mouse	Santa Cruz	1:200
α-Nedd4-1	Mouse	Transduction Lab	1:500
α-Nedd4-1	Rabbit	(Kawabe et al., 2010)	1:1000
α-Nedd4-2	Rabbit	Kind gift from Dr. Daniela Rotin	1:1000

Secondary antibodies used for immunoblotting in this study.

	Host Speices	Conjugated substruct/Dye	Origin	Usage Dilution
α-Mouse IgG	Goat	HRP	Biorad	WB; 1:20000
α-Rabbit IgG	Goat	HRP	Biorad	WB; 1:20000

2.3 Molecular Biology

2.3.1 Plasmid DNA Preparation Using Miniprep and Midiprep

The plasmid DNA preparation was carried out using the PureLink Quick Plasmid Miniprep Kit, HiPure Plasmid Midiprep Kit, and HiPure Plasmid Maxiprep Kit (Invitrogen), following the protocol provided by the manufacturer. The final concentration of the plasmid DNA was adjusted to 2 mg/ml in TE buffer (10 mM Tris-HCl pH 7.4, 1 mM EDTA).

2.3.2 Plasmid Transformation Using Electroporation

An aliquot (50 µl) of electro-competent cells of the appropriate *E.coli* strain was let thaw on ice and 20 ng of plasmid DNA or 1 µl of a ligation reaction were added, mixed gently, and incubated for 1 min on ice in a pre-cooled electroporation

cuvette (0.1 cm, BioRad). Following the application of a short electric pulse (1.8 kV) using an *E.coli* pulser (Biorad), the cells were immediately resuspended in 0.5 ml pre-warmed LB medium. For the recovery and the expression of the antibiotic resistance gene, the *E.coli* was incubated at 37ºC with vigorous shaking for 60 min. The *E.coli* were harvested and plated on an appropriate selection plate.

LB medium: 25 g Lutia Broth (LB; Invitrogen) powder was dissolved in 1 L ddH_2O and autoclaved.

LB plates: 15 g Bacto-agar (Invitrogen) per 1 L of LB medium was dissolved and autoclaved. To prepare a selection antibiotic plate, 100 µg/ml ampicillin or kanamycin was added to a dish and allowed to set.

2.3.3 Measurement of DNA Concentration

For the determination of the DNA concentration, a DU®650 Spectrophotometer (Beckman, USA) was used for measurement of optical densities (ODs) at 260 nm/280 nm wavelength. The DNA concentration was calculated using following equation: dsDNA concentration = OD_{260}* 50 µg/ml* dilution factor. The purity of DNA was estimated by OD_{260}/OD_{280} ratio, with 1.8-2.0 being optimal for use.

2.3.4 DNA Sequencing

All DNA sequencing analysis was performed on an Applied Biosystems 373 DNA Sequencer in the MPI-EM DNA Core Facility.

2.3.5 DNA Digestion with Restriction Endonucleases

The instruction manuals provided from New England BioLabs were referred to for all DNA digestion procedures to find the appropriate conditions. Generally the appropriate quantity of DNA was digested for 1-3 h at the enzyme specific temperature as instructed. The buffer was exchanged using Invisorb MSB spin PCRapace kit (Invitek) when required, e.g. consecutive double-digestion.

2.3.6 Dephosphorylation of 5'DNA-Ends

To prevent religation of a plasmid cut with an identical restriction endonuclease for 3'- and 5'- ends or blunting ends, the 5'-ends of DNA fragments

were dephosphorylated using alkaline phosphatase (Roche) in the supplied buffer according to manufacturer's instructions.

2.3.7 DNA Ligation

The digested plasmid DNA and the insertion of DNA fragments with compatible ends were mixed in the reaction buffer. The molar ratio of the insertion to the vector was 1:1 to 10:1 and the final total volume was adjusted to 20 µl. Lastly, T4 DNA ligase (Invitrogen) was gently added and the mixture was incubated at 16ºC overnight.

2.3.8 Ethanol Precipitation of DNA

A DNA solution was mixed with 3 M potassium acetate and ethanol (DNA solution: 3 M potassium acetate:ethanol=1:0.1:3 in volume) and placed at -80ºC for at least 2 h. The dehydrated DNA was precipitated at 16,000 x g for 30 min using a pre-cooled bench-top centrifuge, and the pellet was washed with 70% ethanol and resuspended in TE buffer.

2.3.9 Agarose Gel Electrophoresis

For size analyses and purification of DNA, DNA products were subjected to agarose-gel electrophoresis. Generally a TBE based-agarose gel (0.7-2%) containing ethidium bromide was used. Negatively charged DNA was separated at a constant voltage (50-150 V) in TBE buffer and visualized by ethidium bromide under an UV-light (254 or 314 nm) exposure. GeneRuler DNA Ladder Mix sample (Fermentas) was loaded in parallel as the marker for the DNA molecular size.

TBE buffer: 50 mM Tris-Base, 50 mM boric acid, 2 mM EDTA, pH 8.0

2.3.10 Purification of DNA Fragments

Following the separation by agarose gel electrophoresis, DNA fragments of interest were excised and isolated from agarose gels with the PureLink Gel Extraction Kit (Invitrogen) according to the protocol supplied by the manufacturer. Long exposure of DNA to UV-light was avoided to protect the DNA from damage.

2.3.11 Polymerase Chain Reaction (PCR)

DNA fragments of interest were amplified in 50 µl of reaction mixtures containing double stranded DNA template, oligonucleotide primers, dNTPs, high-fidelity *Pfu* DNA polymerase (Stratagene), and the reaction buffer. All PCR reactions were run on a Gene Amp 9700 PCR cycler (Applied Biosystems) with basic cycle parameters as below:

Step1: 94ºC for 2 min

Step2: 94ºC for 20 s

Step3: *annealing temperature* for 20 s

Step4: 72ºC for *extension time* (30-40 cycles from Step2 to Step4)

Step5: 72ºC for 10 min

Annealing temperatures and extension times were modified depending on the target DNA fragments. For genotyping PCR, REDTaq DNA polymerase (Sigma-Aldrich) was used.

2.3.12 Subcloning Using the TOPO Cloning Kit

The PCR products were rapidly and easily subcloned into pCR2.1-TOPO or pCRII-TOPO vectors using TOPO TA cloning Kits (Invitrogen) referring to the provided protocol from Invitrogen. LB plates with ampicillin or kanamycin, IPTG and X-gal were used for blue/white screenings.

2.3.13 Cloning Strategies for Constructs Generated and Used in This Study

<u>pCR2.1-Nedd4-2 (WT, -C2 domain)</u>

pEGFPC2-Nedd4-2, containing C2 domain-less mouse Nedd4-2, was used as the template (Accession No. 1300012C07). The insertion was amplified by PCR using primer 12287/12288 and directly subcloned into pCR2.1 vector using TOPO cloning kit.

<u>pCR2.1-C2-Nedd4-2</u>

The cDNA fragment encoding the N-terminal of Nedd4-2 protein containing its C2 domain was amplified by PCR from a mouse cDNA brain library using primers 12687/12344. The obtained fragment was subclonesd into pCR2.1-TOPO vector.

<u>pEGFPC2-Nedd4-2 (WT, +C2 domain)</u>

The insertion encoding C2 domain of Nedd4-2 was obtained from pCR2.1-C2-Nedd4-2 by EcoRI/PstI digestion. This insertion fragment was subcloned into pEGFPC2-

Nedd4-2 (WT, -C2 domain) using EcoRI/PstI sites so as to produce pEGFPC2-Nedd4-2 (WT, full length containing C2 domain).

pEGFPC2-Nedd4-2 (WT, -C2 domain)

The insertion was obtained from pCR2.1-Nedd4-2 (WT, -C2 domain) by EcoRI/XbaI digestion and subcloned into pEGFPC2 vector.

pEGFPC2-Nedd4-2 (CS, +C2 domain)

The cDNA fragment containing the point mutation C971S was obtained from pEGFPC2-Nedd4-2 (CS, -C2 domain) by EcoRI/SalI digestion and exchanged to the corresponding region of pEGFPC2-Nedd4-2 (WT, +C2 domain) plasmid.

pEGFPC2-Nedd4-2 (CS, -C2 domain)

A site-directed mutagenesis (QuickChange®, Stratagene) was carried out using primer 12432/12433 to produce C971S point mutant from pEGFPC2-Nedd4-2 (WT, -C2 domain).

pEGFPC2-Nedd4-2 (WT, -C2 domain) +oligo

pEGFPC2-Nedd4-2 (WT, +C2 domain) +oligo

A PacI restriction site was inserted downstream of the 3'-XbaI restriction site of pEGFPC2-Nedd4-2 (WT, -C2 domain) +oligo. The insertion fragment encoding Nedd4-2 (WT, +C2) was digested by EcoRI/XbaI and exchanged into pEGFPC2-Nedd4-2 (WT, -C2 domain) +oligo vector.

pF(syn)W-RBN-Nedd4-2 (WT, +C2 domain)

pF(syn)W-RBN-Nedd4-2 (WT, -C2 domain)

The cDNA fragment encoding EGFP fused with each Nedd4-2 was obtained from each pEGFPC2-Nedd4-2 +oligo by NheI/PacI digestion and subcloned into pF(syn)W-RBN plasmid.

pClneo Myc-Synaptopodin (short)

The cDNA fragment encoding SYNPO was obtained from pCRII-SYNPO by EcoRI digestion. Following a dephosphorylation of 5'-end of pClneo Myc vector, the insertion fragment was subcloned.

pCR2.1-Mena

pFLAG2b-Mena

The cDNA encoding Mena was amplified by PCR from a mouse cDNA brain library using primers 12302/12303. This DNA fragment was subcloned into pCR2.1-TOPO vector and subsequently into pFLAG2b using EcoRI/SalI site.

2.4 Yeast Two-Hybrid (YTH) Screening

Screening the mouse- and the rat-brain cDNA library was performed by GAL4-based YTH system using PJ69-4A yeast strain.

2.4.1 Media, Buffers, and Stock Solutions

2.4.1.1 Yeast Complete Media and Yeast Selection Media

The following media were prepared using ddH_2O and autoclaved. 2% (w/v) agarose was added into the media before autoclaving to prepare the plates.

20x complete amino acids mix (per 1 L)

0.4 g adenine, 0.4 g uracil, 0.4 g L-tryptophan, 0.4 g L-histidine HCl, 0.4 g L-arginine, 0.4 g L-methionine, 0.6 g L-tyrosine, 0.6 g L-isoleucine, 0.6 g L-lysine HCl, 1.2 g L-phenylalanine, and 0.6 g L-leucine.

20x –WL mix

As above without the following amino acids: L-tryptophan and L-leucine.

20x –WLH mix

As above without the following amino acids: L-tryptophan, L-leucine, and L-histidine HCl.

20x –WLA mix

As above without the following amino acids: L-tryptophan, L-leucine, and adenine.

20x –LA mix

As above without the following amino acids: L-leucine and adenine.

YPAD (per 1 L)

10 g yeast extract, 20 g bacto peptone, 0.4 g adenine, 20 g glucose (dextrose).

SC –W (per 1 L)

6.7 g yeast nitrogen base without amino acids, 20 g glucose, 5 g casamino acids, 0.2 g adenine, and 0.2 g uracil.

SC –WL (per 1L)

6.7 g yeast nitrogen base without amino acids, 20 g glucose, 50 ml 20x –WL mix.

SC –WLH (per 1L)

6.7 g yeast nitrogen base without amino acids, 20 g glucose, 50 ml 20x –WLH mix.

SC –WLH (+3AT) (per 1L)

Add 1 ml of 1 M 3-amino-1, 2, 4 triazol (3AT, sterilized by 0.22 μm filter) to 100 ml of SC- WLH media after autoclave.

SC –WLA (per 1 L)

6.7 g yeast nitrogen base without amino acids, 20 g glucose, 50 ml 20x –WLA mix.

2.4.1.2 Buffers and M9 Medium

1 M Lithium Acetate (LiAc)

10.2 g Lithium Acetate was dissolved in ddH_2O and adjusted to pH at 7.5 with dilute acetic acid. The final volume was adjusted to 100 ml and autoclaved.

10x TE

0.1 M Tris-HCl (pH 7.5), 100 mM EDTA (autoclaved).

LiAc/TE

5 ml of 1M LiAc and 5 ml of 10x TE were mixed and adjusted to 50 ml with ddH_2O.

PEG/LiAc solution

40 ml of 50% PEG, 5 ml of 1 M LiAc, and 5 ml of 10x TE were mixed and adjusted to 50 ml with ddH_2O.

50% PEG

50 g of PEG (3350) was dissolved in ddH_2O and adjusted to 100 ml and sterilized with a 0.22 μm filter (Millipore).

Yeast lysis buffer

1% SDS, 100 mM NaCl, 10 mM Tris-HCl (pH8.0), 1 mM EDTA, 2% Triton X-100.

10x M9 mix

29.0 g Na_2HPO_4, 15.0 g KH_2PO_4, 25.0 g NaCl, and 5.0 g NH_4Cl, adjusted to 500 ml with ddH_2O and autoclaved.

M9 plate (per 600 ml)

1.2 g glucose, 24 mg L-proline, 60 mg thiamine hydrochloride, 12 g agarose, and 510 ml ddH_2O were mixed and autoclaved, then 60 ml 10x M9 mix, 30 ml 20x -LA mix, 0.6 ml 1 M $MgSO_4$, and 0.6 ml 0.1 M $CaCl_2$ were added and stirred. 0.6 ml of 100 mg/ml ampicillin was supplied before making plates.

2.4.2 Generation of Bait Constructs for YTH Screening

The following bait cDNA constructs were generated by PCR using indicated sets of primers and pCR2.1-Nedd4-1 or pCR2.1-Nedd4-2 as templates. The amplified cDNA was cloned into pCRII-TOPO vector, and error-free cDNA clone was subcloned into pGBD-C2 bait vector using EcoRI/BglII sites. All bait constructs were confirmed by sequence analysis before use.

Bait construct	Domain	5' primer ID	3' primer ID
Nedd4-1	WW1	12946	12950
Nedd4-1	WW2	12947	12951
Nedd4-1	WW3	12948	12952
Nedd4-1	WW1+WW2	12946	12951
Nedd4-1	C2+WW1	12945	12950
Nedd4-1	WW2+WW3	12947	12952
Nedd4-1	WW1+WW2	12946	12951
Nedd4-1	HECT	12949	12953
Nedd4-1	HECT CS mutant	12949	12953
Nedd4-2	WW1	12911	12915
Nedd4-2	WW2	12966	12916
Nedd4-2	WW3	12913	12917
Nedd4-2	C2+WW1	12687	12915
Nedd4-2	WW2+WW3, 4	12966	12917
Nedd4-2	WW1+WW2	12911	12916
Nedd4-2	WW1+WW2+WW3, 4	12911	12917
Nedd4-2	HECT	12914	12918
Nedd4-2	HECT CS mutant	12914	12918

2.4.3 Yeast Transformation Using the Lithium Acetate (LiAc) Method

The yeast cells (PJ69-4A strain) were transformed using a heat shock procedure with DMSO and salmon sperm carrier DNA. 200 µl of saturated pre-culture was diluted to an OD_{600} of 0.2 in 10 ml of YPAD medium and shaken at 30ºC for a further 3 h. The cells were collected by centrifugation at 1,000 x g for 5 min and once rinsed with 1 ml of TE. Then the cells were gently suspended twice with centrifugations at 5,000 x g for 5 s at RT, the first in 1 ml and the second in 0.5 ml of LiAc/TE to obtain the yeast competent cells. 100 µl of the competent cells were first mixed with 6 µl of aliquot containing 0.1 µl of bait plasmid and 50 µg of salmon sperm DNA, and then suspended with 600 µl of PEG/LiAc solution. Following a vortex suspension, the cells were shaken at 30ºC for 30 min. The cells were mildly mixed with 70 µl of DMSO by several inversions, and a heat shock at 42ºC for 15 min was applied. The cells were harvested by a centrifugation at 5,000 x g for 5 s, followed by a rinse with 1 ml TE. Finally the cells were spread on an appropriate plate and incubated at 30 ºC for 2-3 days. For the titer examination, the rinsed cells were incubated in 1 mL of YPAD for additional 1 h and streaked on YPAD plate. The transformation efficiency with a single plasmid DNA was about 10^4 to10^5 colonies per microgram DNA.

2.4.4 Selection of Bait Constructs for Screening

To exclude the bait constructions that exhibit auto-activation, first the auto-activity was tested. Each of baits was transformed together with pVP16-3 vector or pGAD424-HA, or alone using the LiAc method. The cells were plated on SC-WL, SC-WLH (+3AT), and SC-WLA plates and incubated for 3 days at 30ºC.

2.4.5 Yeast Two-Hybrid Screening

The transformed yeast cells with each bait construct were subsequently transformed with the prey constructs: the rat brain library in pVP16-3 or the mouse brain library in pGAD. The transformation was carried out using the LiAc method. After the heat shock, cells were resuspended and cultured in SC-WL media at 30ºC overnight. The cells were harvested and plated on SC-WLH (+3AT) plate. Following incubation at 30ºC for 2-3 days, the grown colonies were picked up and streaked on SC-WLA plate for the final selection. The colonies grown on SC-WLA plates were selected as the positive clones.

2.4.6 Plasmid DNA Extraction from Yeast Cells

The prey plasmids of the positive clones were extracted from the yeast cells. The colonies from the positive clones were picked up and rinsed with the ddH_2O. The yeast cells were suspended with 200 µl of yeast extraction buffer and transferred into an eppendorf 1.5 ml tube with glass beads, then 200 µl of phenol/ CH_3Cl was added. The plasmids were extracted by vigorous shaking for 20 min at RT and isolated into aqueous phase separated by centrifugation at 24,000 x g for 5 min at RT. The plasmid DNA was purified and concentrated by the ethanol precipitation method.

2.4.7 Identification of the Positive cDNA Clones

In order to identify the prey construct of the positive clones, the purified prey plasmids were transformed in HB101 *E.coli* competent cells using electroporation. After the incubation for the recovery, the *E.coli* was spread on M9 plates and incubated at 37ºC for 1 or 2 days. The colonies were picked up and the plasmids were purified by miniprep method. The insertion sequences of the prey plasmids were analyzed. To confirm the interaction between the bait and the prey clone, each plasmid pair was again transformed in the yeast cells and grown on the selection plates.

2.5 *In Situ* Hybridization (ISH)

DIG-labeled single strand RNA probes were used for *in situ* hybridization (ISH) analysis. To avoid contamination with RNase, all materials and instruments were isolated from other experiments. Autoclaved 0.1% diethylpyrocarbonate (DEPC) containing-ddH_2O was used instead of ddH_2O. All solutions were DEPC-treated and autoclaved prior to use, except Tris-HCl buffer.

2.5.1 Preparation of RNA Probes

To generate ISH probes, the corresponding cDNA fragments of Nedd4-2 (127 bp-374 bp) were amplified by PCR using primers 14740/14741 and subcloned into pCRII-TOPO. The linearized DNA fragments containing SP6 and T7 promoters on either side of the probe sequence were amplified by PCR using primers 89/91 from the subcloned pCRII-TOPO plasmid. The PCR products were separated on an agarose gel and purified using the PureLink Quick gel extraction kit (Invitrogen) according to the protocol supplied by the manufacturer. The linear DNA fragments were used as the templates for *in vitro* transcription using MEGAscript (SP6 or T7) transcription kit (Ambion) combined with DIG RNA Labeling Mix containing digoxigenin (DIG)-UTP (Roche), following the provided protocols. The reaction mixture was treated by RNase free DNaseI to remove the template DNA fragments, and the labeled probes were purified by ethanol precipitation. The DIG-labeled RNA products were quantified using agarose gel electrophoresis.

2.5.2 Tissue Preparation

The samples were obtained from 2-week-old male C57Black6N mice. Whole brains were removed quickly and immediately frozen. The coronal sections (thickness 20 μm) were cut using cryostat (Leica) and attached on microscope glass slides (SUPERFROST® PLUS, MENZEL-GLASER). The frozen sections were kept at -80ºC until the experiments were carried out.

2.5.3 Hybridization and Detection

The frozen sections were fixed with 4% PFA/PBS at 4ºC for 20 min, washed with PBS three times (5 min each), incubated in 100% Ethanol for 5 min, and dried at

RT. Then the sections were incubated in the pre-hybridization buffer at least 10-15 min. DIG-labeled RNA probes were diluted to approximately 0.5 μg/ml in the hybridization buffer just before use. The hybridization was carried out for 2 days at 37ºC in a humid chamber. After the hybridization, the slides were rinsed with pre-warmed 0.2x SSC buffer at 37ºC for 10 min, washed twice with 1x SSC buffer at RT for 20 min each. To detect the DIG-labeled probes, the slices were incubated with 1:1000 diluted anti-DIG antibody conjugated with alkaline phosphate (Roche) in the blocking buffer at 4ºC overnight, following 2 h blocking reaction. After washing with 1x SSC for 10 min three times, the slides were incubated with pre-warmed BM Purple (Roche) at RT in the dark for an approximate time to develop the conjugated alkaline phosphate.

20x SSC buffer

3 M Sodium chloride, 300 mM tri-Sodium citrate dihydrate, pH 7.0.

Pre-hybridization buffer

4x SSC, 50% dionized formamide.

Hybridization buffer

4x SSC, 40% dionized formamide, 10% dextran sulfate, 1x Denhardt's solution.

2.6 Biochemical Experiments

2.6.1 Protein Measurement

To quantify protein concentration, the bicinchorinic acid (BCA) method was employed. After the reaction with the BCA regents (BCA assay kit, Thermo Piece), the absorbance at 652 nm of each sample was measured using DU®650 Spectrophotometer (Beckman, USA).

2.6.2 Sodium Dodecyl Sulfate-Polyacrylamide Gel Electrophoresis (SDS-PAGE)

To separate proteins based on the molecular size and post-translational modification, for example, phosphorylation, glycosylation, and ubiquitination, protein samples were subjected to SDS-PAGE under denaturing condition. Generally, the protein samples were dissolved in Laemmili's SDS-sample buffer, followed by boiling at 95ºC for 3 min. An SDS-PAGE gel consisting of stacking and resolving gel layers (see recipes below) was prepared and set on the Bio-Rad Mini-PTOTEAN 2

casting system. The protein sample was loaded onto the gel and the electrophoresis was performed with 20 mA for stacking and 30 mA for resolving. Generally 5-20 µg of protein was loaded along side an SDS-PAGE ladder (Bio-Rad).

Laemmili's SDS-sample buffer

10% Glycerol, 50 mM Tris-HCl (pH 6.8), 2 mM EDTA, 2% SDS, 100 mM DTT, 0.05% Bromophenol blue.

Upper stacking gel

5% acrylamide/N,N'-Methylene-bis-Acrylamide (29:1) Solution (AMBA), 125 mM Tris-HCl (pH 6.8), 0.1% SDS, 0.05% ammonium persulfate (APS), 0.005% N,N,N',N'-tetramethylethylenediamine (TEMED).

Lower resolving gel

8-15% acrylamide/N,N'-Methylene-bis-Acrylamide (29:1) Solution (AMBA), 325 mM Tris-HCl (pH 8.8), 0.1% SDS, 0.05% APS, 0.005% TEMED.

Running buffer

25 mM Tris-HCl, 250 mM Glycine, 0.1% SDS (pH 8.8).

2.6.3 Immunoblotting

Protein samples separated by SDS-PAGE were transferred onto an activated PVDF membrane (Millipore, Immobilon-P-Membrane, 0.45 µm pore size) at 200 mA for 10 h at 4ºC in a Western wet-transfer unit (Hoefer, TE22 Mighty Small tank transfer). The membrane was incubated in the blocking buffer for 1 h at RT with gentle shaking. The membrane was incubated with the primary antibody diluted in the antibody buffer for 2 h at RT or at 4ºC overnight. Following 6 x 5 min rinses with the washing buffer, the membrane was exposed to the HRP conjugated-secondary antibody for 1 h at RT. After washing the membrane, the HRP on the membrane was detected by an enhanced chemi-luminescence (ECL) detection system (Amersham).

Transfer buffer

25 mM Tris Base, 190 mM Glycine, 20% Methanol.

TBS

10 mM Tris-HCl, 150 mM NaCl, pH 7.5.

Blocking buffer

5% skim milk, 5% goat serum, 0.1% Tween 20 in TBS.

Antibody buffer

5% skim milk, 0.1% Tween 20 in TBS.

Washing buffer

0.1% Tween 20 in TBS.

2.6.4 Subcellular Fractionation of Rat Brains

Ten male Sprague-Dawley rats (200-250 g) were used for the preparation of subcellular fractionations by following the published methods (Huttner et al., 1983; Mizoguchi et al., 1989). The animals were anesthetized and decapitated, and then the cortices were isolated and kept in cold 0.32 M sucrose solution. All the following procedures were carried out at 0-4ºC. After homogenization with a Teflon-glass homogenizer, debris and the nuclear fraction (P1) were centrifuged at 1,400 x g for 10 min. The supernatant (S1) was next centrifuged at 13,800 x g for 15 min, and the pellet and the supernatant were collected as the crude membrane fraction (P2) and the cytosol fraction (S2). This P2 fraction was further fractionated by a centrifugation using discontinuous sucrose density gradient (0.85 M, 1.0 M, and 1.2 M sucrose layers) at 82,500 x g for 2 h. The interface between 0.32 M and 0.85 M sucrose was collected as the myelin-enriched fraction (P2A), the one between 0.85 M and 1.0 M sucrose as the ER-, Golgi-, and microsome-enriched fraction (P2B), the one between 1.0 M and 1.2 M sucrose as the synaptosome fraction (P2C), and the bottom fraction as the mitochondria-enriched fraction (P2D). The P2C fraction was resuspended in 6 mM Tris/HCl (pH8.0) and centrifuged at 32,800 x g for 20 min, and the pellet was collected as the crude synaptic membrane fraction (CSM). The supernatant was further separated by a centrifugation at 200,000 x g for 2 h, and the supernatant was collected as the synaptic soluble cytoplasm fraction (SS) and the pellet as the crude synaptic vesicle fraction (CSV). The CSM fraction was resuspended in a buffer containing 6 mM Tris/HCl (pH8.0) and 0.32 M sucrose with 0.5% Triton X-100. Following incubation on ice for 15 min, the sample was centrifuged at 32,800 x g for 20 min. The pellet fraction was collected as the postsynaptic density fraction (PSD) and the supernatant as the Triton X-100 soluble-synaptic membrane fraction (TritonX sup).

2.6.5 Purification of Recombinant GST-Fusion Proteins

To purify GST fusion proteins, GST gene fusion system (GE Healthcare Life Sciences) was employed. *E.coli* BL21DE3 was used as host strain for recombinant GST fusion protein expression.

cDNA fragments encoding partial Nedd4-1 (residues 217-549) and Nedd4-2 (residues120-601) were subcloned into pGEX-4T-1 vector, and these vectors were transformed into BL21DE3 *E.coli* by electroporation. A single colony was inoculated in 5 ml LB medium in the presence of ampicillin (LB+Amp) and cultured at 37ºC overnight. This pre-culture was transferred into 50 ml of LB+Amp medium and shaken at 37ºC to start a large culture. After approximate 3-4 h incubation, when the OD_{600} reached at 0.4-0.6, the expression of the GST fusion protein was induced by an addition of 0.1 mM isopropyl-β-D-1-thiogalactopyranoside (IPTG) to the cells. Following 4 h induction at RT, the cells were harvested by centrifugation at 4,500 x g for 20 min at 4ºC followed by a rinse with PBS. These cells were lysed by a sonication using the Macro-tip from the Labsonic U Sonifiers (Braun) (5 pulses x 10 s) in lysis A buffer. To solubilize the protein, the cells were incubated in the presence of 0.1% Triton X-100 for 20 min on ice with a gentle shake. The solubilized GST fusion protein was separated by ultracentrifugation at 100,000 x g for 30 min at 4ºC and the supernatant was collected. The GST-fusion proteins were purified by butch purification using reduced glutathione (GSH) covalently coupled to Sepharose 4B (GE Healthcare) according to the instruction supplied by the manufacturer.

A-buffer

20 mM Tris-HCl pH 7.5 at 4°C, 150 mM NaCl, 1 mM EDTA, 1 mM DTT, 1% Triton X-100, 0.2 mM PMSF, 1 µg/ml Aprotinin, 0.5 µg/ml Leupeptin.

2.6.6 Affinity Purification of GST-Nedd4-1 and -Nedd4-2 Binding Proteins

Recombinant GST-Nedd4-1 (residues 217-549) and GST-Nedd4-2 (residues 120-601) were purified, and 40 µg of these proteins were immobilized on 50 µl Glutathione-Sepharose 4B beads (GE Healthcare). After washing the beads with five bed volumes of A- buffer, a Triton X-100 extract (A-buffer) of rat brain synaptosomes (containing 80 mg protein) was loaded. Beads were washed with five bed volumes of A-buffer, and GST-Nedd4-1 and -Nedd4-2 binding proteins were eluted with B-buffer.

A-buffer

20 mM Tris-HCl pH 7.5 at 4°C, 150 mM NaCl, 1 mM EDTA, 1 mM DTT, 1% Triton X-100, 0.2 mM PMSF, 1 µg/ml Aprotinin, 0.5 µg/ml Leupeptin.

B-buffer

A-buffer with additional 40 mM Glutathione.

2.6.7 Protein identification by Mass Spectrometry

Eluted Nedd4-1 and Nedd4-2 binding proteins from affinity purification were separated under a reducing condition by SDS-PAGE on pre-cast NuPAGE 10% Bis-Tris gels (Invitrogen). A MOPS buffer system was employed as recommended by the manual. The eluate from GST beads were used as controls. After colloidal Coomassie staining of gels, gel plugs were excised manually from bands representing specifically enriched proteins indicative of putative Nedd4-1/2 binding partners. Gel plugs were subjected to an automated platform for the identification of gel-separated proteins (Jahn et al., 2006) as described previously (Reumann et al., 2007; Werner et al., 2007). An Ultraflesx MALDI-TOF-mass spectrometer (Bruker Daltonics) was used to acquire both peptide mass fingerprint and fragment ion spectra, resulting in confident protein identifications based on peptide mass and sequence information. Database searches in the NCBI non-redundant primary sequence database restricted to the taxonomy *Rat* were carried out using the Mascot Software 2.0 (Matrix Science) with parameter settings described earlier (Reumann et al., 2007; Werner et al., 2007). The minimal requirement for accepting a protein as identified was at least one peptide sequence match above homology threshold in coincidence with at least four peptide masses assigned in the peptide mass fingerprints.

2.6.8 *In Vitro* Ubiquitination Assay

Mammalian expression vectors for Myc-tagged Synaptopodin (SYNPO) were co-transfected with various EGFP-tagged E3 ligases and His_6-tagged ubiquitin expression vectors using Lipofectamine2000 (Invitrogen) in HEK293FT cells. The following E3 ligases were examined: Nedd4-1 (WT), Nedd4-1 catalytic inactive mutant, the large (+C2) and short (-C2) forms of Nedd4-2 and Nedd4-2 catalytic inactive mutant. The cells were incubated with MG132, a proteasome inhibitor, for 10 h prior to harvest, and recombinant proteins were extracted in RIPA buffer containing 20 mM NEM and 20 μM MG132. Myc-tagged proteins were immunoprecipitated using anti-myc antibody conjugated to agarose beads (SIGMA-ALDRICH). The immunoprecipitation of Myc-SYNPO was confirmed by immunoblotting using anti-myc monoclonal antibodies. Ubiquitination on Myc-SYNPO was detected by immunoblotting using an anti-ubiquitin mouse P4D1 (Santa Cruz) that recognizes mono- and polyubiquitin conjugated proteins.

RIPA buffer

50 mM Tris-HCl (pH 8.0), 150 mM NaCl, 1% NP40, 0.5% Sodium deoxycholate, 0.1% SDS, 5 mM EDTA, 0.2 μM Aprotinin, 20 μM Leupeptin, 1 mM PMSF.

2.7 Cell Culture

2.7.1 Media and Solutions

10% FCS/DMEM

500 ml DMEM, 50 ml FCS, 5 ml GlutaMAX I (Invitrogen), 5 ml Penicillin/Streptomycin (100x, Invitrogen).

Complete Neurobasal Medium

500 ml Neurobasal A, 5 ml GlutaMAX I (Invitrogen), 10 ml B-27 supplement (Invitrogen), 1 ml Penicillin/Streptomycin (100x, Invitrogen).

Solution 1

0.2 mg/ml Cystein, 1 mM CaCl2, 0.5 mM EDTA in DMEM.

Papain Solution

20-25 units of Papain per 1 ml of solution 1 were added and bubbled with carbogen (95% oxygen, 5% carbon dioxide) for 10-20 min until the solution is clear. The Papain Solution was sterilized using a 0.2 μm filter (Millipore) and kept on the ice until use.

Stop Solution

2.5 mg/ml BSA, 2.5 mg/ml trypsin inhibitor, 10% FCS in DMEM. The solution was kept at 37°C until use.

2.7.2 Coverslip Treatment for Culturing Primary Neurons

The surface of glass coverslips were coated with Poly-L-Lysine (PLL, Sigma) under a sterile condition to attain direct adhesion of cultured neurons. The cover slips were incubated in diluted PLL with PBS (1:12) at least for 3 h (usually overnight) at 37°C. The cover slips were then rinsed twice with PBS and once with HBSS, followed by an incubation in the Complete Neurobasal Medium at 37°C until use.

2.7.3 Preparation of Mouse Primary Neuron Cultures

The brains were quickly removed from newborn pups and collected in cold HBSS. Each pair of hippocampi were dissected on ice and transferred into 0.5 ml of Papain Solution and digested at 37°C for approximately 60 min with a gentle agitation. The Papain Solution was aspirated, and the tissue digestion was stopped by additional gentle incubation in 0.5 ml of the Stop Solution at 37ºC for 15-20 min. The supernatant was carefully removed and exchanged by 200 µl pre-warmed Complete Neurobasal Medium. The tissue were gently triturated 10-20 times using a plastic pipette tip with P-200 Pipetman and 150 µl of cell-suspension-supernatant was transferred in 1 ml of pre-warmed Complete Neurobasal Medium. This trituration process could be repeated 2 to 3 times to increase the yield of the neuron preparation, if necessary. Cells were counted using the Naubauer Counting Chamber (4 x 4 grid x 1000 cells/ml) and approximately 60,000-120,000 cells per well were plated in 24 well plates. The medium was exchanged after the attachment of the neurons onto the coverslips, and the neurons were cultured at 37ºC in a 5% CO_2 incubator.

2.7.4 HEK 293FT Cell Line

Human embryonic kidney (HEK) 293FT cells were used for *in vitro* ubiquitination assay and the preparation of lentivirus. HEK293FT cells were maintained in tissue culture dishes with 10% FCS/DMEM at 37ºC in a 5% CO_2 incubator.

2.7.5 Transfection for HEK 293FT Cells

Transfection using Lipofectamine2000 (Invitrogen) was performed for *in vitro* ubiquitination assay and lentivirus preparation. The manual provided from Invitrogen was referred to for all procedures. The HEK293 cells were maintained at 50-80% confluence at the time of transfection in an antibiotic free DMEM medium. The plasmid mixture was first diluted in DMEM and kept at RT. Separately, Lipofctamine2000 was diluted in DMEM and mixed gently, and kept at RT for 5 min. These mixtures were combined gently and then incubated at least for 20 min at RT. After incubation, the mixture was applied to the culture cells and mixed well. The cells were returned to the incubator for 24 to 48 h to allow for recovery and protein expression.

2.7.6 Lentivirus Preparation

For lentivirus preparation, a packaging plasmid (PACK) and an envelope plasmid (ENV) were co-transfected with the vector plasmid (pFUGW or pFUGW-iCre) in HEK293FT cells. The next day after transfection, 10 mM butylate was added in the medium, and the lentivirus containing-culture medium was harvested after an incubation for 48 h. The medium was roughly cleared using 0.45 μm filter (Millipore) then concentrated through Amicon filter system (Millipore) combined with a repetitive centrifugation at 4,600 x g at 4ºC. Following a rinse with pre-cold Neurobasal A, the concentrated virus containing medium was dialyzed with cold TBS (pH7.5) for overnight at 4ºC. Small aliquots of the final production were stored at -80ºC until use. The viral production was added in the medium of primary culture neurons at DIV1-3. The viral titer was visually estimated by the expression level of EFGP in the neurons.

2.8 Golgi Staining

To visualize the entire morphology of single neurons *in vivo*, the traditional Golgi staining was carried out using FD Rapid GolgiStain^{TM} Kit (MTR Scientific). The whole brains were carefully removed and rinsed with PB, then immersed in the mixture of Solution A and B for 5-6 days in the dark. The samples were next transferred in Solution C and kept for 2-7 days in the dark. Then they were quickly frozen at -40ºC, and the coronal sections (100-200 μm thickness) were cut using a cryotome. The sections were dried in a dark cold room for a few weeks at the longest. After a rinse with ddH_2O, the staining was developed by incubating in the mixture of Solution D and E appropriately for 10 min in the dark. The water-rinsed samples were gradually dehydrated through 50%, 75%, 95%, and finally absolute 100% ethanol then cleared in xylene under a hood. The sections were mounted with Entellan-Neu (Merk). The sample images were acquired using an epifluorescence microscope (Olympus BX-61).

2.9 Electrophysiology

Male mice at the age of postnatal day (P) 21-34 were used for all electrophysiological experiments.

2.9.1 Extracellular Recording

2.9.1.1 Solutions and Media

5x Stock Slicing Solution

1150 mM Sucrose, 130 mM $NaHCO_3$, 10 mM KCl, 5mM KH_2PO_4, 5m M $MgCl_2$, 50 mM Glucose in ddH_2O. After bubbling with 95% O_2/5% CO_2 (carbogen), the stock solution was sterilized using a 0.22 μm filter and stored at 4°C.

Slicing Solution

To prepare 1x slicing solution, 1M $CaCl_2$ was added for a final concentration of 2 mM. After bubbling with carbogen, the solution was frozen, and the ice was finely crushed. The mixed-ice solution was again bubbled with carbogen and chilled on ice until use.

10x Artificial Cerebrospinal Fluid (ACSF)

1200 mM NaCl, 260 mM $NaHCO_3$,, 20 mM KCl, 10 mM KH_2PO_4, and 100 mM Glucose in ddH_2O. After bubbling with carbogen, the stock solution was sterilized using a 0.22 μm filter and stored at 4°C.

ACSF

To prepare 1x ACSF, 1 M $CaCl_2$ and $MgCl_2$ were added to final concentrations of 2 mM. The solution was bubbled with carbogen until use.

2.9.1.2 Acute Slice Preparation

The whole brain was quickly and carefully removed from the skull and immediately transferred in the ice-cold slicing solution, and the hippocampi were isolated carefully. Transverse hippocampal slices (400-450 μm) were cut using a tissue chopper (McILWAIN). The slices were immediately transferred and recovered in a submerged chamber filled with carbogen supplied ACSF for 30 min at 30ºC. After the recovery, the slices were kept at RT for at least 30 min before recording.

2.9.1.3 Extracellular Field Recording

The acute slice was transferred and maintained in a submerged recording chamber (HARVARD apparatus, 64-1525) perfused with carbogen-supplied ACSF containing 100 μM picrotoxin (PTX) and maintained at 25ºC. Electric stimulations on the SC afferents were delivered using a concentric metal bipolar electrode (FHC Inc.) with a 100 μs duration time. The recording electrode (2-3 MΩ) was prepared using a pipette puller (Sutter Instrument), filled with 3M NaCl, and positioned in the stratum radiatum of the CA1 area (Fig. 1-2A). The recordings were performed using a Multiclamp 700B amplifier and a Digidata 1440A (Axon Instruments). For the analysis, the data were analized using Clampfit (Molecular devices) and the statistics

were carried out using KaleidaGraph (Synergy Software). Slopes of field excitatory postsynaptic potentials (fEPSPs) were measured at the initial linear parts of fEPSP (0.5 ms duration), and amplitudes of fiber volley (FV) were measured at the negative peaks of FV.

Paired Pulse Ratio (PPR)

The stimulation intensity was adjusted so as to yield around 1 mV of fEPSP response. Pairs of stimuli were applied with varying interpulse intervals between 25-1000 ms (25, 50, 100, 250, 500, and 1000 ms). The ratio of the second response to the first response was analyzed. Four repetitive trials were averaged for each point per slice.

Synaptic Plasticity

The stimulation intensity was adjusted so as to yield 50% or 30% of the max response for LTD or LTP, respectively. After establishing a stable baseline recording at least for 20 min, LTD or LTP was induced. To induce LTD, a low frequency stimulation (LFS), 900 pulses at 1 Hz was delivered. To induce early phase-LTP (E-LTP), a single train of high frequency stimulation (HFS) consisted of 100 pulses at 100 Hz was delivered. As an induction of relatively strong LTP, three trains of HFSs spaced 20 s apart were applied. The fEPSP was continuously monitored every 30 s during the recoding. If fEPSP after LTP induction declined lower than baseline level, the recording was discarded.

2.9.2 Whole-cell Voltage Clamp Recording

2.9.2.1 Solutions and Media

Slicing Solution

188 mM Sucrose, 26 mM $NaHCO_3$, 1.9 mM KCl, 1.2 mM NaH_2PO_4, 10 mM $MgSO_4$, 25 mM Glucose in ddH_2O. After the preparation, the solution was immediately bubbled with carbogen for more than 10 min and frozen. The ice was finely crushed and bubbled again with a carbogen. The ice-mixed solution was chilled on ice till use.

ACSF

124 mM NaCl, 25 mM $NaHCO_3$, 2.4 mM KCl, 1.0 mM NaH_2PO_4, 4 mM $MgCl_2$, 10 mM Glucose in ddH_2O (pH 7.4, 300 mOsm). 1M $CaCl_2$ was lastly added to a final concentration of 4 mM. Then the solution was immediately bubbled with a carbogen and kept in the dark until use.

Intracellular Solution

117.5 mM $MeSOH_3H$, 10 mM HEPES, 17.75 mM CsCl, 10 mM TEA-Cl, 0.25 mM EGTA, 10 mM Glucose, 2 mM $MgCl_2$, 4 mM Na_2ATP, 0.3 mM NaGTP in ddH_2O (adjusted pH to 7.2 with CsOH, osmolarity to 290 mOsm with CsCl). The solution was chilled on ice before and after the addition of NaGTP and Na_2ATP. For AMPA/NMDA ratio measurement, 3 mM QX314-Cl (Tocris) was added in the intracellular solution. After the preparation, the solution was filtrated using a 0.2 μm filter and stored in -80ºC. The solution was filtered again using a 0.2 μm filter just before use.

2.9.2.2 Acute Slice Preparation

The animal was anesthetized with Isofluran (DeltaSelect) and subsequently decapitated following a negative response to the pinch test. The whole brain was quickly and carefully removed from the brain skull and immediately transferred into the ice-cold slicing solution. The brain was trimmed and transverse sections (400 μm) were cut using a vibratome (Leica VT1200S). The slices were immediately transferred and recovered in a submerged chamber filled with carbogen supplied ACSF for 30 min at 30ºC. After the recovery, the slices were kept at RT for at least 60 min before recording.

2.9.2.3 Whole-Cell Voltage Clamp Recording

The acute slice was transferred and weighed down with a U-shaped platinum wire across which nylon threads are strung. The recordings were performed in a submerged recording chamber perfused with carbogen-supplied ACSF containing 100 μM PTX and maintained at 30ºC. The recording pipettes (2.8-4 MΩ) were prepared using a pipette puller (Sutter Instrument) and filled with the intracellular solution. Single CA1 pyramidal neurons were identified by infrared-differential interference contrast with a high-magnification water immersion objective (Zeiss w-plan-Apochromat 63x/1.0 M27), and whole-cell voltage clamp recordings were performed. The series resistance (SR) and the input resistance (IR) were simultaneously monitored during recording by 5 mV of a hyperpolarizing step pulse. The SR and the IR were kept less than 20 MΩ and more than 100 MΩ, respectively. All recordings were performed using ELC-03XS (npi) and DIZITYZER, and the signals were filtered at 3k Hz and gain of 10. The data acquisition and analysis were carried out using Igor Pro (WaveMetrics Inc.), Mini Analysis software (Synaptosoft Inc.), and KaleidaGraph (Synergy Software).

<u>mEPSC</u>

mEPSC was recorded at the holding potential of -60mV in the presence of 0.5 μM TTX, and the SR and the IR were monitored every 10 s during the recording.

AMPAR/NMDAR Ratio

The Schaffer collateral (SC) afferents were stimulated with theta glass pipette filled with ACSF and the stimulation intensity was adjusted so as to obtain 100-200 pA of EPSCs at the holding potential of –70 mV. AMPAR- and NMDAR-mediated currents were determined based on their distinctive channel properties, kinetics, and voltage dependencies; an AMPAR-mediated current was measured as the peak current of EPSC at -70 mV, while an NMDAR-mediated current was measured as the EPSC current at 50 ms after the stimulation at +40 mV.

3 Results

3.1 Nedd4-1 and Nedd4-2 are Neural E3 Ubiquitin Ligases Localized at the Synapse

Nedd4-1 was originally identified in a screen for cDNA clones whose expression levels are developmentally downregulated in mouse neural precursor cells (Kumar et al., 1992), and a subsequent study identified its close homolog Nedd4-2 (Kamynina et al., 2001). To determine which brain regions to focus on for functional analyses of these E3 ligases, I first studied the expression patterns of Nedd4-1 and Nedd4-2.

To explore the expression patterns of Nedd4-1 and Nedd4-2 mRNA, *in situ* hybridization was carried out. Nedd4-1 and Nedd4-2 mRNAs were detected using a radioactive and DIG-labeled anti-sense RNA probes, respectively. Nedd4-1 mRNA expression was relatively limited to the hippocampus, the olfactory bulb, the hypothalamus, the cortex, and the cerebellar granular cell layer (Fig. 3-1Aa). Nedd4-2 mRNA expression was detected in the granule cells and the pyramidal neurons of the hippocampus and in the granule cells and the Purkinje cells of the cerebellum (Fig. 3-1Ab).

Next, the distribution patterns of Nedd4-1 and Nedd4-2 proteins in adult rat brains were examined biochemically. Homogenates of several brain regions, including cerebellum, brain stem, olfactory bulb, striatum, hippocampus, cerebral cortex, and basal brain, were subjected to SDS-PAGE and immunoblotting with anti-Nedd4-1 and anti-Nedd4-2 antibodies (Fig. 3-1B). The fidelity of the sample preparation was verified by the distribution pattern of synaptopodin (SYNPO), which had previously been reported to be expressed in olfactory bulb, striatum, hippocampus, and cortex (Mundel et al., 1997). Nedd4-1 was detected in all tested brain regions at similar expression levels, while the doublet signal of Nedd4-2 was more prominent in cerebellum, striatum, hippocampus, and cerebral cortex than in the other regions. It was reported that two Nedd4-2 splicing variants with or without the N-terminal C2-domain are expressed in the kidney and the adrenal gland (Dunn et al., 2002). The anti-Nedd4-2 antibody used in this study detects a part of the WW domain containing sequence, which is present in both variants. Based on their molecular weights, I concluded that the short and long proteins detected by the anti-Nedd4-2 antibody correspond to variants with and without the N-terminal C2 domain.

Interestingly, the expression ratios of these variants were variable among the brain regions tested. The variant with C2 domain was highly expressed in cerebellum and cortex while the short variant without the C2 domain was dominant in the striatum. One of the closest homologs of Nedd4-2, Smurf2, forms an intramolecular fold via its N-terminal C2 and C-terminal HECT domains in the absence of Ca^{2+}, exerting an autoinhibition of the catalytic activity of this ligase (Wiesner et al., 2007). Thus, Nedd4-2 may operate differently depending on the brain regions.

I next examined the developmental expression profiles of Nedd4-1 and Nedd4-2 proteins (Fig. 3-1C). For this purpose, a series of homogenates of hippocampi and cortices were prepared from embryonic, neonatal, and adult mice. Although protein levels of the two ligases were developmentally down regulated, substantial levels of these ligases were still expressed in the adult mouse brain, indicating that Nedd4-1 and Nedd4-2 may play roles in the adult as well as in the developing brain.

To determine if Nedd4-1 and Nedd4-2 are localized at synapses, rat cortices were fractionated biochemically, and equal amounts of each subcellular fraction were subjected to SDS-PAGE and immunoblotting (Fig. 3-1D). The fidelity of the subcellular fractionation was verified by antibodies for marker proteins [synaptophysin for the crude synaptic vesicle fraction (CSV); post-synaptic density 95 (PSD95) for the postsynaptic density fraction (PSD)]. Although Nedd4-1 displayed a relatively broad subcellular distribution, Nedd4-1 and Nedd4-2 were enriched in the PSD fraction as well as the ER and Golgi complex fraction (P2B), the synaptosome fraction (P2C), and the synaptosomal soluble fraction (SS). Partial enrichment of Nedd4-1 and Nedd4-2 in synaptic fractions may indicate functional roles in the regulation of synaptic function.

To further study the distribution patterns in the adult brain and the neural subcellular localizations of Nedd4-1 and Nedd4-2 proteins, immunostaining using sections from adult mouse brains and primary cultured neurons was performed. However, the all antibodies tested showed indistingusishable staining patterns and levels between control and *Nedd4-1* and *Nedd4-2* lacking samples, indicating that staining signals are not specific for Nedd4-1 and Nedd4-2.

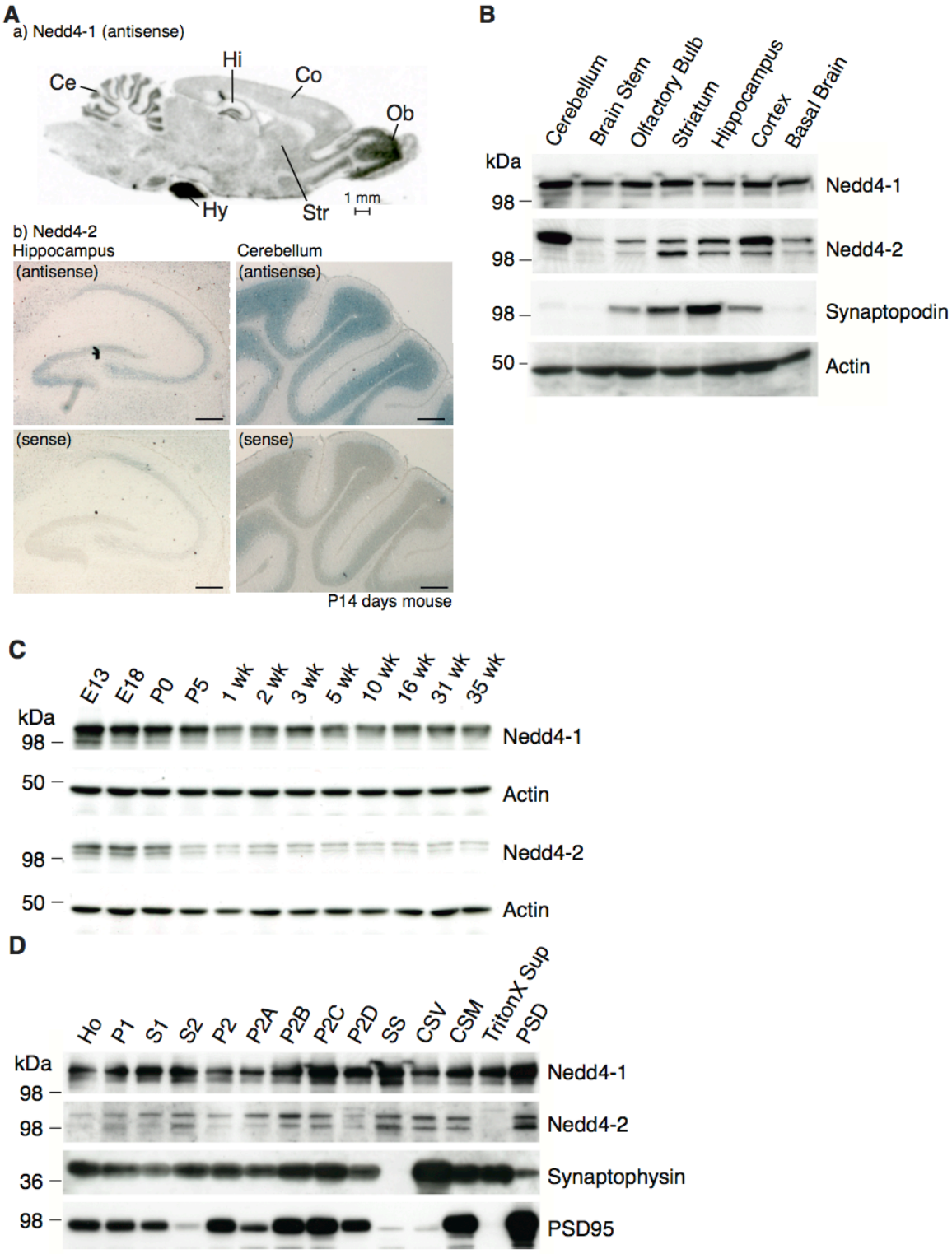

Figure 3-1 Nedd4-1 and Nedd4-2 are expressed in the adult rodent brain

(A) *In situ* hybridization analysis of *Nedd4-1* and *Nedd4-2* mRNA. Nedd4-1 and Nedd4-2 transcripts are expressed in the hippocampus and cerebellum. a) Nedd4-1 mRNA was detected with an [^{35}S] dATPαS-labled RNA probe in the adult rat brain. Scale bar, 1 mm. Ce, cerebellum; Co, cerebral cortex; Hi, hippocampus; Hy, hypophysis; Ob, olfactory bulb; Str, striatum. This result was contributed by Dr. Antje Neeb. b) Nedd4-2 mRNA was detected with a digoxigenin (DIG)-labeled *anti-sense* RNA probe in the mouse hippocampus (left

upper panel) and cerebellum (right upper panel) at the age of postnatal day 14. No signals were detected with the DIG-labeled *sense* RNA probe (lower panels). Scale bar, 300 μm.
(B) Distribution patterns of Nedd4-1 and Nedd4-2 proteins in the indicated regions of adult rat brain. 7.5 μg of homogenates were separated on SDS-PAGE gels followed by immunoblotting using the indicated antibodies. The anti-synaptopodin antibody was used to verify the fidelity of the sample preparation and actin was detected as a loading control.
(C) Developmental expression profiles of Nedd4-1 and Nedd4-2 proteins. 7.5 μg of homogenates prepared from mouse cortices at the indicated ages were subjected to SDS-PAGE and immunoblotting using anti-Nedd4-1 and anti-Nedd4-2 antibodies. E13, embryonic day 13; E18, embryonic day 18; P0, postnatal day 0; P5, postnatal day 5; 1 wk, postnatal week 1; 2 wk, postnatal week 2; 3 wk, postnatal week 3; 5 wk, postnatal week 5; 10 wk, postnatal week 10; 16 wk, postnatal week 16; 31 wk, postnatal week 31; 35 wk, postnatal week 35.
(D) Subcellular distribution of Nedd4-1 and Nedd4-2 proteins. Adult rat brain homogenates were subjected to subcellular fractionation, and 10 μg of protein from each fraction was analyzed by SDS-PAGE and immunoblotting using the indicated antibodies. Ho, homogenate; P1, debris and nuclear fraction; S1, supernatant of Ho excluding P1; S2, cytosol fraction; P2, crude membrane fraction; P2A, myelin-enriched fraction; P2B, ER- Golgi- and microsome-enriched fraction; P2C, synaptosome fraction; P2D, mitochondria-enriched fraction; SS, synaptic soluble cytoplasm fraction; CSV, crude synaptic vesicle fraction; CSM, crude synaptic membrane fraction; TritonX sup, Triton X-100 soluble- synaptic membrane fraction; PSD, post synaptic density (PSD) fraction.

3.2 Generation of Excitatory Neuron Specific Conditional *Nedd4-1* and *Nedd4-2* Double Knockout Mouse Lines

To investigate the functions of Nedd4-1 and Nedd4-2 in mammalian neurons *in vivo*, we generated mutant mouse lines for Nedd4-1 and Nedd4-2. It has been reported that *Nedd4-1* deficient mice exhibit severe growth retardation during embryogenesis and die during late gestation probably because of impaired vasculogenesis or angiogenesis (Kawabe et al., 2010). Mice with a null allele of *Nedd4-2* die perinatally due to increased expression and activity of epithelial sodium channel (ENaC) in the lung, leading to a failure to inflate the lung (Boase et al., 2011). Among the reported knockout (KO) mice lacking E3 ubiquitin ligases (Bloom et al., 2007; Jiang et al., 1998; Lotz et al., 2004; Luna et al., 1995; Yamashita et al., 2005; Yao et al., 2007), the phenotypes of *Nedd4-1* and *Nedd4-2* KO mice are at the most severe levels, indicating that these E3 ligases play critical roles in cellular functions. Nedd4-1 and Nedd4-2 are highly homologous at the amino acid level and are expressed in the same population of cortical neurons (Fig. 3-1B), indicating that loss of function of one isoform might be partially compensated by the other. Considering the lethal phenotypes of *Nedd4-1* and *Nedd4-2* conventional KO mice,

we generated excitatory neuron specific conditional *Nedd4-1* and *Nedd4-2* double KO mouse using the Cre/loxP recombination system.

The Cre/loxP recombination system is a genetic method to control deletion or activation of a target gene in a spatially and temporally restricted manner. The Cre recombinase catalyzes loxP site-specific recombination by cleaving and removing one of the two pairs of genomic DNA strands. Therefore, it is required to cross two mouse lines to operate this system; an established flox mouse line carrying a pair of loxP cassettes flanking exon(s) of a target gene and a Cre driver line carrying the Cre expression cassette under the control of a certain promoter (e.g. CaMKII, GFAP, or Thy-I promoters).

My host lab designed the gene targeting strategy of Nedd4-1 and Nedd4-2 flox alleles. The exon 9 of *Nedd4-1* encoding amino acid (aa) 194-227 and the exon 15 of *Nedd4-2* encoding aa 492-568 were flanked by pairs of loxP sites (Figs. 3-2A and B). After confirming homologous recombination by Southern blotting (Figs. 3-2C and F), the mice were genotyped by PCR analyses routinely (Figs. 3-2D and G). Immunoblotting using anti-Nedd4-1 and -Nedd4-2 antibodies verified elimination of Nedd4-1 and Nedd4-2 proteins in primary cultured neurons prepared from Nedd4-$1^{flox/flox}$ and Nedd4-$2^{flox/flox}$ mice upon overexpression of Cre recombinase by lentiviral infection (Figs. 3-2E and H). To establish excitatory neuron-specific *Nedd4-1* and *Nedd4-2* conditional double KO (Nedd4 cDKO) mice, Nedd4-1 and Nedd4-2 flox mice (Nedd4-$1^{flox/+}$; Nedd4-$2^{flox/+}$) were crossed with the NEX-Cre mouse. This Cre driver mouse expresses Cre recombinase from embryonic day 11.5 in dorsal telencephalic postmitotic neurons, including the pyramidal neurons, the dentate gyrus mossy and granule cells, but not in the proliferating neural precursors of the ventricular zone, in the interneurons, or in the glial cells (Fig. 3-2I) (Goebbels et al., 2006). Nedd4 cDKO mice (NEX-Cre; Nedd4-$1^{flox/flox}$; Nedd4-$2^{flox/flox}$) were viable and fertile, and were indistinguishable from control littermates (Nedd4-$1^{flox/flox}$; Nedd4-$2^{flox/flox}$) in the cage environment. Immunoblotting analyses confirmed a marked reduction of Nedd4-1 and Nedd4-2 proteins in crude hippocampal homogenates prepared from the Nedd4 cDKO mouse at 3 weeks of age (Fig. 3-2J). Trace expression of these proteins likely results from expression in inhibitory neurons and/or in glial cells. In the present study, I analyzed the Nedd4 cDKO mouse to investigate functions of Nedd4-1 and Nedd4-2 in mature neurons.

In addition to the Nedd4 cDKO mouse, tamoxifen-inducible *Nedd4-1* and *Nedd4-2* double KO mice were established using *NEX-CreERT2* mouse line that carries *CreERT2* in the *Nex1* locus (Agarwal et. al., 2011). *CreERT2* encodes a Cre recombinase fused to human estradiol receptor ligand binding domain (ERT2) that is mutated in order to bind to exogenous tamoxifen with high affinity, but not to endogenous estradiol. Binding of tamoxifen to ERT2 causes translocation of CreERT2 to the nucleus where the Cre recombinase excises the exon flanked by the two loxP cassettes in the genomic DNA. Nedd4 cDKO mice were crossed with NEX-CreERT2 mice to obtain NEX-CreERT2; Nedd4-1$^{flox/flox}$; Nedd4-2$^{flox/flox}$ (tamoxifen-inducible Nedd4 cDKO), NEX-Cre; Nedd4-1$^{flox/flox}$; Nedd4-2$^{flox/flox}$, and Nedd4-1$^{flox/flox}$; Nedd4-2$^{flox/flox}$ littermates. As shown in Fig. 3-2K, tamoxifen was injected to all littermates at a dose of 80 mg/kg body weight for 10 consecutive days from P11 onwards, and the hippocampi were sampled at P25. Immunoblotting analyses showed a reduced expression level of Nedd4-1 and Nedd4-2 proteins in tamoxifen-induced Nedd4 cDKO (NEX-CreERT2; Nedd4-1$^{flox/flox}$; Nedd4-2$^{flox/flox}$) mice comparable to those in Nedd4 cDKO mice (Fig. 3-2L). This result together with previously published papers (Goebbels et al., 2006)(Agarwal et. al., 2011) indicates that the Nex-1 promoter is active in the early postnatal hippocampus and that Nedd4-1 and Nedd4-2 are dominantly expressed in glutamatergic neurons in the hippocampus.

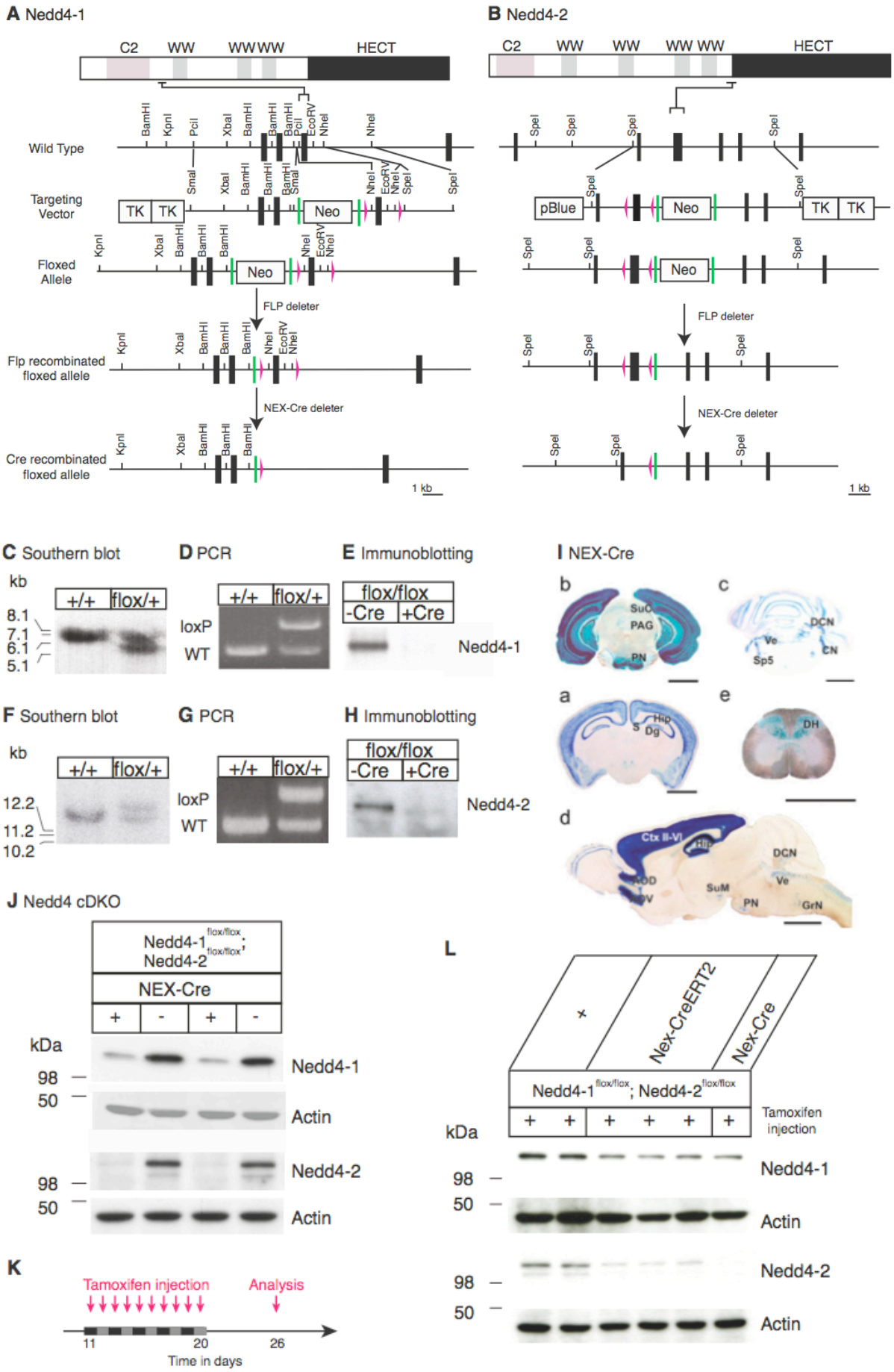
A Nedd4-1
C2
WW
WW WW
HECT
Wild Type
Targeting Vector
TK
TK
Neo
Floxed Allele
FLP deleter
Flp recombinated floxed allele
NEX-Cre deleter
Cre recombinated floxed allele
1 kb
B Nedd4-2
pBlue
C Southern blot
kb
+/+
flox/+
8.1
7.1
6.1
5.1
D PCR
loxP
WT
E Immunoblotting
flox/flox
-Cre
+Cre
Nedd4-1
I NEX-Cre
F Southern blot
12.2
11.2
10.2
G PCR
H Immunoblotting
Nedd4-2
J Nedd4 cDKO
Nedd4-1flox/flox; Nedd4-2flox/flox
NEX-Cre
kDa
98
50
Actin
K
Tamoxifen injection
Analysis
11
20
26
Time in days
L
Nex-CreERT2
Nex-Cre
Tamoxifen injection

Figure 3-2 Generation of *Nedd4-1* and *Nedd4-2* conditional knockout mice

(A and B) Targeting strategies for *Nedd4-1* (A) and *Nedd4-2* (B). The domain structures of Nedd4-1 and Nedd4-2 (top schemes), structures of the wild type *Nedd4-1* and *Nedd4-2* alleles (Wild Type), Nedd4-1^{flox} and Nedd4-2^{flox} targeting vectors (Targeting Vector), and floxed mutant alleles of *Nedd4-1* and *Nedd4-2* (Floxed Allele). Exons are indicated as black boxes. Flip recombinase targets (FRT) and loxP sites are indicated as green boxes and red triangles, respectively. The exon 9 of *Nedd4-1* and the exon 15 of *Nedd4-2* were floxed. Following homologous recombination and germline transmission of the mutant alleles, floxed mice were crossed with FLP deleter mice and subsequently with NEX-Cre mice. pBlue, pBluescript; Neo, neomycin resistance cassette; TK, herpes simplex virus thymidine kinase expression cassette.
(C and F) Southern blot analyses of genomic DNA prepared from targeted embryonic stem cells. The genomic DNA was digested with PvuII for *Nedd4-1* and with BamHI for *Nedd4-2*, and digested fragments were detected by the specific probes. (C) The 7.4 kb and the 6.3 kb bands report the wild type (WT) and Nedd4-1 floxed alleles, respectively. +/+, WT; flox/+, heterozygous Nedd4-1$^{flox/+}$. (F) The 15 kb and the 17 kb bands report the WT and Nedd4-2 floxed alleles, respectively. +/+, WT; flox/+, heterozygous Nedd4-2$^{flox/+}$.
(D and G) PCR analyses of genomic DNA prepared from WT (+/+) and heterozygous Nedd4-1 flox (flox/+) mice (D) or from WT (+/+) and heterozygous Nedd4-2 flox (flox/+) mice (G).
(E and H) Nedd4-1 and Nedd4-2 proteins were eliminated in the presence of Cre recombinase. Hippocampal cultured neurons were prepared from homozygous Nedd4-1$^{flox/flox}$ (E) and Nedd4-2$^{flox/flox}$ (H) pups and infected with lentivirus to overexpress EGFP together with Cre recombinase (+Cre) or EGFP alone (-Cre). The cell lysates were analyzed by immunoblotting using anti-Nedd4-1 and anti-Nedd4-2 antibodies.
(I) LacZ reporter gene expression in NEX-Cre; R26R (b and c) and NEX-Cre; floxLacZ (a, d and e) adult mice (modified from Goebbels et. al., 2006). Activities of Cre-mediated recombination was detected by X-gal staining in the olfactory bulb, the amygdala, the hippocampus, and the neocortex.
(J) Immunoblotting analyses of Nedd4 cDKO and control hippocampi. The crude homogenates were prepared from Nedd4 cDKO (NEX-Cre; Nedd4-1$^{flox/flox}$; Nedd4-2$^{flox/flox}$) and control (Nedd4-1$^{flox/flox}$; Nedd4-2$^{flox/flox}$) mice at 3 weeks of age and analyzed by SDS-PAGE and immunoblotting using the indicated antibodies. Note the massive reduction of Nedd4-1 and Nedd4-2 protein levels in Nedd4 cDKO hippocampi.
(K and L) Establishment of tamoxifen-inducible Nedd4 cDKO mice. (K) The outline of treatment protocols for tamoxifen applications. (L) NEX-CreERT2; Nedd4-1$^{flox/flox}$; Nedd4-2$^{flox/flox}$, NEX-Cre; Nedd4-1$^{flox/flox}$; Nedd4-2$^{flox/flox}$, and Nedd4-1$^{flox/flox}$; Nedd4-2$^{flox/flox}$ mice were intraperitoneally injected with tamoxifen for 10 consecutive days at a dose of 80 mg/kg body weight. The crude hippocampal homogenates were prepared at 6 days after the last injection and analyzed by immunoblotting using the indicated antibodies.

3.3 Neuronal loss of *Nedd4-1* and *Nedd4-2* Causes Morphological Defects in the Mature Brain *in vivo*

In a previous study, we showed that Nedd4-1 is a critical positive regulator of neurite development and arborization in developing rodent neurons *in vitro* and *in vivo* and that Nedd4-1 monoubiquitinates Rap2 to inhibit Rap2-dependent TNIK activation that leads to slow-down of dendritic growth (Kawabe et al., 2010). As shown in Figs. 1-5, postmitotic-neuron specific inactivation of *Nedd4-1* resulted in

reduced thickness of the cerebral cortex and in impaired neurite arborization in the mature brain.

In order to study the effects of deletions of *Nedd4-1* and its closest homolog *Nedd4-2* on glutamatergic neurons, I analysed the gross brain morphology of the Nedd4 cDKO mice at P21. The Nedd4 cDKO mouse displayed a reduced size of the cerebral cortex (Fig. 3-3A), accompanied by a reduction in the thickness of the cerebral cortex (data not shown). In the next set of experiments, I examined the morphology of individual Golgi-impregnated neurons in the hippocampal CA1 region. As shown in Fig. 3-3B, the arborization of individual apical dendrites was reduced in the Nedd4 cDKO mouse, resembling the Nedd4-1 cKO mouse (Fig. 1-5C). Furthermore, the impact of the loss of *Nedd4-1* and *Nedd4-2* on the cytoarchitecture at the synaptic level was examined by quantifying the spine density at secondary branches of proximal apical dendrites (Fig. 3-3C). As shown in Fig. 3-3D, the spine density was indistinguishable between Nedd4 cDKO and control mice (Fig. 3-3D; control, 0.97 ± 0.09 µm, n=16, N=2; cDKO, 0.96 ± 0.07 µm, n=20, N=2; Student's *t*-test, p=0.887), indicating that the total spine number of an individual CA1 neuron of the Nedd4 cDKO mouse is reduced because of the reduced complexity of dendrites.

Given that Nedd4-2 also has the potential to interact with TNIK (data not shown), Nedd4-2 may be also involved in the Nedd4-1-dependent pathway that promotes the development of dendrites by inactivating Rap2 and TNIK in immature neurons. Nedd4-1 and Nedd4-2 do not regulate spine density, although it remains unclear if these enzymes regulate the volume or the length of spines. It would be also interesting to address whether and how Nedd4-1 and Nedd4-2 maintain dendritic morphology and impact the size of certain brain regions in the mature brain.

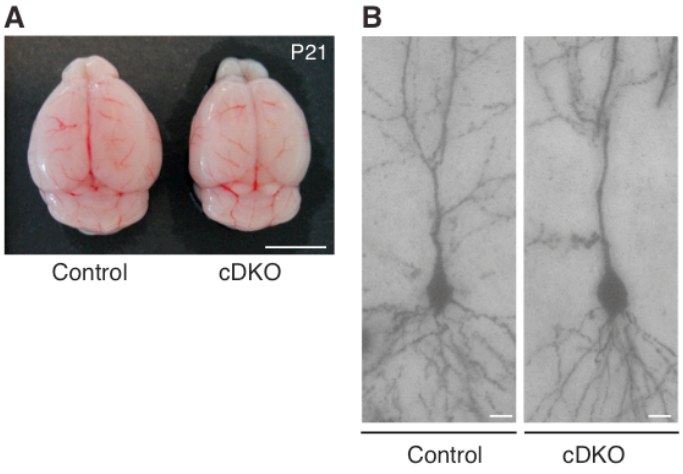

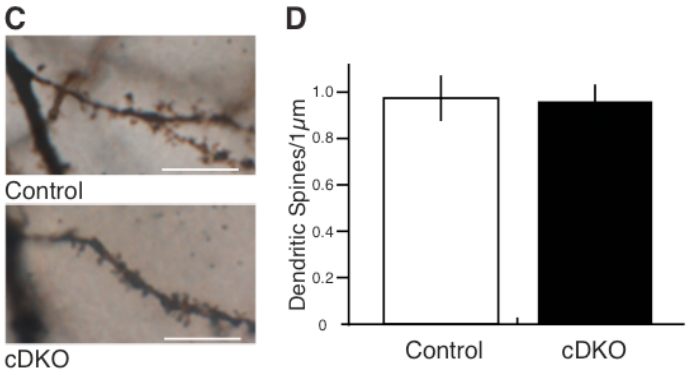

Figure 3-3 Simultaneous inactivation of *Nedd4-1* and *Nedd4-2* leads to defective dendrite development *in vivo*

(A) Nedd4 cDKO mice (right) display a smaller cerebrum than control mice (left) at P21. Note that the size of the cerebellum is comparable between the two genotypes. Scale bars, 5 mm.
(B) Apical dendrites of Golgi-impregnated CA1 pyramidal neurons. The left panel shows a control neuron; the right panel shows a Nedd4 cDKO neuron. Scale bars, 10 μm.
(C) High-power images of spines at secondary branches of apical dendrites. The upper panel shows a control neuron; the lower panel shows a Nedd4 cDKO neuron. Scale bars, 10 μm.
(D) Quantification of spine densities at secondary branches of apical dendrites. Control and Nedd4 cDKO mice displayed similar spine densities per μm dendrite (control, 0.9747 ± 0.0932, n=16, N=2; cDKO, 0.9587 ± 0.0666, n=20, N=2; Student's *t*-test, p=0.887).

3.4 Nedd4-1 and Nedd4-2 are Required for LTP, but Not for Basal Synaptic Transmission and LTD

In my analysis of the role of Nedd4-1 and Nedd4-2 in adult neurons, I focused on the electrophysiological consequences of *Nedd4-1* and *Nedd4-2* loss-of-function mutations in glutamatergic neurons using hippocampal acute slices.

The hippocampus has been studied extensively as a model system for synaptic plasticity because of its key role in learning and memory formation (Milner et al., 2004). The major signal flow through the hippocampus is relayed via a "trisynaptic loop" that is made up from three groups of neurons; the granule cells, the CA3 pyramidal neurons, and the CA1 pyramidal neurons (Fig. 1-2A). The granule cells in the DG project their axons to the CA3 neurons. In turn, the CA3 neurons excite the CA1 neurons through the Schaffer collateral (SC) axons, forming SC-CA1 synapses (Fig. 1-2A). These SC-CA1 synapses were analyzed in the present study. I applied an electric stimulation to the SC afferents and measured excitatory postsynaptic currents (EPSC) or field excitatory postsynaptic potential (fEPSP) of the CA1 pyramidal neurons (Fig. 1-2A). In order to avoid interference by inhibitory postsynaptic

potentials (IPSP), all recordings were performed in the presence of 100 μM picrotoxin (PTX).

3.4.1 Basal Synaptic Transmission is not Affected in the Nedd4 cDKO Mouse

I first characterized basal synaptic transmission in the Nedd4 cDKO mice. An action potential propagating along the axon of a presynaptic neuron triggers an influx of calcium at the presynaptic terminal. Such transient elevation of the calcium concentration is essential for synchronous release of neurotransmitters. On the other hand, spontaneous release occurs at all synapses in an action potential independent manner, but requires an elevation of calcium (Xu et al., 2009a). Released neurotransmitters are in turn received by glutamate receptors in the postsynapses leading to depolarization. Basal synaptic transmission can be affected by alterations in the number of functional synapses, the release probability, and the number and function of postsynaptic receptors. Functional synaptic connectivity, characterized by the correlation between the transmitter release and the postsynaptic response, was examined under basal conditions using two distinct measurements, miniature excitatory postsynaptic currents (mEPSCs) and input/output relationships.

3.4.1.1 mEPSC

mEPSCs are small electrical signals excited by the spontaneous release of neurotransmitters from a single synaptic vesicle. mEPSC frequency is generally affected by the number of functional synapses and the release probability, while mEPSC amplitude is generally affected by the quantal size of presynaptic vesicles and the number and functional properties of glutamate receptors in the postsynapse.

Our previous study showed that mEPSC frequency is significantly reduced in developing autaptic cultured neurons lacking *Nedd4-1*, due to a reduced number of synapses caused by impaired dendritic development (Kawabe and Brose, 2010). On the other hand, an independent study showed that mEPSC amplitudes are reduced in Nedd4-1 overexpressing neurons owing to enhanced endocytosis of GluR1 (Schwarz et al., 2010). To gain a deeper insight into the roles of Nedd4-1 and Nedd4-2 in basal synaptic transmission, I sought to determine whether Nedd4-1 and Nedd4-2 affect mEPSCs in more physiological condition using hippocampal acute slices.

Whole-cell patch clamp recording was performed to measure mEPSCs in CA1 pyramidal neurons. mEPSCs were recorded at -60 mV, a holding potential near the resting membrane potential of neurons, in ACSF (4 mM Ca^{2+}, 4 mM Mg^{2+}). TTX (0.5

μM) was applied to exclude generation of action potentials. Under this condition, AMPAR-mediated mEPSCs are more dominant than NMDAR-mediated mEPSCs. As shown in Figs. 3-4B and C, the mEPSC amplitudes and frequencies in the Nedd4 cDKO mice were slightly but not significantly reduced as compared to control mice (Fig. 3-4C, mEPSC amplitude; control, 28.55 ± 1.22 pA, n=15, N=9; cDKO, 26.99 ± 1.55 pA, n=17, N=9; Student's *t* test, p=0.4426) (Fig. 3-4C, mEPSC frequency; control, 0.7159 ± 0.05747 Hz, n=15, N=9; cDKO, 0.7138 ± 0.062 Hz, n=17, N=9; Student's *t* test, p=0.9809). These results indicate that Nedd4-1 and Nedd4-2 do not affect the number of functional synapses, release probability, the size of quanta release, and/or the number of functional AMPARs at SC-CA1 synapses.

3.4.1.2 Input-Output Relationship

In order to examine the relationship between an evoked presynaptic input and the corresponding postsynaptic output, evoked fEPSPs were measured using extracellular field recording. Fig. 1-2B displays a typical trace of evoked fEPSP recorded in CA1 stratum radiatum, which consists of, first, a fiber volley (FV) caused by the inward current of the action potential and, second, an fEPSP (Bortolotto et. al., 2011). The magnitude of the FV reflects the number of excited axons activated by an electric stimulation of the SC afferents, while the initial slope of fEPSP displays the intensity of the postsynaptic response. Evoked fEPSPs were recorded under submerged conditions and with superfusion with ACSF (2 mM Ca^{2+}, 2 mM Mg^{2+}). As shown in Fig. 3-4D, the input-output relationship was not significantly different between Nedd4 cDKO and control mice (Fig. 3-4D, control, n=13, N=7; cDKO, n=14, N=6), indicating that the loss of *Nedd4-1* and *Nedd4-2* does not affect the relative balance between presynaptic inputs and postsynaptic responses in evoked synaptic transmission.

3.4.1.3 Paired-Pulse Ratio (PPR)

To examine effects of *Nedd4-1* and *Nedd4-2* loss on presynaptic function, I measured PPR as an indirect readout for presynaptic release probability. PPR is the ratio of the second response to the first response when a pair of stimuli are given at the same intensity and in rapid succession. The SC-CA1 synapses exhibit paired-pulse facilitation (PPF), which is characterized by a PPR>1. PPR in the SC-CA synapses generally reaches the maximum at short (e.g. 50 ms) interpulse intervals and decreases exponentially with increased interpulse intervals (to 500 ms). PPF, a form of presynaptic short-term plasticity, occurs as the result of a transient increase of the

residual calcium level after the first stimulation, and is prominent at synapses with a low initial probability of release (Katz and Miledi, 1968). As expected, I found that PPR peaked at an interpulse interval of 50 ms, followed by exponential decline, both in the Nedd4 cDKO and control mice (Fig. 3-4E, control, n=12 N=6; cDKO, n=17, N=6). However, no significant differences in PPR were found between the two genotypes over a range of the interpulse intervals from 25 ms to 1,000 ms, indicating that presynaptic function in evoked synaptic transmission is unaffected by the loss of *Nedd4-1* and *Nedd4-2*.

3.4.1.4 AMPAR/NMDAR Ratio

EPSCs consist of AMPAR- and NMDAR-mediated currents, which can be electrophysiologically and pharmacologically separated by their distinct channel properties. The AMPAR/NMDAR ratio is controlled locally, developmentally, and pathologically (Collingridge et al., 2004). Immature synapses are often 'silent' because they only contain NMDARs and are insensitive to glutamate stimuli under basal conditions, hence AMPAR/MNDAR ratios indicate synapse maturation (Isaac et al., 1995; Liao et al., 1995).

In order to study the effects of *Nedd4-1* and *Nedd4-2* deficiencies on AMPAR/NMDAR ratios, evoked EPSCs were measured by whole-cell patch clamp recording at -70 mV and +40 mV holding potential. As indicated in Fig. 3-4F, AMPAR-mediated EPSCs were analyzed at -70 mV as the peak currents of the EPSCs, while NMDA-mediated EPSCs were analyzed at +40 mV as the currents at 50 ms after the stimulation, when AMPAR-mediated currents are mostly absent. Although Nedd4 cDKO mice showed slightly increased AMPAR/MNDAR ratios (Fig. 3-4F; control, 2.90 ± 0.28, n=11, N=8; cDKO, 3.16 ± 0.25, n=9, N=6; Student's *t* test, p=0.5129), there was no significant difference between the two groups, indicating that Nedd4-1 and Nedd4-2 do not affect AMPAR/NMDAR ratios under basal conditions and at the age tested.

Taken together, above data show that Nedd4-1 and Nedd4-2 do not significantly impact basal synaptic transmission in mature excitatory neurons.

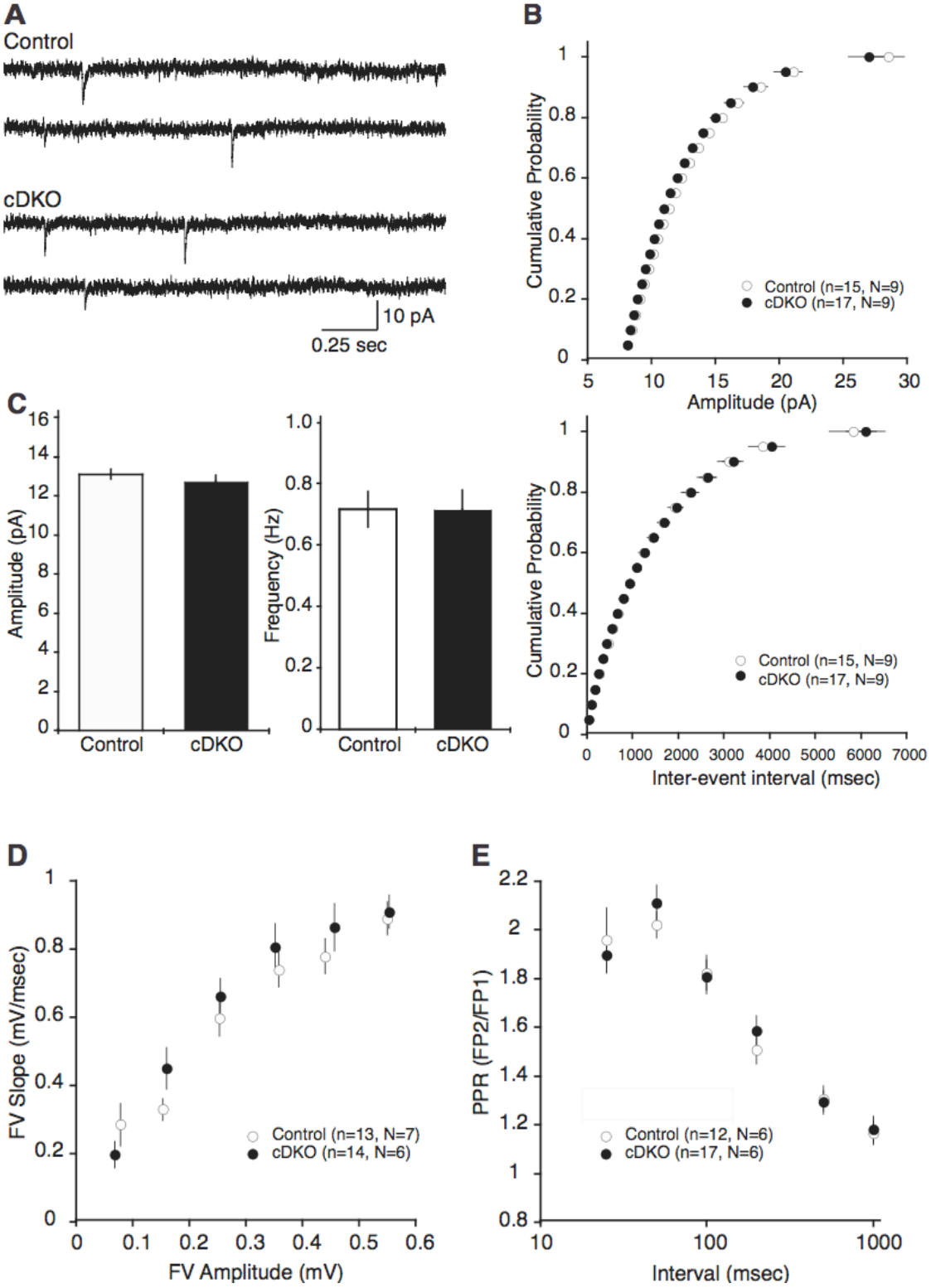
A
Control
cDKO
10 pA
0.25 sec
B
Cumulative Probability
Amplitude (pA)
Control (n=15, N=9)
cDKO (n=17, N=9)
C
Amplitude (pA)
Control
cDKO
Frequency (Hz)
Control
cDKO
Cumulative Probability
Inter-event interval (msec)
Control (n=15, N=9)
cDKO (n=17, N=9)
D
FV Slope (mV/msec)
FV Amplitude (mV)
Control (n=13, N=7)
cDKO (n=14, N=6)
E
PPR (FP2/FP1)
Interval (msec)
Control (n=12, N=6)
cDKO (n=17, N=6)

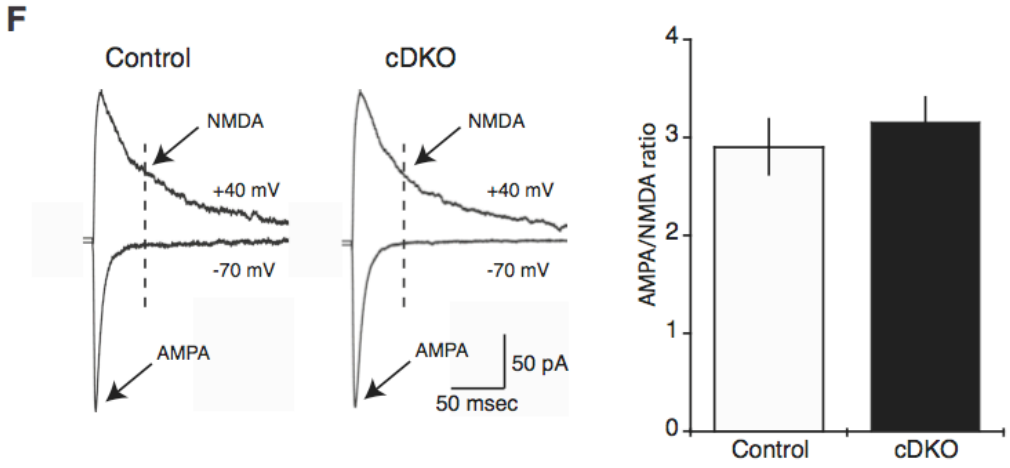

Figure 3-4 Intact basal synaptic transmission in SC-CA1 synapses of Nedd4 cDKO mice

(A-C) Nedd4 cDKO mice exhibit intact mEPSCs. mEPSCs were recorded by whole-cell voltage-clamp mode at -60 mV holding potential in the presence of 0.5 μM TTX and 100 mM PTX. (A) Sample traces of mEPSCs from control (upper two panels) and Nedd4 cDKO (lower two panels) mice. Scale bars, 10 pA, 0.25 s. (B) Cumulative probability of amplitudes (top) and inter-event interval time (bottom) of mEPSCs. (C) Averaged mEPSC amplitude (left) and frequency (right).
(D) Input-output relationship is intact in the Nedd4 cDKO mouse. Summary graph of the input-output relationship obtained by plotting the amplitude of the fiber volley against the fEPSP slope.
(E) PPR is intact in the Nedd4 cDKO mouse. A set of paired stimulations were applied at different interval times, 25, 50, 100, 200, 500, and 1000 ms.
(F) AMPAR/NMDAR ratios were comparable between the two genotypes. Sample traces (left two panels) measured at -70 and +40 mV holding potentials. AMPAR- and NMDAR-mediated currents were measured at the indicated points (arrow). Scale bars, 50 pA, 50 ms. The summary graph of the averaged AMPAR/NMDAR ratios showed no significant difference between two groups (right panel).

3.4.2 Nedd4-1 and Nedd4-2 are Required for LTP

In order to further explore the physiological functions of Nedd4-1 and Nedd4-2 in mature neurons, I studied the roles of Nedd4-1 and Nedd4-2 in synaptic plasticity. At the hippocampal SC-CA1 synapse, the induction of LTP and LTD requires a calcium influx into the activated postsynaptic spine through NMDARs, which in turn activates multiple intracellular signaling pathways, including kinases, phosphatases, and small GTPases. While early-phase LTP (E-LTP) and LTD are consequences of recycling and/or activation or inactivation of AMPARs, a robust plasticity, such as late-phase LTP (L-LTP), requires gene transcription and protein synthesis. Recent studies showed that L-LTP is based on the balance of protein synthesis and proteasomal degradation (Fonseca et al., 2006) and that a synaptic

activation induces synaptic accumulation of the ubiquitin-proteasome system (UPS) (Bingol and Schuman, 2006). Considering a possible synaptic localization of Nedd4-1 and Nedd4-2 (Fig. 3-1D) and the involvement of the UPS in the regulation of synaptic plasticity, I examined LTP and LTD in the Nedd4 cDKO mice using the extracellular field recording technique.

3.4.2.1 LTD

In order to determine whether the loss of *Nedd4-1* and *Nedd4-2* affects LTD, the SC afferents were stimulated using a low frequency stimulation (LFS) protocol, consisting of 900 pulses at 1 Hz. This form of LTD had been reported to be age-dependent. Starting from P10, the magnitude of LTD declines with age and cannot be induced in acute slices prepared from mice older than P50 (Milner et al., 2004). Synaptic weakening by LTD is mainly mediated by dephosphorylation and endocytosis of AMPARs (Collingridge et al., 2004; Ehlers, 2000; Lee et al., 2003).

As shown in Fig. 3-5A, LTD was reliably induced, with a robust and a stable depression of fEPSP for more than 1 h after the induction, in the control (Fig. 3-5A, 80.43 ± 3.2%, n=19, N=10) and the Nedd4 cDKO mice (Fig. 3-5A, 77.6584 ± 2.4184%, n=20, N=12, Student's *t*-test, p=0.4904) without any significant differences. This result indicates that Nedd4-1 and Nedd4-2 are not involved in the process of low calcium influx via NMDARs and consequent removal of synaptic AMPARs during LTD.

3.4.2.2 LTP

In order to examine whether Nedd4-1 and Nedd4-2 are involved in LTP, SC afferents were stimulated by a single train of high frequency stimulation (HFS), consisting of 100 pulses at 100 Hz. As shown in Fig. 3-5B, the magnitude of LTP at 60 min after the induction was not significantly different between the two genotypes tested (Fig. 3-5B, control, 139.001 ± 9.17%, n=8, N=6; cDKO, 128.8475 ± 8.3166%, n=7, N=5; Student's *t*-test, p=0.1902), although there was a slight tendency of a reduction of LTP in Nedd4 DKO mice (Fig. 3-5B).

Considering the tendency towards reduced LTP in Nedd4 DKO mice after stimulation with a single train of pulses (Fig. 3-5B), LTP was next induced by a relatively strong induction protocol using three trains of HFSs spaced 20 s apart. Previous studies had shown that this form of LTP, induced using three trains of HFSs, is independent of protein translation (Abbas et al., 2009), voltage-dependent-calcium-channel (VDCC) (Swant and Wagner, 2006), and presumably PKA (Woo et al.,

2003), implying that this LTP may not belong to the L-LTP category. Although the initiation of LTP was comparable between the two genotypes using this protocol, LTP in the Nedd4 cDKO mice was significantly reduced at 120 min after the induction as compared to control mice (Fig. 3-5C, control, 136.2774 ± 6.9631%, n=10, N=8; cDKO, 108.3049 ± 6.7488%, n=15, N=7; Student's *t*-test, *p*=0.01054).

These results indicate that Nedd4-1 and Nedd4-2 participate in the maintenance of LTP, which involves synaptic insertion of AMPARs and modification of the conductance of AMPARs. As the initiation of LTP was intact in the Nedd4 cDKO mice, Nedd4-1 and Nedd4-2 are dispensable for the process of calcium influx through NMDARs activation during LTP. It remains unclear if Nedd4-1 and Nedd4-2 are required for L-LTP, therefore the question as to whether Nedd4-1 and Nedd4-2 play roles in L-LTP needs to be examined.

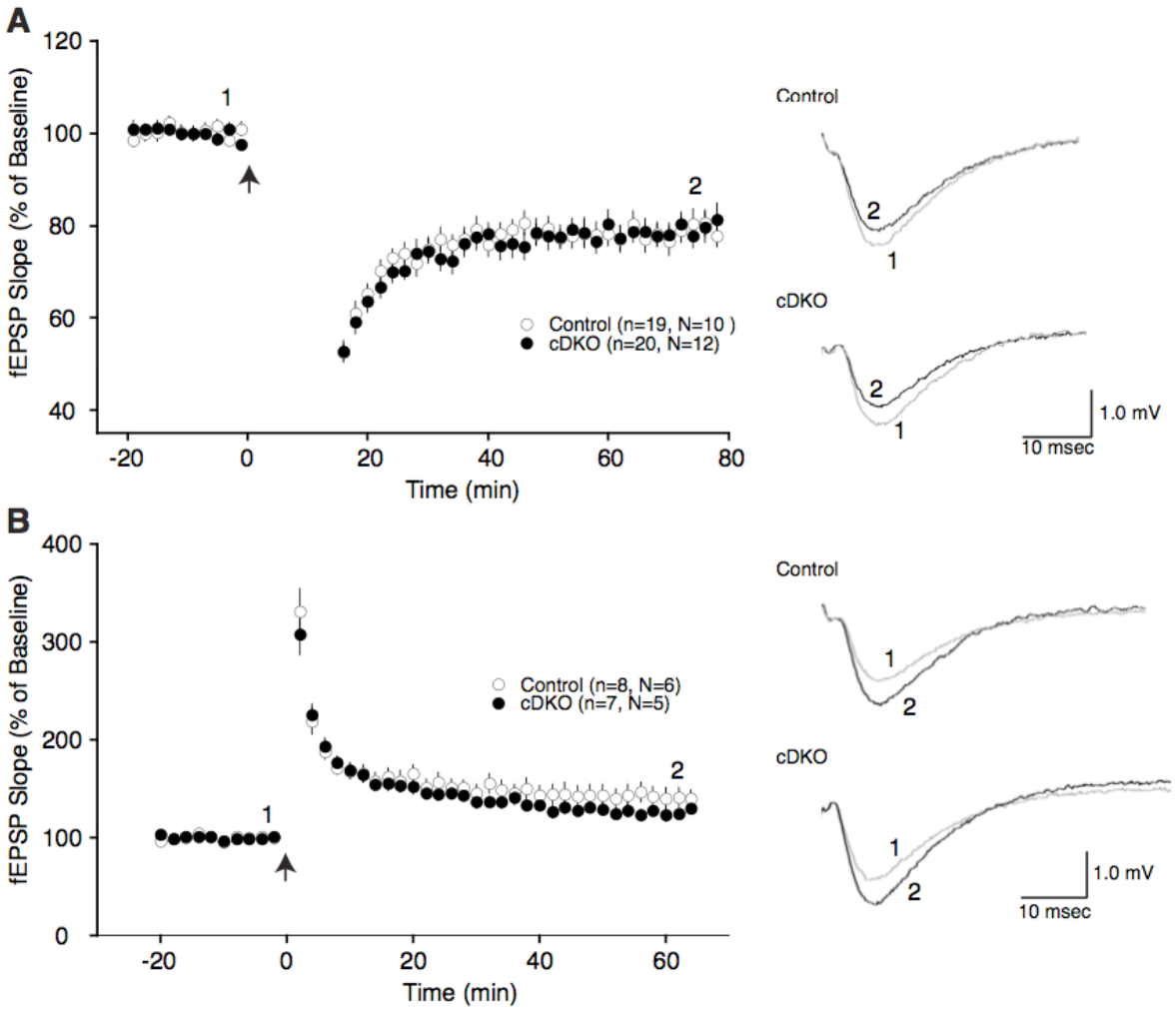

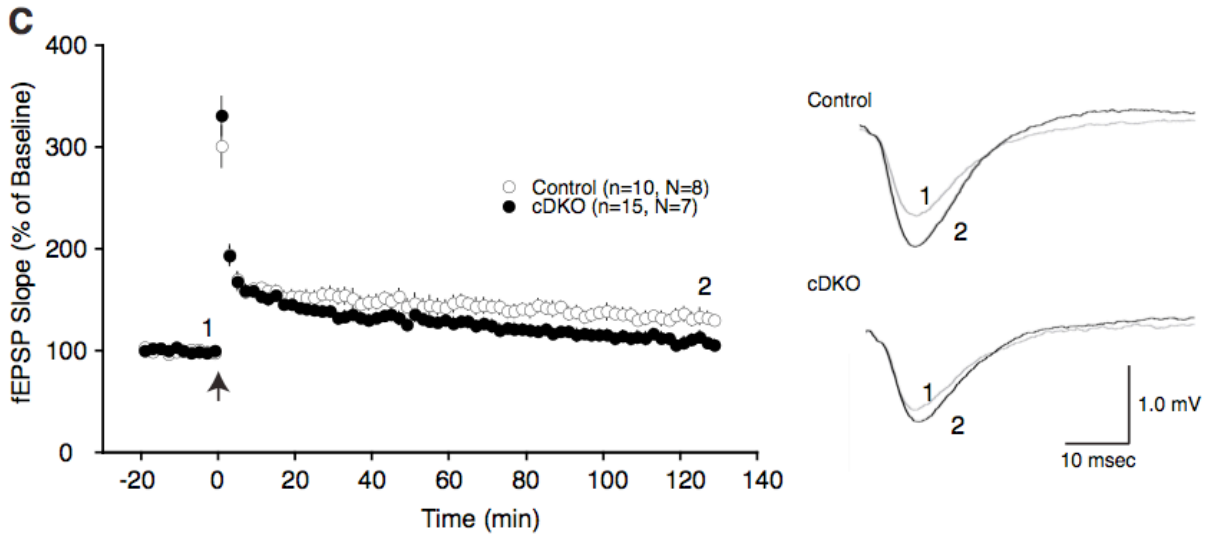

Figure 3-5 Nedd4-1 and Nedd4-2 are required for the maintenance of LTP

All measurements were performed under submerged conditions in the presence of 100 μM PTX. The slope of fEPSPs was monitored every 30 s during recording and 4 sequential points were averaged in the analysis. The open and closed circles show the results from control and Nedd4 cDKO mice, respectively. Arrowheads indicate the time point of induction. Right panels show the representative traces of control (top) and Nedd4 cDKO mice (bottom) at base measurement (time point at 1 in the left panels, grey line) and at the indicated time points (time point at 2 in the left panels, black line). Scale bar, 10 ms, 1 mV.
(A) Time courses of the normalized fEPSP slopes before and after LTD induction (900 pulses at 1 Hz) showed that LTD is intact in Nedd4 cDKO mice.
(B) Time courses of normalized fEPSP slopes before and after LTP induction (a single train of HFS) shows a slight tendency of a reduction in LTP in Nedd4 cDKO mice.
(C) Induction of a relatively strong LTP induced by three trains of HFSs spaced 20 s apart revealed a significant reduction in cDKO mice (Student's *t*-test, p=0.01054) at 120 min after the induction.

3.5 Identifying Interacting Proteins of Nedd4-1 and Nedd4-2

In order to identify substrates of Nedd4-1 and Nedd4-2 that might be involved in the regulation of LTP, I performed yeast two-hybrid (YTH) screening using rat and mouse brain cDNA libraries.

3.5.1 YTH Screening

As a first approach, a Gal4-based YTH screening was carried out. This system is based on the detection of physical protein-protein interactions of bait and prey proteins that are fused to a DNA-binding domain (DNA-BD) and an activating domain (AD) of a transcription factor, respectively. When a DNA-BD and an AD domain form a stable protein complex via interaction between bait and prey proteins, the expression of a reporter gene is activated.

Bait constructs with partial sequences of Nedd4-1 and Nedd4-2 were cloned as listed below (see also Fig. 3-6A).

Nedd4-1

1) Nedd4-1 (WW1)/pGBDC2
2) Nedd4-1 (WW2)/pGBDC2
3) Nedd4-1 (WW3)/pGBDC2
4) Nedd4-1 (C2+WW1)/pGBDC2
5) Nedd4-1 (WW1+WW2)/pGBDC2
6) Nedd4-1 (WW2+WW3)/pGBDC2
7) Nedd4-1 (WW1+WW2+WW3)/pGBDC2
8) Nedd4-1 (HECT)/pGBDC2
9) Nedd4-1 (HECT C/S mutant)/pGBDC2

Nedd4-2

1) Nedd4-2 (WW1)/pGBDC2
2) Nedd4-2 (WW2)/pGBDC2
3) Nedd4-2 (WW3, 4)/pGBDC2
4) Nedd4-2 (C2+WW1)/pGBDC2
5) Nedd4-2 (WW1+WW2)/pGBDC2
6) Nedd4-2 (WW2+WW3, 4)/pGBDC2
7) Nedd4-2 (WW1+WW2+WW3, 4)/pGBDC2
8) Nedd4-2 (HECT)/pGBDC2
9) Nedd4-2 (HECT C/S mutant)/pGBDC2

First, transcriptional auto-activity of each bait construct was examined by transformation of a yeast cell line, PJ169-4A, with bait plasmids encoding the GAL4 DNA binding domain fused with Nedd4 together with an empty prey plasmid encoding only the GAL4 activating domain. Eight constructs showed no auto-activities and were used as baits for YTH screening using adult rat and mouse brain cDNA libraries (Table 3-1). The positive prey clones were sequenced, and a total of 31 in-frame cDNAs were identified as Nedd4-1 and Nedd4-2 binding partners (Table 3-2).

Among the identified binding partners, Sec24c and Sec31, core components of the COPII vesicles, were of particular interest. ER-to-Golgi trafficking is the initial phase of the secretory pathway of newly synthesized proteins and lipids and is

mediated by the transport of COPII vesicles. In the process of COPII vesicle formation, one of the first proteins recruited to the ER is the small GTPase Sar1, which sequentially recruits Sec23/Sec24 and Sec13/Sec31 complexes. Sec24 determines and recruits the cargo proteins into the vesicle, and Sec31 forms the 'outer shell' of the vesicle. Forward morphometric genetic screening in *D. melanogaster* identified orthologs of Sec23 and Sar1 as regulators of dendritogenesis (Ye et al., 2007).

Ubiquitination is involved in multiple vesicle trafficking pathways. The most well-known is endocytosis of transmembrane type tyrosine kinases (e.g. EGFR and c-Met (Huang et al., 2006; Li et al., 2007)). Upon activation of these kinases by extracellular ligands, they are autophosphorylated and recruit Nedd4-1 and Cbl (Marmor and Yarden, 2004; Vecchione et al., 2003). Monoubiquitination of such transmembrane type kinases is critical for recruitment of adaptor proteins such as Esp15 or epsin1 to drive endocytosis. Given that Eps15 and epsin1 are also exposed to monoubiquitination, I attempted to demonstrate the ubiquitination of Sec23 by Nedd4-1. However, it was not possible to purify recombinant Sec23 for this purpose (data not shown).

Table 3-1 Results of YTH screening

The domains and amino acid residues of Nedd4-1 and Nedd4-2 encoded in each bait construct, screening sizes, and the numbers of the final positive clones are given. "-" indicates the constructs which were not used for screening because of high transcriptional auto-activity.

	Bait construct		Rat brain library		Mouse brain library	
	Bait construct (Subcloned into pGBDC2)	Amino acid residues (aa)	Screened clones ($x10^6$)	Number of positive clones	Screened clones ($x10^6$)	Number of positive clones
Nedd4-1						
1	WW1	239-342	-	-	-	-
2	WW2	367-457	1.14	7	0.61	0
3	WW3	446-538	1.36	8	0.56	5
4	C2+WW1	31-342	1.1	2	0.4	3
5	WW1+WW2	239-457	-	-	-	-
6	WW2+WW3	367-538	-	-	-	-
7	WW1+WW2+WW3	239-538	-	-	-	-
8	HECT	500-887	-	-	-	-
9	HECT C/S mutant	500-887	0.7	0	1.78	0
Nedd4-2						
1	WW1	141-326	-	-	-	-
2	WW2	320-475	-	-	-	-
3	WW3, 4	474-595	-	-	-	-
4	C2+WW1	1-326	1.3	0	0.9	0

5	WW1+WW2	141-475	-	-	-	-
6	WW2+WW3, 4	320-595	-	-	-	-
7	WW1+WW2+WW3, 4	141-595	0.43	0	0.65	0
8	HECT	611-976	0.75	3	0.86	0
9	HECT C/S mutant	611-976	0.58	3	0.83	0

Table 3-2 The identified proteins encoded by the positive interacting clones

Proteins encoded by the positive clones	GeneBank accession number	Prey library	Number of positive clones	Bait domain
Transmembrane protein 55A	NP_082540	Rat	4	Nedd4-1 /WW2
rCG50614, isoform CRA_b	EDL86931	Rat	4	Nedd4-1 /WW3
Hypothetical protein LOC362374	NP_001102100	Rat	3	Nedd4-1 /WW3
Sec24c protein	AAH27157	Mouse	3	Nedd4-1 /WW3
ADH dehydrogenase subunit 1	YP_220563	Rat	2	Nedd4-1 /WW3
mKIAA1764	BAD32534	Mouse	2	Nedd4-1 /C2+WW1
rCG54809	EDL98732	Rat	2	Nedd4-1 /C2+WW1 Nedd4-2 /HECT C/S
rCG57266	EDL93739	Rat	2	Nedd4-2 /HECT C/S
SEC31	Q9Z2Q1	Rat	1	Nedd4-1 /WW2
SEC31 like	EDL99573	Rat	1	Nedd4-1 /WW2
Nedd4 family interaction protein 1	NP_001013077	Rat	1	Nedd4-1 /WW2
Tyrosine 3-monooxygenase	NP_037185	Rat	1	Nedd4-1 /WW3
Similar to CG17265-PA	XP_001076332	Rat	1	Nedd4-1 /WW3
Hypothetical protein	XP_001065363	Rat	1	Nedd4-1 /C2+WW1
Cytoplasmic FMR1 interaction protein 1	NP_001100987	Rat	1	Nedd4-2 /HECT
rCG43799	EDL85025	Rat	1	Nedd4-2 /HECT
Unnamed protein	BAE30321	Mouse	1	Nedd4-1 /C2+WW1

3.5.2 Affinity Purification of Nedd4-1 and Nedd4-2 Binding Proteins from Rat Synaptosomes

As a second approach to identify physiological targets of Nedd4-1 and Nedd4-2, Nedd4-1 and Nedd4-2 binding proteins were purified by affinity chromatography. A Triton X-100 synaptosome extract (P2 fraction) of adult rat brain was incubated with Glutathione-Sepharose beads coupled with purified GST-Nedd4-1 (residues 217-549) or GST-Nedd4-2 (residues 120-601). To remove non-specific interacting partners, beads were washed with extraction buffer containing 1 M NaCl. Bound proteins were eluted along with GST-Nedd4-1 or GST-Nedd4-2 by 40 mM glutathione and separated by SDS-PAGE (Fig. 3-6B). The bands enriched in the eluate from the GST-Nedd4-1 and GST-Nedd4-2 columns were analyzed, and Mammalian enabled (Mena) and synaptopodin (SYNPO) were identified by mass spectrometry (MS) as binding partners.

3.5.3 Mena is not Ubiquitinated by Nedd4-1 and Nedd4-2 *in vitro*

Mena, the mammalian ortholog of *Drosophila* Enabled (Ena), is an Ena/ vasodilator-stimulated phosphoprotein (Vasp) family protein, which links Abl, Arg, and Src-meditated signaling with actin polymerization through protein-protein interactions. This protein family consists of Mena, Vasp, and EVH, which share highly conserved domain structures, including a proline-rich domain and Ena-VASP homology 1 and 2 domains (EVH1 and EVH2). The EVH1 determines the cellular localization of Vasp family proteins by interacting with the focal adhesion proteins Zyxin and Vinculin. The proline-rich domain regulates reorganization of the actin cytoskeleton by interacting with Profilin, a regulator of actin depolymerization, whereas the EVH2 domain stabilizes actin filament bundles through a direct interaction with F-actin (Bachmann et al., 1999).

Among the Vasp family proteins, Mena is particularly highly expressed in the brain (Lanier et al., 1999), indicating that it may be the dominant family member in the brain. Loss of the *Vasp* gene alone is irrelevant for neural development and function and instead leads to hyperplasia of megakaryocytes in bone marrow and spleen (Lanier et al., 1999). *Mena* deficient mice are viable, but behave abnormally with less mobility, and show misguidance of the axonal projections from the hippocampus and the pons, leading to a failure in the midline crossing of axons

(Lanier et al., 1999). A genetic interaction between *Mena* and *profilin* is indicated by the fact that neural tube closure is aberrant in *Mena* -/-; *profilin* +/- animals. Thus, Mena plays an important role in the regulation of the reorganization of the actin cytoskeleton in the developing brain (Goh et al., 2002). The *Mena* gene produces two splicing isoforms, a ubiquitously expressed short isoform (80 kDa) and a brain specific long isoform (140 kDa) (Lanier et al., 1999).

Considering the dendritic localization of Mena (Lanier et al., 1999) and the known involvement of actin remodeling in LTP, I examined the ubiquitination of Mena by Nedd4-1 and Nedd4-2 based on the hypothesis that this ubqiuitination might be involved in the synaptic plasticity defects seen in the Nedd4 cDKO. For this purpose, I cloned the mouse cDNA encoding the short isoform of Mena that was identified in the affinity chromatography to overexpress Mena in heterologous cells. However, *in vitro* ubiquitination assays failed to report ubiquitination of Mena by Nedd4-1 and Nedd4-2 (Fig. 3-6C).

3.5.4 Nedd4-1 and Nedd4-2 Ubiquitinate SYNPO *in vitro*

SYNPO is a proline rich and an actin-associated protein highly expressed in the mature brain and in the kidney. In the mammalian forebrain, SYNPO is closely associated with the spine apparatus, a cellular organelle present in a subset of dendritic spines. Ultrastructural analysis showed that the spine apparatus is composed of a stack of lengthened lumenal structures surrounded by a lipid bilayer. A study using *SYNPO* deficient mice revealed that SYNPO is critical for the formation of the spine apparatus, for LTP, and for spatial learning (Deller et al., 2003). Given that SYNPO contains two PPxY motifs (Mundel et al., 1997), Nedd4-1 and Nedd4-2 may regulate LTP through direct binding and/or ubiquitination of SYNPO.

In order to examine whether SYNPO is ubiquitinated by Nedd4-1 and Nedd4-2, an *in vitro* ubiquitination assay using heterologous cells was performed. Both, the large (+C2) and the short (–C2) isoforms of Nedd4-2 (Fig. 3-1B) were examined. EGFP-tagged Nedd4-1 or Nedd4-2 was overexpressed together with myc-tagged SYNPO and His_6-tagged ubiquitin in HEK293FT cells. The cells were incubated with MG132, a proteasome inhibitor, for 10 h prior to harvest, and Myc-tagged SYNPO was immunoprecipitated from the cell extract using an anti-myc antibody. Immunoprecipitated Myc-SYNPO cross-reacted with an anti-ubiquitin antibody in the

presence of overexpressed EGFP-Nedd4-1 and of both isoforms of EGFP-Nedd4-2s, but not if catalytically inactive mutants (C/S) of Nedd4s or other Nedd4 family proteins (EGFP-WWP1 or EGFP-WWP2) were expressed (Fig. 3-6D). Although EGFP-Nedd4-2 was expressed at lower levels than EGFP-Nedd4-1 in these assays (Fig. 3-6D, lower panel), SYNPO was ubiquitinated more robustly in the EGFP-Nedd4-2-expressing cells (Fig. 3-6D, upper panel). Therefore, Nedd4-2 may have stronger enzymatic ubiquitination activity towards SYNPO than Nedd4-1.

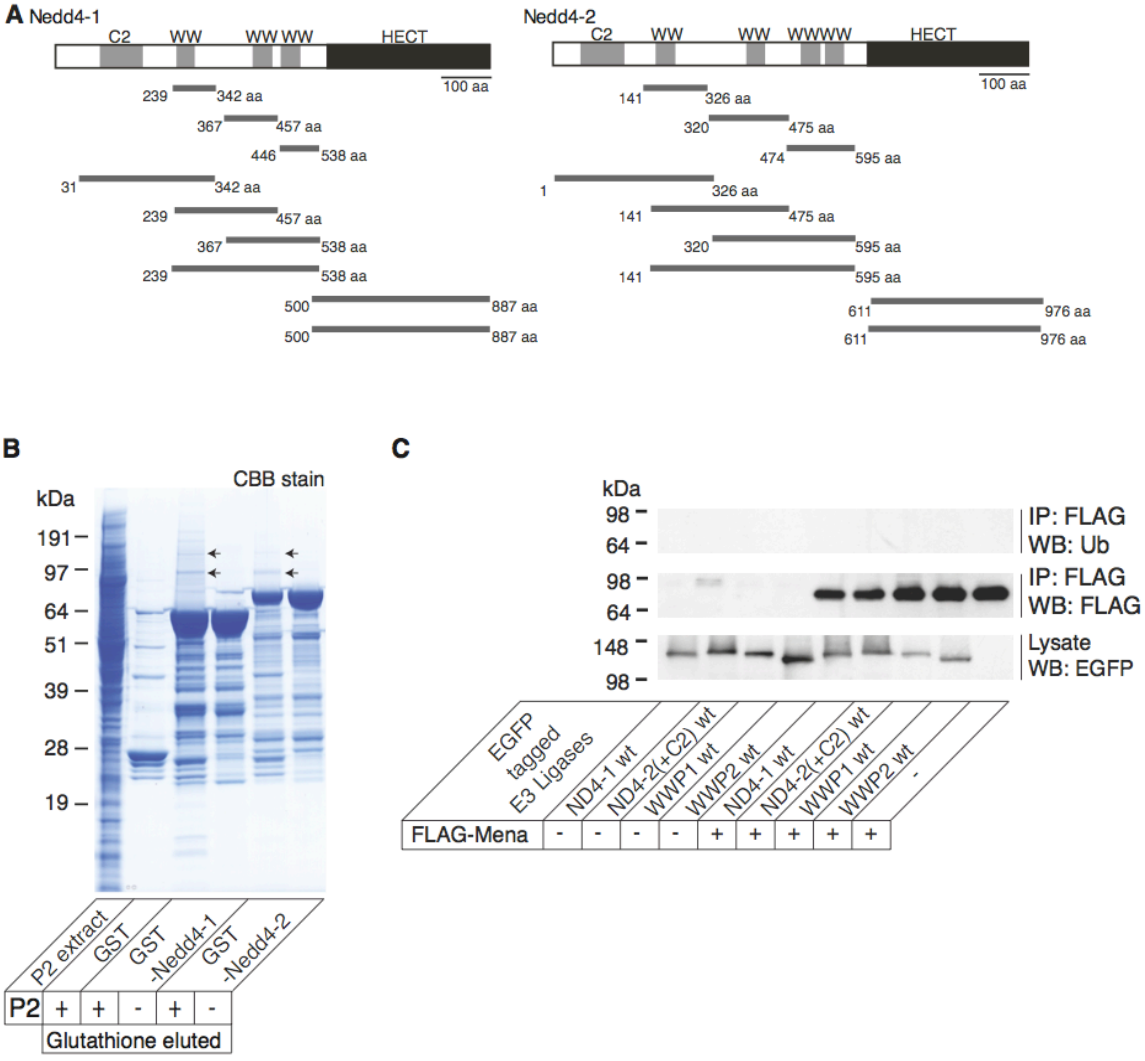

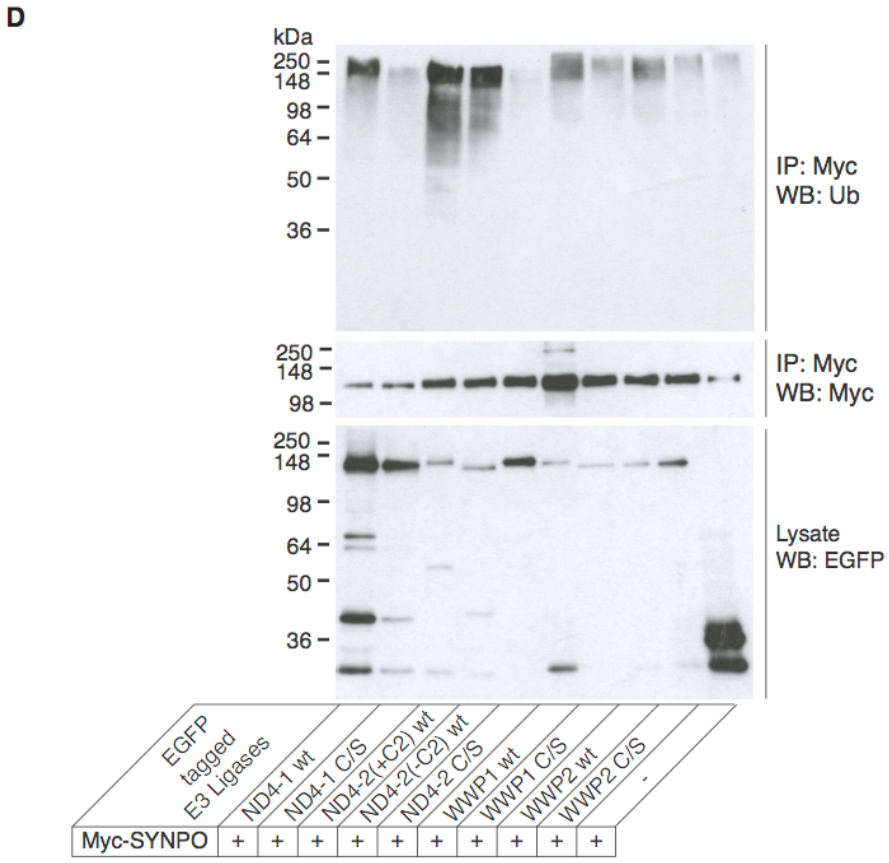

Figure 3-6 Identification and characterization of proteins associated with Nedd4-1 and Nedd4-2

(A) Schematic diagram of Nedd4-1 and Nedd4-2 bait proteins used in the present study. Each construct is indicated with the corresponding amino acid residues. C2, C2 domain; WW, WW domain; HECT, HECT domain.
(B) Affinity purification of Nedd4-1 and Nedd4-2 binding proteins. 40 µg of GST alone, GST-Nedd4-1 (residues 217–549), or GST-Nedd4-2 (residues 120-601) were immobilized on Glutathione-Sepharose beads, and a Triton X-100 extract of rat brain synaptosomes (P2, +) or the buffer only (P2, -) were loaded. Bound proteins were eluted with 40 mM glutathione, separated by SDS-PAGE, and stained with CBB. Protein bands enriched in the eluate from the GST-Nedd4-1 and the GST-Nedd4-2 beads were analyzed by mass spectrometry. Mena (lower arrows) and SYNPO (upper arrows) were identified as binding proteins of Nedd4-1 and Nedd4-2. This result was incorporated from Dr. Kalina Dimova, Dr. Olaf Jahn, and Dr. Hiroshi Kawabe.
(C and D) Nedd4-1 and Nedd4-2 ubiquitinate SYNPO, but not Mena, *in vitro*. EGFP-tagged E3 ligases or EGFP alone (-) were coexpressed with FLAG-Mena (C) or Myc-SYNPO (D) and His_6-Ubiquitin. FLAG-Mena or Myc-SYNPO were immunoprecipitated using anti-FLAG or myc antibodies, and the precipitates were subjected to immunoblotting with anti-FLAG (C) or myc (D) antibodies (middle panels), respectively, and an anti-ubiquitin antibody (upper panels). The expression of EGFP-tagged Nedd4 family proteins was confirmed by immunoblotting using an anti-GFP antibody (lower panels). wt, wild type; C/S, catalytic inactive mutant; +C2, the larger isoform of Nedd4-2; -C2, the shorter form of Nedd4-2.

4 Discussion

In view of the synaptic enrichment of Nedd4-1 and Nedd4-2 in neurons from adult rodent brain (Fig. 3-1D), I investigated the functions of Nedd4-1 and Nedd4-2 by morphological and electrophysiological analyses in the brains of control and Nedd4 cDKO mice. Nedd4-1 and Nedd4-2 are involved in neurite development and are size determinants of certain brain regions without affecting spine density and basal synaptic transmission. Strikingly, these E3 ligases are specifically required for the maintenance of LTP, indicating that they may play important roles in cognitive function in the mature brain, such as learning and memory formation. Furthermore, the finding that Nedd4-1 and Nedd4-2 ubiquitinate synaptopodin (SYNPO), which plays a critical role in LTP, may indicate a possible mechanism by which Nedd4-1 and Nedd4-2 positively regulate LTP through ubiquitinating SYNPO.

4.1 Roles of Nedd4-1 and Nedd4-2 in Neuronal Morphogenesis

The morphological consequences of *Nedd4-1* and simultaneous *Nedd4-1* and *Nedd4-2* disruptions are very similar (Figs. 1-5 and Figs. 3-3A and B). Given that Nedd4-2 has the potential to interact with TNIK (data not shown), Nedd4-2, as well as Nedd4-1, might be part of the TNIK/Rap2 pathway by which Nedd4s regulate neurite growth (Kawabe et al., 2010). It remains to be determined whether Nedd4-2 directly ubiquitinates Rap2, as Nedd4-1 does, and what the developmental and morphological consequences occur after single *Nedd4-2* deletion in developing and mature neurons. Another open question is whether and how Nedd4-1 and Nedd4-2 maintain neural morphology in mature neurons. Considering the massive impairment in dendritic development in Nedd4 cDKO mice, other effects of *Nedd4-1* and *Nedd4-2* deficiencies in mature neurons, e.g. on spine density through possible activation of Rap2, could be masked in the Nedd4 cDKO. An analysis using tamoxifen inducible Nedd4 cDKO mice would be a favorable approach owing to the advantage of temporal control of the KO onset, which would allow to isolate morphological effects of Nedd4-1 and Nedd4-2 deletion in mature neuron from developmental effects.

Several lines of evidence imply that Nedd4-2, rather than Nedd4-1, might be involved in axon development, leading to the hypothesis that Nedd4-1 and Nedd4-2 activities may be coordinated to promote neurite development in a spatially independent manner. It has been reported that *Xenopus tropicalis* Nedd4-1 (xNedd4-

1) promotes axon branching through ubiquitination and proteasomal degradation of PTEN in developing *Xenopus* neurons (Drinjakovic et al., 2010). However, it is still under debate whether or not PTEN is a physiological target of Nedd4-1. Several studies using heterologous expression systems combined with overexpression and RNAi-mediated knockdown of Nedd4-1 have shown that Nedd4-1 mono- and polyubiquitinates PTEN, which leads to nuclear localization and proteasomal degradation of PTEN, respectively (Trotman et al., 2007; Wang et al., 2007). On the other hand, independent studies using *Nedd4-1* deficient mouse cells have shown that Nedd4-1 is dispensable for the degradation and the nuclear localization of PTEN (Cao et al., 2008; Fouladkou et al., 2008). Considering that the results obtained from KO cells are more reliable than those from RNAi cells, it is unlikely that PTEN is a target of Nedd4-1 in mammals, except that Nedd4-1 may target PTEN in a manner dependent on cell type and developmental stage. Alternatively, phylogenic analysis demonstrates that xNedd4-1 is more homologous to mammalian Nedd4-2 than to Nedd4-1 (Fig. 4-1) (Yang and Kumar, 2010), indicating that Nedd4-2, instead of Nedd4-1, may ubiquitinate PTEN to promote axon branching in mammalian neurons. Therefore, it may be hypothesized that Nedd4-1 and Nedd4-2 promote dendritic and axonal development independently through targeting Rap2 and PTEN, respectively, much like Smurf1 and Smurf2, which form another subfamily in the Nedd4 superfamily and coordinate axon acquisition by targeting RhoA and Rap1B, respectively, in developing neurons (Cheng et al., 2011; Schwamborn et al., 2007).

The present study shows that loss of *Nedd4-1* and *Nedd4-2* causes a reduced size of the cerebral cortex (Fig. 3-3A). It is generally believed that glial cells are a major factor in the determination of brain size, because glial cells surround, support, and nourish neurons and are more tightly packed than neurons are in the brain. However, changes in neuron number and morphology are seemingly capable of affecting the brain size, as neuron specific conditional *PTEN* or *IGF1-R* KOs lead to enlarged and reduced brain volume, respectively (Kwon et al., 2006; Liu et al., 2009). Given that all glial cells and inhibitory neurons are genetically intact in the Nedd4 cDKO mouse, the size reduction in cortical regions of the cDKO is likely caused by the shorter dendrites with poor arborization of the pyramidal neurons, though a contribution from a neuronal change in the cell number was not addressed in the present study. Considering the large number of glial cells surrounding neurons, another question to address in the future could be whether the reduced cortical volume

in the *Nedd4-1* and *Nedd4-2* KO is also partly caused by alterations of glial cells, which might arise by a primary neuronal change (e.g. in Notch-Delta and Eph-ephrin pathways). It would be therefore interesting to determine whether the degree of reduction in somata and dendrite sizes of cDKO neurons are correlated with the size reductions in the affected brain regions in the Nedd4 cDKO mice. Alternatively, it could be addressed whether the number and the size of glial cells are affected in the Nedd4 cDKO mouse.

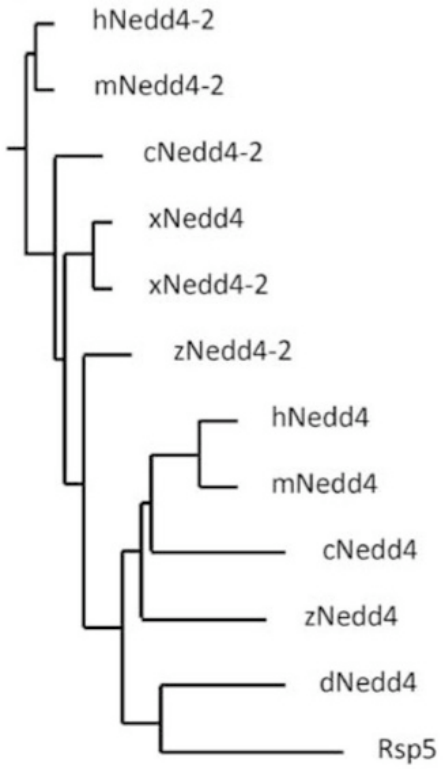

Figure 4-1 Phylogenic tree of Nedd4-1 and Nedd4-2 ubiquitin ligases

c, chicken (*Gallus gallus*); d, fruitfly (*Drosophila melanogaster*); h, human (*Homo sapiens*); m, mouse (*Mus musculus*); x, frog (*Xenopus tropicalis*); and z, zebrafish (*Danio rerio*). (Adapted from Yang and Kumar, 2010)

4.2 Minor Roles of Nedd4-1 and Nedd4-2 in Basal Synaptic Transmission

The roles of Nedd4-1 and Nedd4-2 in basal synaptic transmission were investigated using electrophysiological measurements. The present study showed that mEPSC amplitudes and frequencies, the input/output relationship, PPR, and AMPAR/NMDAR ratios at SC-CA1 synapses are not significantly affected by the loss of *Nedd4-1* and *Nedd4-2* (Figs. 3-4). Consistently, it has been reported that the

surface expression levels of AMPARs and mEPSCs are unchanged in *Nedd4-1*RNAi neurons under basal conditions (Schwarz et al., 2010). Structural analysis of a member of the Nedd4 E3 ligase family showed that the N-terminal C2 domain inhibits the activity of the C-terminal catalytical HECT domain by forming an intramolecular fold in the absence of calcium ions (Bruce et al., 2008; Wiesner et al., 2007). Calcium binding to the C2 domain releases this intramolecular interaction, thus making the HECT domain freely accessible for E2 and substrates. Without robust stimulation of the postsynaptic neuron, the calcium concentration at the spine remains below the threshold for such de-inactivation of Nedd4 E3 ligases, which may limit their activity under basal conditions.

The morphological and electrophysiological consequences of *Nedd4-1* and *Nedd4-2* deficiencies, however, seem to be inconsistent. Spines are actin-rich protrusion on dendrites and the postsynaptic sites that receive neurotransmitters from presynaptic neurons. Therefore the mEPSC frequency generally correlates with the number of dendritic spines. In the Nedd4 cDKO mouse, estimated total spine number in individual CA1 pyramidal neurons is decreased (i.e. normal spine density but reduced dendrite size), whereas mEPSC frequency was unaltered. Additionally, a previous study had shown that mEPSC frequency is reduced in developing *Nedd4-1* deficient autaptic cultured neurons, which is consistent with the reduced synapse number in *Nedd4-1* deficient autaptic neurons (Kawabe et al., 2010). This discrepant result with regard to mEPSC frequency in the Nedd4 cDKO mouse (Figs. 3-4B and C) could be explained by several possibilities.

(1) The negative effects of *Nedd4-1* and *Nedd4-2* deficiencies on mEPSC frequency, which were seen in developing autaptic *Nedd4-1* deficient neurons, may be attenuated in mature neurons, because the expression levels of Nedd4-1 and Nedd4-2 proteins decrease with neuronal maturation (Fig. 3-1C). The previous study used developing autaptic cultured neurons at DIV10-14, whereas the present study used mature brain slices at postnatal week 3-4, when expression levels of both Nedd4-1 and Nedd4-2 are already substantially diminished.

(2) The loss of *Nedd4-2* might counteract the effects of Nedd4-1 KO on mEPSP frequency, so that Nedd4 cDKO mice exhibit normal mEPSC frequency.

(3) The loss of *Nedd4-1* and *Nedd4-2* might lead to an increased release probability of spontaneous release. The spontaneous release is a ubiquitous synaptic activity at rest, independent of action potentials, and may be required for maturation and stability of

synaptic networks (McKinney et al., 1999; Verhage et al., 2000) and inhibition of local dendritic protein synthesis (Sutton et al., 2004). However, its nature and biological relevance remain enigmatic (Xu et al., 2009a), in contrast to action potential dependent synchronous release. Whether or not and to what extent the two major modes of vesicle release (spontaneous 'mini' and evoked synchronous) share similar mechanisms remains unclear. These two forms of release might also operate at different synapses on the same dendrite, or they may exist at the same synapse but employ different types of presynaptic vesicles. In both release modes, neurotransmitters are released through exocytosis in a calcium-dependent manner (Xu et al., 2009a), and synaptic vesicles are recycled back through endocytosis after a release event (Murthy and Stevens, 1999; Ryan et al., 1997; Sun et al., 2002). However, Sara et. al. reported that distinct vesicle pools are used for spontaneous and evoked release (Sara et al., 2005), and Xu et al. showed that synaptotagmin 1 differentially regulates neurotransmitter release in these two modes (Xu et al., 2009a). Effects of a mutation on evoked release, therefore, cannot simply be correlated with mEPSC characteristics, and the release probability of spontaneous release might not be a reliable predictor of Pvr of evoked release. Therefore, the possibility remains that release probability of spontaneous 'mini' release might be increased in the Nedd4 DKO mouse, which would compensate for any reduction in the number of synapses in Nedd4 cDKOs and result in intact mEPSC characteristics.

(4) The loss of *Nedd4-1* and *Nedd4-2* might decrease the ratio of silent vs. responsive synapses (Durand and Konnerth, 1996; Isaac et al., 1995). This would lead to a larger population of responsive synapses. In this case, the detectable mEPSC frequency in Nedd4 cDKOs could be increased to reach control levels.

(5) It is possible that the total spine number is indeed normal in the Nedd4 cDKO mouse. In the present study, spine density was assessed only in parts of the dendrites of CA1 neurons (Figs. 3-3C and D), and the notion of reduced spine numebr in Nedd4 cDKO neurons was deduced based on the normal spine density and reduced dendrite complexity. Considering the possibility that the stability of spines and spinogenesis could be differently regulated depending on the specific dendritic area, the total spine number in Nedd4 cDKO neurons may have to be determined more systematically throughout the entire dendritic tree.

4.3 Roles of Nedd4-1 and Nedd4-2 in Synaptic Plasticity

4.3.1 Pathways Involved in the LTP Forms Studied

Based on its duration, LTP is categorized as E-LTP or L-LTP. L-LTP is mainly distinguishable from E-LTP by its dependency on gene transcription, protein translation, and PKA activity. In the present study, roles of Nedd4-1 and Nedd4-2 in the regulation of LTP were examined using two types of induction protocols, a single train of HFS and three trains of HFSs spaced 20 s apart (a relatively strong type of induction protocol). In contrast to the E-LTP induced by a single train of HFS, the type of LTP induced by our protocol with three trains of HFSs is less well defined.

According to two studies on the properties of LTP induced with three trains of HFSs spaced 20 s apart, this induction protocol is assumed to induce E-LTP, rather than L-LTP. The first report showed that this LTP is insensitive to an antagonist of voltage dependent calcium channels (VDCC), which are required for robust L-LTP (Raymond, 2007; Swant and Wagner, 2006). In the second report, the authors showed that this LTP can last for 4-8 h in the presence of translation inhibitors (Abbas et al., 2009). Additionally, the robustness of LTP depends on the interval between HFS trains as well as the number of imposed stimulations. For instance, typical L-LTP is induced with four trains of HFSs spaced 5 min apart (a spaced stimulation) while four trains of HFSs spaced 20 s apart (a massed stimulation) evokes LTP with different properties. L-LTP induced by a spaced stimulation is PKA and translation dependent, whereas LTP induced by a massed stimulation is PKA independent and weakly translation dependent (Nguyen and Woo, 2003; Scharf et al., 2002; Woo et al., 2003). Therefore, the relatively strong LTP in the present study, induced with three trains of HFSs spaced 20 s apart, is assumed to be an PKA-independent and slightly translation-dependent LTP. This LTP is enhanced by dopamine transporter (DAT) inhibition (Swant and Wagner, 2006), *$IP_3$3-kinase* deficiency (Jun et al., 1998), and erythropoietin (EPO) (Adamcio et al., 2008), which are not involved in regulation of typical L-LTP. Thus, based on the present study, Nedd4-1 and Nedd4-2 appear to be involved in the process of E-LTP, where protein translation is not required and AMPAR trafficking is strictly regulated, which might be subject to modulation by dopaminergic signaling, $IP_3$3-kinase (IP3K), and/or EPO signaling. However, the underlying mechanisms must now be defined directly using pharmacological tools.

The present study shows that Nedd4-1 and Nedd4-2 are required for the maintenance of E-LTP. This indicates possible functions of these E3 ligases in activity dependent GluR1 trafficking, e.g. in inhibiting receptor endocytosis, in accelerating exocytosis, in altering lateral diffusion, and/or in enhancing tethering at activated synapses. In contrast, several recent studies have shown that Nedd4-1 ubiquitinates and accelerates GluR1 endocytosis and proteolytic degradation upon glutamate stimuli (Lin et al., 2011; Schwarz et al., 2010). While the conditional targeting strategy using the Nedd4-1 flox mouse allows to inactivate *Nedd4-1* in a specifically controlled manner, it is possible that prenatal and chronic inactivation of *Nedd4-1* could be compensated by other homologous E3 ligases, especially by Nedd4-2. Indeed, several groups reported that Nedd4-1 and Nedd4-2 share functions in various cellular processes (Ingham et al., 2004; Yang and Kumar, 2010). In order to avoid possible compensation of loss of function of *Nedd4-1* by endogenous *Nedd4-2*, I analyzed the postmitotic neuron specific Nedd4 cDKO mouse line. Given that the contradictory studies published by others relied on overexpression and RNAi-mediated KD of Nedd4-1, which can lead to non-physiological consequences and off-target effects, I conclude based on the present results obtained with Nedd4 cDKOs that Nedd4 E3 ligases play critical role in retaining AMPARs at synapses during LTP induction and maintenance and not in their endocytosis.

4.3.2 Roles of Nedd4-1 and Nedd4-2 in UPS-dependent Protein Degradation during LTP

Several recent studies indicated a critical role of protein turnover and degradation through the UPS system in synaptic plasticity. The involvement of the UPS in these processes seems to be limited to postsynaptic spines, either by local ubiquitination of postsynaptic substrates [e.g., polyubiquitinaion of PSD-95 by Mdm2 (Colledge et al., 2003)] or by activity dependent recruitment of proteasomal components to the spine (Bingol and Schuman, 2006). Furthermore, the balance between protein synthesis and protein degradation via the UPS has been shown to be an essential parameter in the regulation of E-LTP and L-LTP (Dong et al., 2008; Fonseca et al., 2006). Inhibition of the UPS leads to an increase in the initial phase of E-LTP without affecting the maintenance of E-LTP (Dong et al., 2008). Given that LTP in the Nedd4 cDKO mouse was intact in the first 30 min after induction (Figs. 3-5B and C), Nedd4-1 and Nedd4-2 are not involved in the UPS dependent initial phase

of E-LTP. Importantly, the UPS is dispensable for the maintenance of E-LTP, indicating that the loss of *Nedd4-1* and *Nedd4-2* may interfere with LTP via a nonproteolytic pathway (i.e. monoubiuitination and K63-linked polyubiquitination).

4.3.3 Possible Mechanisms by which Nedd4-1 and Nedd4-2 Could Positively Regulate LTP

4.3.3.1 Ubiquitination of Synaptopodin (SYNPO) by Nedd4-1 and Nedd4-2

My host lab identified SYNPO as a binding protein of Nedd4-1 and Nedd4-2. I demonstrated in the present study that Nedd4-1 and Nedd4-2 ubiquitinate SYNPO *in vitro* (Fig. 3-6D), indicating that Nedd4-1 and Nedd4-2 may positively regulate LTP through mono- or polyubiquitination of SYNPO.

SYNPO is highly enriched in the spine apparatus. Spine apparatuses were first reported five decades ago by Gray (Gray and Guillery, 1963) while their function in synaptic transmission had remained enigmatic. An analysis of deletion mutant mice demonstrated the essential role of SYNPO in the formation of spine apparatuses. Intriguingly, *SYNPO* KO mice show an impairment of E-LTP and special learning, indicating that the spine apparatus is a subcellular organelle critical for the regulation of synaptic plasticity (Deller et al., 2003). A functional analysis using a photolysis approach revealed that spines containing SYNPO and spine apparatuses exhibit increased synaptic responses due to increased calcium release via Ryanodine receptors (RyRs) (Vlachos et al., 2009). RyRs, calcium-induced calcium release channels, are present throughout spine apparatuses and the dendritic ERs in hippocampal neurons. SYNPO promotes intracellular calcium release from RyRs (Vlachos et al., 2009). Given that RyRs are exclusively required for E-LTP (Balschun et al., 1999), SYNPO may regulate E-LTP through RyRs.

It has been reported that SYNPO interacts with GDP-bound RhoA. This interaction blocks association of Smurf1 with GDP-bound RhoA, thereby preventing the targeting of RhoA for polyubquitination and proteasomal degradation (Asanuma et al., 2006). RhoA signaling plays a critical role in synaptic plasticity. The loss of *LIMK1*, a downstream target of RhoA, causes abnormally enhanced LTP (Meng et al., 2002).

Given that Nedd4-1 and Nedd4-2 interact with and ubiquitinate SYNPO, this protein could be a substrate of Nedd4 E3 ligases *in vivo*, promoting LTP by regulating intracellular calcium release via RyR or RhoA expression.

4.3.3.2 Nedd4-1 and Nedd4-2 may not Regulate LTP through Overactivation of Rap2

Ryu et. al. showed that overexpression of a constitutively active mutant of Rap2 in neurons leads to enhanced LTD in acute hippocampal slices but does not affect E-LTP or depotentiation (Ryu et. al., 2008). An independent study has shown that overexpression of a constitutively active form of Rap2 by viral infection in a hippocampal organotypic slice culture causes depressed AMPAR-mediated responses and impaired depotentiation (Zhu et al., 2005). The loss of *Nedd4-1* and *Nedd4-2,* on the other hand, results in reduced LTP, but intact LTD and normal basal synaptic transmission (Figs. 3-4 and -5), which thus cannot be explained by overactivated Rap2 in the Nedd4 cDKO mouse. Thus, I conclude that while Rap2 is a target of Nedd4-1 in developing neurons, other substrates of Nedd4 E3 ligases must be responsible for the Nedd4 effects on LTP in mature neurons.

4.3.3.3 Nedd4-2 may Regulate Dopaminergic Inputs through Dopamine Transporters (DAT) during LTP

Nedd4-2 has been identified as a regulator of endocytosis of DAT (Sorkina et al., 2006), indicating that Nedd4-2 may tune dopaminergic inputs to promote LTP. The hippocampus receives various inputs from a range of other brain regions that are active during learning and memory formation. Dopamine is one of the biogenic monoamines and plays key roles in synaptic plasticity as well as in the reward system, and is thus deeply related with motivational behavior and addiction, and certain motor functions. The ventral tegmental area (VTA) and the substantia nigra (SN) in the midbrain dominantly contain dopaminergic neurons projecting axons in complex patterns to many parts of the brain, including the hippocampus. Indeed, hippocampal neurons express G-protein coupled dopamine receptors (D1-D5). D1 and D5 receptors are Gs-protein coupled receptors and activate adenyl cyclase, while D2, D3, and D4 are Gi-coupled receptors that inactivate adenyl cyclase upon stimulation by dopamine. DAT is localized at the periphery of presynaptic dopaminergic terminals and tunes dopaminergic inputs through dopamine reuptake from the synaptic clefts.

Pharmacological treatment of acute hippocampal slices with an antagonist of D1/D5 receptors revealed that activation of these receptors is required for the maintenance of L-LTP (Frey et al., 1990). A recent study using *D1* receptor deficient mice demonstrated that the D1 receptor-mediated signal is required for both E- and L-LTP and for the expression of immediate early genes (EIGs), such as Zif268 and

activity-regulated cytoskeleton-associated protein (Arc) (Granado et al., 2008). Enhancement of LTP by a DAT blocker, which increases the dopamine level in the synaptic cleft, indicates that tuning of dopaminergic inputs through endogenous DATs may underlie certain mechanisms of LTP (Thompson et al., 2005). Nedd4-2 governs PKC-dependent endocytosis of DAT (Sorkina et al., 2006), leading to the hypothesis that Nedd4-2 may positively regulate LTP through tuning endogenous dopaminergic inputs and activating D1 receptors by controlling the endocytosis of DAT.

4.3.3.4 Nedd4-1 and Nedd4-2 may Regulate LTP through the Mammalian Target of Rapamycin (mTOR) Pathway

The $IP_3$3-kinase (PI3K)/Akt/mTOR pathway is a major cellular signaling pathway, and its misregulation contributes to the pathophysiological characteristics of a variety of diseases, including cancer, diabetes, autistic spectrum disorder, and epilepsy. This pathway generally transduces extracellular stimuli, such as growth factors or cytokines, to modulate cell survival, growth, and proliferation.

Receptor tyrosine kinases, including the Insulin receptor (IR) and the IGF1 receptor (IGF1-R) activate PI3K and the downstream protein kinase Akt. Tuberous sclerosis complex 1 and 2 (TSC1 and -2) are substrates of Akt and function as GAPs for the small GTPase RheB (Fig. 4-2). Phosphorylation of TSC1 and -2 results in suppression of their GAP activities, leading to activation of RheB and its target protein mTOR. Phosphatase and tensin homologue deleted on chromosome 10 (PTEN) is a lipid phosphatase converting PIP3 to PIP2, thus inactivating Akt. The pivotal role of mTOR is the initiation of translation of mRNA for a wide variety of synaptic proteins, including Arc, αCaMKII, and GluR1 (Slipczuk et al., 2009). In the mature brain, the PI3K/Akt/mTOR pathway is critical for induction of E-LTP (Ehninger et al., 2008; Sanna et al., 2002; Wang et al., 2006) as well as for maintenance of L-LTP (Karpova et al., 2006; Tang et al., 2002; von der Brelie et al., 2006). It has been reported that Nedd4-1 ubiquitinates IGF-1R by forming a trimeric protein complex with Grb10 and IGF1-R (Vecchione et al., 2003). A recent report showed that surface expression of IGF1-R is reduced in *Nedd4-1* KO fibroblasts indicating that ubiquitinaiton of IGF-1R is critical for the recruitment or retention of this receptor to/at the plasma membrane (Cao et al., 2008). Although controversial, PTEN has been reported as a target of Nedd4-1 and Nedd4-2. Monoubiquitination and polyubiquitination by Nedd4 triggers nuclear transport and proteasomal degradation of PTEN, respectively (Trotman et al., 2007; Wang et al., 2007). Misregulation of

IGF-1R or PTEN in the PI3K/AKT/mTOR pathway may be involved in the impaired LTP in the loss of function mutant of *Nedd4-1* and *Nedd4-2*.

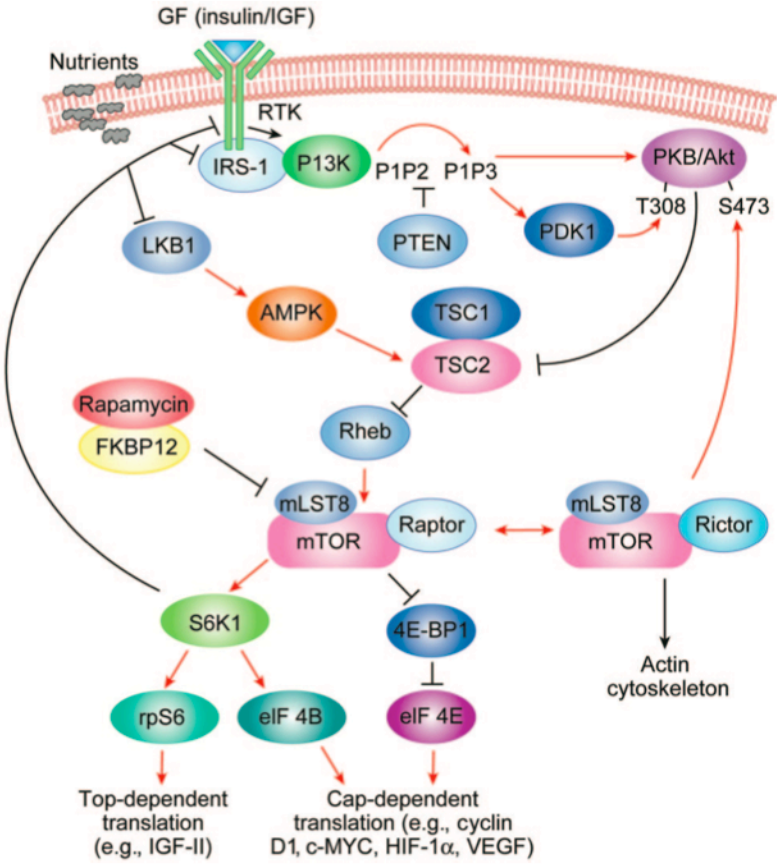

Figure 4-2 A model of mTOR signaling cascade and its function

Growth factors (e.g. insulin and IGF) bind to RTKs and activate PI3K and Akt. Phosphorylation of Akt T308 by PDK1 and Akt S473 by mTORC2 (a complex of mTOR, mLST8, and rictor) leads to its full activation. Activated Akt activates Rheb GTPase and mTORC1 (a complex of mTOR, mLST8, and raptor) via phosphorylation of TSC1 and -2. Phosphorylation of S6K1 and 4E-BP by activated mTORC1 leads to release of 4E-BP1 from elF-4E. This process plays fundamental roles in top-dependent and cap-dependent translation, respectively. mTOR signaling is also linked to the energy-sensing pathway (i.e., through amino acids and ATP) through LKB1. LKB1 sequentially activates AMPK and TSC1/2, resulting in mTORC1 inhibition.
4E-BP1, eukaryotic initiation factor 4E binding protein-1; AMPK, AMP-activated kinase; elF-4E, eukaryotic initiation factor 4E; FKBP12, FK506 binding protein 12; GF, growth factor; HIF-1α, hypoxia inducible factor 1α; IGF, insulin-like growth factor; IRS-1, insulin receptor substrate 1; LKB1, serine threonine kinase 11; mLST8, G protein subunit-like; mTOR, mammalian target of rapamycin; PDK1, 3-phosphoinositide-dependent protein kinase 1; PI3K, phosphatidylinositol 3 kinase; PIP2, phosphatidylinositol-4,5-bisphosphate; PIP3, phosphatidylinositol-3,4,5-triphosphate; PKB, phosphate kinase B; PTEN, phosphatase and tensin homologue deleted on chromosome ten; Rheb, Ras homologue enriched in brain; RTK, receptor tyrosine kinase; S6K1, protein S6 kinase 1; TSC1 and 2, tuberous sclerosis complex 1 and 2; VEGF, vascular endothelial growth factor; T308, Akt threonine 308; S473, Akt serine 473. (Adapted from Wan and Helman, 2007)

4.4 Summary and Outlook

In the present study, Nedd4-1 and Nedd4-2 are characterized as E3 ligases involved in neuronal morphogenesis and activity dependent synaptic plasticity. These E3 ligases are enriched in synapses of mature neurons, and their activity might be regulated depending on synaptic activity.

The morphological analysis of Nedd4 cDKO mice revealed that these E3 ligases are dispensable for spine formation. In contrast to the very subtle effects on basal synaptic transmission, the loss of *Nedd4-1* and *Nedd4-2* causes a significant impairment of LTP. Thus, Nedd4-1 and Nedd4-2 participate in a process of synaptic strengthening in an activity dependent manner. The present study identified synaptopodin as a potential target of Nedd4-1 and Nedd4-2 that might mediate the effects of Nedd4 on LTP. Other possible pathways include the regulation of dopaminergic inputs and PTEN/mTOR signaling.

The present study provides a first insight into roles of Nedd4-1 and Nedd4-2 in mature neurons. It shows that Nedd4-1 and Nedd4-2 could be important E3 ubiquitin ligases in higher functions of the mature brain.

Several questions are raised from the present study. In order to dissect the molecular mechanism by which Nedd4-1 and Nedd4-2 positively regulate LTP, the involved pathways, such as DAT, remain to be determined using pharmacological applications during LTP recordings. The roles of Nedd4-1 and Nedd4-2 on activity-dependent GluR1 endocytosis need to be clarified using *Nedd4-1* and *Nedd4-2* deficient neurons. The morphological effects caused by *Nedd4-1* and *Nedd4-2* deficiencies also remain to be quantified. Further questions to be addressed would be whether the loss of these E3 ligases impairs the maintenance of L-LTP and hippocampus-dependent learning and memory.

5 References

Abbas, A.K., Dozmorov, M., Li, R., Huang, F.S., Hellberg, F., Danielson, J., Tian, Y., Ekstrom, J., Sandberg, M., and Wigstrom, H. (2009). Persistent LTP without triggered protein synthesis. Neurosci Res *63*, 59-65.

Adamcio, B., Sargin, D., Stradomska, A., Medrihan, L., Gertler, C., Theis, F., Zhang, M.Y., Muller, M., Hassouna, I., Hannke, K.*, et al.* (2008). Erythropoietin enhances hippocampal long-term potentiation and memory. Bmc Biol *6*.

Agarwal, A., Dibaj, P., Kassmann, C. M., Goebbels, S., Nave, K. A., and Schwab, M. H. (2011). In Vivo Imaging and Noninvasive Ablation of Pyramidal Neurons in Adult NEX-CreERT2 Mice. Cerebral Cortex [Epub ahead of print]

Andersen, P., Bliss, T.V.P., and Skrede, K.K. (1971). Lamellar Organization of Hippocampal Excitatory Pathways. Exp Brain Res *13*, 222-&.

Asanuma, K., Yanagida-Asanuma, E., Faul, C., Tomino, Y., Kim, K., and Mundel, P. (2006). Synaptopodin orchestrates actin organization and cell motility via regulation of RhoA signalling. Nat Cell Biol *8*, 485-U109.

Azevedo, F.A.C., Carvalho, L.R.B., Grinberg, L.T., Farfel, J.M., Ferretti, R.E.L., Leite, R.E.P., Jacob, W., Lent, R., and Herculano-Houzel, S. (2009). Equal Numbers of Neuronal and Nonneuronal Cells Make the Human Brain an Isometrically Scaled-Up Primate Brain. J Comp Neurol *513*, 532-541.

Bachmann, C., Ahern-Djamali, S.M., and Walter, U. (1999). The Ena/VASP family of proteins: Involvement in signal transduction pathways and regulation of the cytoskeleton. Nato Adv Sci I a-Lif *309*, 279-289.

Balschun, D., Wolfer, D.P., Bertocchini, F., Barone, V., Conti, A., Zuschratter, W., Missiaen, L., Lipp, H.P., Frey, J.U., and Sorrentino, V. (1999). Deletion of the ryanodine receptor type 3 (RyR3) impairs forms of synaptic plasticity and spatial learning. Embo Journal *18*, 5264-5273.

Banke, T.G., Bowie, D., Lee, H.K., Huganir, R.L., Schousboe, A., and Traynelis, S.F. (2000). Control of GluR1 AMPA receptor function by cAMP-dependent protein kinase. Journal of Neuroscience *20*, 89-102.

Barrionuevo, G., Schottler, F., and Lynch, G. (1980). The Effects of Repetitive Low-Frequency Stimulation on Control and Potentiated Synaptic Responses in the Hippocampus. Life Sci *27*, 2385-2391.

Barth, A.M.I., and Mody, I. (2011). Changes in Hippocampal Neuronal Activity During and After Unilateral Selective Hippocampal Ischemia In Vivo. Journal of Neuroscience *31*, 851-860.

Behnisch, T., and Reymann, K.G. (1995). Thapsigargin Blocks Long-Term Potentiation Induced by Weak, but Not Strong Tetanisation in Rat Hippocampal Ca1 Neurons. Neurosci Lett *192*, 185-188.

Bingol, B., and Schuman, E.M. (2006). Activity-dependent dynamics and sequestration of proteasomes in dendritic spines. Nature *441*, 1144-1148.

Bliss, T.V.P., and Collingridge, G.L. (1993). A Synaptic Model of Memory - Long-Term

Potentiation in the Hippocampus. Nature *361*, 31-39.

Bliss, T.V.P., and Lomo, T. (1973). Long-Lasting Potentiation of Synaptic Transmission in Dentate Area of Anesthetized Rabbit Following Stimulation of Perforant Path. J Physiol-London *232*, 331-356.

Bloom, A.J., Miller, B.R., Sanes, J.R., and DiAntonio, A. (2007). The requirement for Phr1 in CNS axon tract formation reveals the corticostriatal boundary as a choice point for cortical axons. Genes Dev *21*, 2593-2606.

Boase, N.A., Rychkov, G.Y., Townley, S.L., Dinudom, A., Candi, E., Voss, A.K., Tsoutsman, T., Semsarian, C., Melino, G., Koentgen, F.*, et al.* (2011). Respiratory distress and perinatal lethality in Nedd4-2-deficient mice. Nat Commun *2*.

Bortolotto, A., Amici, M., Anderson, W. W., Issac, J. T. R., and Collingridge, G. L. (2011). Curre. Protocol in Neurosci. 6.13.1-6.13.26, Synaptic Plasticity in the Hippocampal Slice Preparation

Bruce, M.C., Kanelis, V., Fouladkou, F., Debonneville, A., Staub, O., and Rotin, D. (2008). Regulation of Nedd4-2 self-ubiquitination and stability by a PY motif located within its HECT-domain. Biochem J *415*, 155-163.

Cao, X.R., Lill, N.L., Boase, N., Shi, P.P., Croucher, D.R., Shan, H.B., Qu, J., Sweezer, E.M., Place, T., Kirby, P.A.*, et al.* (2008). Nedd4 Controls Animal Growth by Regulating IGF-1 Signaling. Sci Signal *1*.

Chen, L., Chetkovich, D.M., Petralia, R.S., Sweeney, N.T., Kawasaki, Y., Wenthold, R.J., Bredt, D.S., and Nicoll, R.A. (2000). Stargazin regulates synaptic targeting of AMPA receptors by two distinct mechanisms. Nature *408*, 936-943.

Cheng, P.L., Lu, H., Shelly, M., Geo, H.F., and Poo, M.M. (2011). Phosphorylation of E3 Ligase Smurf1 Switches Its Substrate Preference in Support of Axon Development. Neuron *69*, 231-243.

Chung, H.J., Xia, J., Scannevin, R.H., Zhang, X.Q., and Huganir, R.L. (2000). Phosphorylation of the AMPA receptor subunit GluR2 differentially regulates its interaction with PDZ domain-containing proteins. Journal of Neuroscience *20*, 7258-7267.

Colledge, M., Snyder, E.M., Crozier, R.A., Soderling, J.A., Jin, Y.T., Langeberg, L.K., Lu, H., Bear, M.F., and Scott, J.D. (2003). Ubiquitination regulates PSD-95 degradation and AMPA receptor surface expression. Neuron *40*, 595-607.

Collingridge, G.L., and Bliss, T.V.P. (1995). Memories of Nmda Receptors and Ltp. Trends Neurosci *18*, 54-56.

Collingridge, G.L., Isaac, J.T.R., and Wang, Y.T. (2004). Receptor trafficking and synaptic plasticity. Nature Reviews Neuroscience *5*, 952-962.

Corkin, S., Amaral, D.G., Gonzalez, R.G., Johnson, K.A., and Hyman, B.T. (1997). HM's medial temporal lobe lesion: Findings from magnetic resonance imaging. Journal of Neuroscience *17*, 3964-3979.

Deller, T., Korte, M., Chabanis, S., Drakew, A., Schwegler, H., Stefani, G.G., Zuniga, A., Schwarz, K., Bonhoeffer, T., Zeller, R.*, et al.* (2003). Synaptopodin-deficient mice lack a spine apparatus and show deficits in synaptic plasticity. Proc Natl Acad Sci U S A *100*,

10494-10499.

Derkach, V., Barria, A., and Soderling, T.R. (1999). Ca2+/calmodulin-kinase II enhances channel conductance of alpha-amino-3-hydroxy-5-methyl-4-isoxazolepropionate type glutamate receptors. Proc Natl Acad Sci U S A *96*, 3269-3274.

DeSouza, S., Fu, J., States, B.A., and Ziff, E.B. (2002). Differential palmitoylation directs the AMPA receptor-binding protein ABP to spines or to intracellular clusters. Journal of Neuroscience *22*, 3493-3503.

Dong, C.G., Upadhya, S.C., Ding, L., Smith, T.K., and Hegde, A.N. (2008). Proteasome inhibition enhances the induction and impairs the maintenance of late-phase long-term potentiation. Learn Memory *15*, 335-347.

Drinjakovic, J., Jung, H.S., Campbell, D.S., Strochlic, L., Dwivedy, A., and Holt, C.E. (2010). E3 Ligase Nedd4 Promotes Axon Branching by Downregulating PTEN. Neuron *65*, 341-357.

Dudek, S.M., and Bear, M.F. (1992). Homosynaptic Long-Term Depression in Area Ca1 of Hippocampus and Effects of N-Methyl-D-Aspartate Receptor Blockade. Proc Natl Acad Sci U S A *89*, 4363-4367.

Dunn, D.M., Ishigami, T., Pankow, J., von Niederhausern, A., Alder, J., Hunt, S.C., Leppert, M.F., Lalouel, J.M., and Weiss, R.B. (2002). Common variant of human NEDD4L activates a cryptic splice site to form a frameshifted transcript. J Hum Genet *47*, 665-676.

Durand, G.M., and Konnerth, A. (1996). Long-term potentiation as a mechanism of functional synapse induction in the developing hippocampus. J Physiology-Paris *90*, 313-315.

Ehlers, M.D. (2000). Reinsertion or degradation of AMPA receptors determined by activity-dependent endocytic sorting. Neuron *28*, 511-525.

Ehninger, D., Han, S., Shilyansky, C., Zhou, Y., Li, W.D., Kwiatkowski, D.J., Ramesh, V., and Silva, A.J. (2008). Reversal of learning deficits in a Tsc2(+/-) mouse model of tuberous sclerosis. Nat Med *14*, 843-848.

Ehrlich, I., and Malinow, R. (2004). Postsynaptic density 95 controls AMPA receptor incorporation during long-term potentiation and experience-driven synaptic plasticity. Journal of Neuroscience *24*, 916-927.

Fonseca, R. (2012). Activity-dependent actin dynamics are required for the maintenance of long-term plasticity and for synaptic capture. European Journal of Neuroscience *35*, 195-206.

Fonseca, R., Vabulas, R.M., Hartl, F.U., Bonhoeffer, T., and Nagerl, U.V. (2006). A balance of protein synthesis and proteasome-dependent degradation determines the maintenance of LTP. Neuron *52*, 239-245.

Fotia, A.B., Ekberg, J., Adams, D.J., Cook, D.I., Poronnik, P., and Kumar, S. (2004). Regulation of neuronal voltage-gated sodium channels by the ubiquitin-protein ligases Nedd4 and Nedd4-2. Journal of Biological Chemistry *279*, 28930-28935.

Fouladkou, F., Landry, T., Kawabe, H., Neeb, A., Lu, C., Brose, N., Stambolic, V., and Rotin, D. (2008). The ubiquitin ligase Nedd4-1 is dispensable for the regulation of PTEN stability and localization. Proc Natl Acad Sci U S A *105*, 8585-8590.

Frey, U., Krug, M., Reymann, K.G., and Matthies, H. (1988). Anisomycin, an Inhibitor of

Protein-Synthesis, Blocks Late Phases of Ltp Phenomena in the Hippocampal Ca1 Region Invitro. Brain Res *452*, 57-65.

Frey, U., and Morris, R.G.M. (1997). Synaptic tagging and long-term potentiation. Nature *385*, 533-536.

Frey, U., Schroeder, H., and Matthies, H. (1990). Dopaminergic Antagonists Prevent Long-Term Maintenance of Posttetanic Ltp in the Ca1 Region of Rat Hippocampal Slices. Brain Res *522*, 69-75.

Garty, H., and Palmer, L.G. (1997). Epithelial sodium channels: Function, structure, and regulation. Physiol Rev *77*, 359-396.

Givens, B.S., and Olton, D.S. (1990). Cholinergic and Gabaergic Modulation of Medial Septal Area - Effect on Working Memory. Behav Neurosci *104*, 849-855.

Goebbels, S., Bormuth, I., Bode, U., Hermanson, O., Schwab, M.H., and Nave, K.A. (2006). Genetic targeting of principal neurons in neocortex and hippocampus of NEX-Cre mice. Genesis *44*, 611-621.

Goh, K.L., Cai, L., Cepko, C.L., and Gertler, F.B. (2002). EnaNASP proteins regulate cortical neuronal positioning. Curr Biol *12*, 565-569.

Granado, N., Ortiz, O., Suarez, L.M., Martin, E.D., Cena, V., Solis, J.M., and Moratalla, R. (2008). D-1 but not D-5 dopamine receptors are critical for LTP, spatial learning, and LTP-Induced arc and zif268 expression in the hippocampus. Cereb Cortex *18*, 1-12.

Gray, E.G., and Guillery, R.W. (1963). A Note on Dendritic Spine Apparatus. J Anat *97*, 389-&.

Grover, L.M., and Teyler, T.J. (1990). 2 Components of Long-Term Potentiation Induced by Different Patterns of Afferent Activation. Nature *347*, 477-479.

Hayashi, Y., Shi, S.H., Esteban, J.A., Piccini, A., Poncer, J.C., and Malinow, R. (2000). Driving AMPA receptors into synapses by LTP and CaMKII: Requirement for GluR1 and PDZ domain interaction. Science *287*, 2262-2267.
Hollmann, M., Hartley, M., and Heinemann, S. (1991). Ca2+ Permeability of Ka-Ampa Gated Glutamate Receptor Channels Depends on Subunit Composition. Science *252*, 851-853.

Hou, Q.M., Gilbert, J., and Man, H.Y. (2011). Homeostatic Regulation of AMPA Receptor Trafficking and Degradation by Light-Controlled Single-Synaptic Activation. Neuron *72*, 806-818.

Howitt, J., Lackovic, J., Low, L.H., Naguib, A., Macintyre, A., Goh, C.P., Callaway, J.K., Hammond, V., Thomas, T., Dixon, M.*, et al.* (2012). Ndfip1 regulates nuclear Pten import in vivo to promote neuronal survival following cerebral ischemia. J Cell Biol *196*, 29-36.

Huang, F.T., Kirkpatrick, D., Jiang, X.J., Gygi, S., and Sorkin, A. (2006). Differential regulation of EGF receptor internalization and degradation by multiubiquitination within the kinase domain. Mol Cell *21*, 737-748.

Huttner, W.B., Schiebler, W., Greengard, P., and Decamilli, P. (1983). Synapsin-I (Protein-I), a Nerve Terminal-Specific Phosphoprotein .3. Its Association with Synaptic Vesicles Studied in a Highly Purified Synaptic Vesicle Preparation. J Cell Biol *96*, 1374-1388.

Hyman, B.T., Vanhoesen, G.W., Damasio, A.R., and Barnes, C.L. (1984). Alzheimers-Disease - Cell-Specific Pathology Isolates the Hippocampal-Formation. Science *225*, 1168-1170.

Ingham, R.J., Gish, G., and Pawson, T. (2004). The Nedd4 family of E3 ubiquitin ligases: functional diversity within a common modular architecture. Oncogene *23*, 1972-1984.

Isaac, J.T.R., Nicoll, R.A., and Malenka, R.C. (1995). Evidence for Silent Synapses - Implications for the Expression of Ltp. Neuron *15*, 427-434.

Jahn, O., Hesse, D., Reinelt, M., and Kratzin, H.D. (2006). Technical innovations for the automated identification of gel-separated proteins by MALDI-TOF mass spectrometry. Anal Bioanal Chem *386*, 92-103.

Jiang, Y.H., Armstrong, D., Albrecht, U., Atkins, C.M., Noebels, J.L., Eichele, G., Sweatt, J.D., and Beaudet, A.L. (1998). Mutation of the angelman ubiquitin ligase in mice causes increased cytoplasmic p53 and deficits of contextual learning and long-term potentiation. Neuron *21*, 799-811.

Jones, R.S.G. (1993). Entorhinal Hippocampal Connections - a Speculative View of Their Function. Trends Neurosci *16*, 58-64.

Jun, K.S., Choi, G.D., Yang, S.G., Choi, K.Y., Kim, H., Chan, G.C.K., Storm, D.R., Albert, C., Mayr, G.W., Lee, C.J.*, et al.* (1998). Enhanced hippocampal CA1 LTP but normal spatial learning in inositol 1,4,5-trisphosphate 3-kinase(A)-deficient mice. Learn Memory *5*, 317-330.

Kamynina, E., Debonneville, C., Bens, M., Vandewalle, A., and Staub, O. (2001). A novel mouse Nedd4 protein suppresses the activity of the epithelial Na+ channel. Faseb J *15*, 204-214.

Karpova, A., Sanna, P.P., and Behnisch, T. (2006). Involvement of multiple phosphatidylinositol 3-kinase-dependent pathways in the persistence of late-phase long term potentiation expression. Neuroscience *137*, 833-841.

Katz, B., and Miledi, R. (1968). Role of Calcium in Neuromuscular Facilitation. J Physiol-London *195*, 481-&.

Kawabe, H., and Brose, N. (2010). The ubiquitin E3 ligase Nedd4-1 controls neurite development. Cell Cycle *9*, 2477-2478.

Kawabe, H., Neeb, A., Dimova, K., Young, S.M., Takeda, M., Katsurabayashi, S., Mitkovski, M., Malakhova, O.A., Zhang, D.E., Ulmilkawa, M.*, et al.* (2010a). Regulation of Rap2A by the Ubiquitin Ligase Nedd4-1 Controls Neurite Development. Neuron *65*, 358-372.

Kessels, H.W., and Malinow, R. (2009). Synaptic AMPA Receptor Plasticity and Behavior. Neuron *61*, 340-350.

Kim, C.H., and Lisman, J.E. (1999). A role of actin filament in synaptic transmission and long-term potentiation. Journal of Neuroscience *19*, 4314-4324.

Kim, H.C., and Huibregtse, J.M. (2009). Polyubiquitination by HECT E3s and the Determinants of Chain Type Specificity. Mol Cell Biol *29*, 3307-3318.

Kimura, T., Kawabe, H., Jiang, C., Zhang, W.B., Xiang, Y.Y., Lu, C., Salter, M.W., Brose, N., Lu, W.Y., and Rotin, D. (2011). Deletion of the ubiquitin ligase Nedd4L in lung epithelia

causes cystic fibrosis-like disease. Proc Natl Acad Sci U S A *108*, 3216-3221.

Kopec, C.D., Real, E., Kessels, H.W., and Malinow, R. (2007). GluR1 links structural and functional plasticity at excitatory synapses. Journal of Neuroscience *27*, 13706-13718.

Krucker, T., Siggins, G.R., and Halpain, S. (2000). Dynamic actin filaments are required for stable long-term potentiation (LTP) in area CA1 of the hippocampus. Proc Natl Acad Sci U S A *97*, 6856-6861.

Kumar, S., Tomooka, Y., and Noda, M. (1992). Identification of a Set of Genes with Developmentally down-Regulated Expression in the Mouse-Brain. Biochem Biophys Res Commun *185*, 1155-1161.

Kwon, C.H., Luikart, B.W., Powell, C.M., Zhou, J., Matheny, S.A., Zhang, W., Li, Y.J., Baker, S.J., and Parada, L.F. (2006). Pten regulates neuronal arborization and social interaction in mice. Neuron *50*, 377-388.

Lanier, L.M., Gates, M.A., Witke, W., Menzies, A.S., Wehman, A.M., Macklis, J.D., Kwiatkowski, D., Soriano, P., and Gertler, F.B. (1999). Mena is required for neurulation and commissure formation. Neuron *22*, 313-325.

Lee, H.K., Takamiya, K., Han, J.S., Man, H.Y., Kim, C.H., Rumbaugh, G., Yu, S., Ding, L., He, C., Petralia, R.S.*, et al.* (2003). Phosphorylation of the AMPA receptor GluR1 subunit is required for synaptic plasticity and retention of spatial memory. Cell *112*, 631-643.

Lee, S.H., Choi, J.H., Lee, N., Lee, H.R., Kim, J.I., Yu, N.K., Choi, S.L., Lee, S.H., Kim, H., and Kaang, B.K. (2008). Synaptic protein degradation underlies destabilization of retrieved fear memory. Science *319*, 1253-1256.

Lee, S.H., Liu, L.D., Wang, Y.T., and Sheng, M. (2002). Clathrin adaptor AP2 and NSF interact with overlapping sites of GluR2 and play distinct roles in AMPA receptor trafficking and hippocampal LTD. Neuron *36*, 661-674.

Li, M., Shin, Y.H., Hou, L.F., Huang, X.X., Wei, Z.B., Klann, E., and Zhang, P.M. (2008a). The adaptor protein of the anaphase promoting complex Cdh1 is essential in maintaining replicative lifespan and in learning and memory. Nat Cell Biol *10*, 1083-1089.

Li, N., Lorinczi, M., Ireton, K., and Elferink, L.A. (2007). Specific Grb2-mediated interactions regulate clathrin-dependent endocytosis of the cMet-tyrosine kinase. Journal of Biological Chemistry *282*, 16764-16775.

Li, W., Bengtson, M.H., Ulbrich, A., Matsuda, A., Reddy, V.A., Orth, A., Chanda, S.K., Batalov, S., and Joazeiro, C.A.P. (2008b). Genome-Wide and Functional Annotation of Human E3 Ubiquitin Ligases Identifies MULAN, a Mitochondrial E3 that Regulates the Organelle's Dynamics and Signaling. PLoS One *3*.

Liao, D.Z., Hessler, N.A., and Malinow, R. (1995). Activation of Postsynaptically Silent Synapses during Pairing-Induced Ltp in Ca1 Region of Hippocampal Slice. Nature *375*, 400-404.

Lin, A., Hou, Q.M., Jarzylo, L., Amato, S., Gilbert, J., Shang, F., and Man, H.Y. (2011). Nedd4-mediated AMPA receptor ubiquitination regulates receptor turnover and trafficking. J Neurochem *119*, 27-39.

Lisman, J.E., and Otmakhova, N.A. (2001). Storage, recall, and novelty detection of

sequences by the hippocampus: Elaborating on the SOCRATIC model to account for normal and aberrant effects of dopamine. Hippocampus *11*, 551-568.

Liu, W., Ye, P., O'Kusky, J.R., and D'Ercole, A.J. (2009). Type 1 Insulin-Like Growth Factor Receptor Signaling Is Essential for the Development of the Hippocampal Formation and Dentate Gyrus. J Neurosci Res *87*, 2821-2832.

Lopez-Salon, M., Alonso, M., Vianna, M.R.M., Viola, H., Souza, T.M.E., Izquierdo, I., Pasquini, J.M., and Medina, J.H. (2001). The ubiquitin-proteasome cascade is required for mammalian long-term memory formation. European Journal of Neuroscience *14*, 1820-1826.

Lotz, K., Pyrowolakis, G., and Jentsch, S. (2004). BRUCE, a giant E2/E3 ubiquitin ligase and inhibitor of apoptosis protein of the trans-Golgi network, is required for normal placenta development and mouse survival. Mol Cell Biol *24*, 9339-9350.

Lu, Y., Christian, K., and Lu, B. (2008). BDNF: A key regulator for protein synthesis-dependent LTP and long-term memory? Neurobiol Learn Mem *89*, 312-323.

Luna, R.M.D., Wagner, D.S., and Lozano, G. (1995). Rescue of Early Embryonic Lethality in Mdm2-Deficient Mice by Deletion of P53. Nature *378*, 203-206.

Luscher, C., Xia, H.H., Beattie, E.C., Carroll, R.C., von Zastrow, M., Malenka, R.C., and Nicoll, R.A. (1999). Role of AMPA receptor cycling in synaptic transmission and plasticity. Neuron *24*, 649-658.

Luthi, A., Chittajallu, R., Duprat, F., Palmer, M.J., Benke, T.A., Kidd, F.L., Henley, J.M., Isaac, J.T.R., and Collingridge, G.L. (1999). Hippocampal LTD expression involves a pool of AMPARs regulated by the NSF-GluR2 interaction. Neuron *24*, 389-399.

Mabb, A.M., and Ehlers, M.D. (2010). Ubiquitination in Postsynaptic Function and Plasticity. Annu Rev Cell Dev Bi *26*, 179-210.

Malenka, R.C., and Bear, M.F. (2004). LTP and LTD: An embarrassment of riches. Neuron *44*, 5-21.

Maletic-Savatic, M., Malinow, R., and Svoboda, K. (1999). Rapid dendritic morphogenesis in CA1 hippocampal dendrites induced by synaptic activity. Science *283*, 1923-1927.

Malinow, R., and Malenka, R.C. (2002). AMPA receptor trafficking and synaptic plasticity. Annu Rev Neurosci *25*, 103-126.

Marmor, M.D., and Yarden, Y. (2004). Role of protein ubiquitylation in regulating endocytosis of receptor tyrosine kinases. Oncogene *23*, 2057-2070.

Masson, J., Sagne, C., Hamon, M., and El Mestikawy, S. (1999). Neurotransmitter transporters in the central nervous system. Pharmacol Rev *51*, 439-464.

Matsuda, S., Mikawa, S., and Hirai, H. (1999). Phosphorylation of serine-880 in GluR2 by protein kinase C prevents its C terminus from binding with glutamate receptor-interacting protein. J Neurochem *73*, 1765-1768.

Matsuda, S., Mikawa, S., and Hirai, H. (2000). Phosphorylation of serine 880 in GluR2 by protein kinase C prevents its C-terminus binding with the glutamate receptor interacting protein, GR. European Journal of Neuroscience *12*, 465-465.

Mauceri, D., Cattabeni, F., Di Luca, M., and Gardoni, F. (2004). Calcium/calmodulin-dependent protein kinase II phosphorylation drives synapse-associated protein 97 into spines. Journal of Biological Chemistry *279*, 23813-23821.

McKinney, R.A., Capogna, M., Durr, R., Gahwiler, B.H., and Thompson, S.M. (1999). Miniature synaptic events maintain dendritic spines via AMPA receptor activation. Nat Neurosci *2*, 44-49.

Meng, Y.H., Zhang, Y., Tregoubov, V., Janus, C., Cruz, L., Jackson, M., Lu, W.Y., MacDonald, J.F., Wang, J.Y., Falls, D.L*., et al.* (2002). Abnormal spine morphology and enhanced LTP in LIMK-1 knockout mice. Neuron *35*, 121-133.

Miles, R., Traub, R.D., and Wong, R.K.S. (1988). Spread of Synchronous Firing in Longitudinal Slices from the Ca3 Region of the Hippocampus. J Neurophysiol *60*, 1481-1496.

Milner, A.J., Cummings, D.M., Spencer, J.P., and Murphy, K.P.S.J. (2004). Bi-directional plasticity and age-dependent long-term depression at mouse CA3-CA1 hippocampal synapses. Neurosci Lett *367*, 1-5.

Mizoguchi, A., Ueda, T., Ikeda, K., Shiku, H., Mizoguti, H., and Takai, Y. (1989). Localization and Subcellular-Distribution of Cellular Ras Gene-Products in Rat-Brain. Mol Brain Res *5*, 31-44.

Montgomery, J.M., Zamorano, P.L., and Garner, C.C. (2004). MAGUKs in synapse assembly and function: an emerging view. Cellular and Molecular Life Sciences *61*, 911-929.

Mundel, P., Heid, H.W., Mundel, T.M., Kruger, M., Reiser, J., and Kriz, W. (1997). Synaptopodin: An actin-associated protein in telencephalic dendrites and renal podocytes. J Cell Biol *139*, 193-204.

Murthy, V.N., and Stevens, C.F. (1999). Reversal of synaptic vesicle docking at central synapses. Nat Neurosci *2*, 503-507.

Navakkode, S., Sajikumar, S., Sacktor, T.C., and Frey, J.U. (2010). Protein kinase M zeta is essential for the induction and maintenance of dopamine-induced long-term potentiation in apical CA1 dendrites. Learn Memory *17*, 605-611.

Nguyen, P.V., and Woo, N.H. (2003). Regulation of hippocampal synaptic plasticity by cyclic AMP-dependent protein kinases. Prog Neurobiol *71*, 401-437.

Nicoll, R.A., Tomita, S., and Bredt, D.S. (2006). Auxiliary subunits assist AMPA-type glutamate receptors. Science *311*, 1253-1256.

Nikonenko, A.G., Radenovic, L., Andjus, P.R., and Skibo, G.G. (2009). Structural Features of Ischemic Damage in the Hippocampus. Anat Rec *292*, 1914-1921.

Nishimune, A., Isaac, J.T.R., Molnar, E., Noel, J., Nash, S.R., Tagaya, M., Collingridge, G.L., Nakanishi, S., and Henley, J.M. (1998). NSF binding to GluR2 regulates synaptic transmission. Neuron *21*, 87-97.

Okamoto, K.I., Nagai, T., Miyawaki, A., and Hayashi, Y. (2004). Rapid and persistent modulation of actin dynamics regulates postsynaptic reorganization underlying bidirectional plasticity. Nat Neurosci *7*, 1104-1112.

Okano, H., Hirano, T., and Balaban, E. (2000). Learning and memory. Proc Natl Acad Sci U

S A *97*, 12403-12404.

Opazo, P., and Choquet, D. (2011). A three-step model for the synaptic recruitment of AMPA receptors. Molecular and Cellular Neuroscience *46*, 1-8.

Peng, J.M., Schwartz, D., Elias, J.E., Thoreen, C.C., Cheng, D.M., Marsischky, G., Roelofs, J., Finley, D., and Gygi, S.P. (2003). A proteomics approach to understanding protein ubiquitination. Nat Biotechnol *21*, 921-926.

Pirozzi, G., McConnell, S.J., Uveges, A.J., Carter, J.M., Sparks, A.B., Kay, B.K., and Fowlkes, D.M. (1997). Identification of novel human WW domain-containing proteins by cloning of ligand targets. Journal of Biological Chemistry *272*, 14611-14616.

Pradervand, S., Vandewalle, A., Bens, M., Gautschi, I., Loffing, J., Hummler, E., Schild, L., and Rossier, B.C. (2003). Dysfunction of the epithelial sodium channel expressed in the kidney of a mouse model for Liddle syndrome. J Am Soc Nephrol *14*, 2219-2228.

Raymond, C.R. (2007). LTP forms 1, 2 and 3: different mechanisms for the 'long' in long-term potentiation. Trends Neurosci *30*, 167-175.

Redondo, R.L., and Morris, R.G.M. (2011). Making memories last: the synaptic tagging and capture hypothesis. Nature Reviews Neuroscience *12*, 17-30.

Reumann, S., Babujee, L., Ma, C.L., Wienkoop, S., Siemsen, T., Antonicelli, G.E., Rasche, N., Luder, F., Weckwerth, W., and Jahn, O. (2007). Proteome analysis of Arabidopsis leaf peroxisomes reveals novel targeting peptides, metabolic pathways, and defense mechanisms. Plant Cell *19*, 3170-3193.

Robb, S.A., Pohl, K.R.E., Baraitser, M., Wilson, J., and Brett, E.M. (1989). The Happy Puppet Syndrome of Angelman - Review of the Clinical-Features. Arch Dis Child *64*, 83-86.

Rosenmund, C., Rettig, J., and Brose, N. (2003). Molecular mechanisms of active zone function. Curr Opin Neurobiol *13*, 509-519.

Rougier, J.S., van Bemmelen, M.X., Bruce, M.C., Jespersen, T., Gavillet, B., Apotheloz, F., Cordonier, S., Staub, O., Rotin, D., and Abriel, H. (2005). Molecular determinants of voltage-gated sodium channel regulation by the Nedd4/Nedd4-like proteins. Am J Physiol-Cell Ph *288*, C692-C701.

Ryan, T.A., Reuter, H., and Smith, S.J. (1997). Optical detection of a quantal presynaptic membrane turnover. Nature *388*, 478-482.

Sacktor, T.C. (2008). PKM zeta, LTP maintenance, and the dynamic molecular biology of memory storage. Prog Brain Res *169*, 27-40.

Sanna, P.P., Cammalleri, M., Berton, F., Simpson, C., Lutjens, R., Bloom, F.E., and Francesconi, W. (2002). Phosphatidylinositol 3-kinase is required for the expression but not for the induction or the maintenance of long-term potentiation in the hippocampal CA1 region (vol 22, pg 3359, 2002). Journal of Neuroscience *22*, 10507-10507.

Sara, Y., Virmani, T., Deak, F., Liu, X.R., and Kavalali, E.T. (2005). An isolated pool of vesicles recycles at rest and drives spontaneous neurotransmission. Neuron *45*, 563-573.

Scharf, M.T., Woo, N.H., Lattal, K.M., Young, J.Z., Nguyen, P.V., and Abel, T. (2002). Protein synthesis is required for the enhancement of long-term potentiation and long-term

memory by spaced training. J Neurophysiol *87*, 2770-2777.

Schousboe, A., Hertz, L., and Svenneby, G. (1977). Uptake and Metabolism of Gaba in Astrocytes Cultured from Dissociated Mouse-Brain Hemispheres. Neurochem Res *2*, 217-229.

Schwamborn, J.C., Muller, M., Becker, A.H.M., and Puschel, A.W. (2007). Ubiquitination of the GTPase Rap1B by the ubiquitin ligase Smurf2 is required for the establishment of neuronal polarity. Embo Journal *26*, 1410-1422.

Schwarz, L.A., Hall, B.J., and Patrick, G.N. (2010). Activity-Dependent Ubiquitination of GluA1 Mediates a Distinct AMPA Receptor Endocytosis and Sorting Pathway. Journal of Neuroscience *30*, 16718-16729.

Scoville, W.B., and Milner, B. (1957). Loss of Recent Memory after Bilateral Hippocampal Lesions. J Neurol Neurosur Ps *20*, 11-21.

Setou, M., Seog, D.H., Tanaka, Y., Kanai, Y., Takei, Y., Kawagishi, M., and Hirokawa, N. (2002). Glutamate-receptor-interacting protein GRIP1 directly steers kinesin to dendrites. Nature *417*, 83-87.

Shepherd, J.D., and Huganirl, R.L. (2007). The cell biology of synaptic plasticity: AMPA receptor trafficking. Annu Rev Cell Dev Biol *23*, 613-643.

Shi, S.H., Hayashi, Y., Esteban, J.A., and Malinow, R. (2001). Subunit-specific rules governing AMPA receptor trafficking to synapses in hippocampal pyramidal neurons. Cell *105*, 331-343.

Slipczuk, L., Bekinschtein, P., Katche, C., Cammarota, M., Izquierdo, I., and Medina, J.H. (2009). BDNF Activates mTOR to Regulate GluR1 Expression Required for Memory Formation. PLoS One *4*.

Soderling, T.R., and Derkach, V.A. (2000). Postsynaptic protein phosphorylation and LTP. Trends Neurosci *23*, 75-80.

Sorkina, T., Miranda, M., Dionne, K.R., Hoover, B.R., Zahniser, N.R., and Sorkin, A. (2006). RNA interference screen reveals an essential role of Nedd4-2 in dopamine transporter ubiquitination and endocytosis. Journal of Neuroscience *26*, 8195-8205.

Sprengel, R., Suchanek, B., Amico, C., Brusa, R., Burnashev, N., Rozov, A., Hvalby, O., Jensen, V., Paulsen, O., Andersen, P*., et al.* (1998). Importance of the intracellular domain of NR2 subunits for NMDA receptor function in vivo. Cell *92*, 279-289.

Spruston, N., Jonas, P., and Sakmann, B. (1995). Dendritic Glutamate-Receptor Channels in Rat Hippocampal Ca3 and Ca1 Pyramidal Neurons. J Physiol-London *482*, 325-352.

Sudhof, T.C. (2004). The synaptic vesicle cycle. Annu Rev Neurosci *27*, 509-547.
Sun, J.Y., Wu, X.S., and Wu, L.G. (2002). Single and multiple vesicle fusion induce different rates of endocytosis at a central synapse. Nature *417*, 555-559.

Sutton, M.A., Wall, N.R., Aakalu, G.N., and Schuman, E.M. (2004). Regulation of dendritic protein synthesis by miniature synaptic events. Science *304*, 1979-1983.

Swanson, L.W. (1982). The Projections of the Ventral Tegmental Area and Adjacent Regions - a Combined Fluorescent Retrograde Tracer and Immunofluorescence Study in the Rat. Brain Res Bull *9*, 321-353.

Swant, J., and Wagner, J.J. (2006). Dopamine transporter blockade increases LTP in the CA1 region of the rat hippocampus via activation of the D3 dopamine receptor. Learn Memory *13*, 161-167.

Tang, S.J., Reis, G., Kang, H., Gingras, A.C., Sonenberg, N., and Schuman, E.M. (2002). A rapamycin-sensitive signaling pathway contributes to long-term synaptic plasticity in the hippocampus. Proc Natl Acad Sci U S A *99*, 467-472.

Thompson, A.M., Swant, J., and Wagner, J.J. (2005). Cocaine-induced modulation of long-term potentiation in the CA1 region of rat hippocampus. Neuropharmacology *49*, 185-194.

Trotman, L.C., Wang, X.J., Alimonti, A., Chen, Z.B., Teruya-Feldstein, J., Yang, H.J., Pavletich, N.P., Carver, B.S., Cordon-Cardo, C., Erdjument-Bromage, H.*, et al.* (2007). Ubiquitination regulates PTEN nuclear import and tumor suppression. Cell *128*, 141-156.

Vecchione, A., Marchese, A., Henry, P., Rotin, D., and Morrione, A. (2003). The Grb10/Nedd4 complex regulates ligand-induced ubiquitination and stability of the insulin-like growth factor I receptor. Mol Cell Biol *23*, 3363-3372.

Verhage, M., Maia, A.S., Plomp, J.J., Brussaard, A.B., Heeroma, J.H., Vermeer, H., Toonen, R.F., Hammer, R.E., van den Berg, T.K., Missler, M.*, et al.* (2000). Synaptic assembly of the brain in the absence of neurotransmitter secretion. Science *287*, 864-869.

Vina-Vilaseca, A., and Sorkin, A. (2010). Lysine 63-linked Polyubiquitination of the Dopamine Transporter Requires WW3 and WW4 Domains of Nedd4-2 and UBE2D Ubiquitin-conjugating Enzymes. Journal of Biological Chemistry *285*, 7645-7656.

Vlachos, A., Korkotian, E., Schonfeld, E., Copanaki, E., Deller, T., and Segal, M. (2009). Synaptopodin Regulates Plasticity of Dendritic Spines in Hippocampal Neurons. Journal of Neuroscience *29*, 1017-1033.

von der Brelie, C., Waltereit, R., Zhang, L., Beck, H., and Kirschstein, T. (2006). Impaired synaptic plasticity in a rat model of tuberous sclerosis. European Journal of Neuroscience *23*, 686-692.

Wang, X.J., Trotman, L.C., Koppie, T., Alimonti, A., Chen, Z.B., Gao, Z.H., Wang, J.R., Erdjument-Bromage, H., Tempst, P., Cordon-Cardo, C.*, et al.* (2007). NEDD4-1 is a proto-oncogenic ubiquitin ligase for PTEN. Cell *128*, 129-139.

Wang, Y., Cheng, A.W., and Mattson, M.P. (2006). The PTEN phosphatase is essential for long-term depression of hippocampal synapses. Neuromol Med *8*, 329-335.

Wang, Z.P., Edwards, J.G., Riley, N., Provance, D.W., Karcher, R., Li, X.D., Davison, I.G., Ikebe, M., Mercer, J.A., Kauer, J.A.*, et al.* (2008). Myosin Vb Mobilizes Recycling Endosomes and AMPA Receptors for Postsynaptic Plasticity. Cell *135*, 535-548.

Wenthold, R.J., Petralia, R.S., Blahos, J., and Niedzielski, A.S. (1996). Evidence for multiple AMPA receptor complexes in hippocampal CA1/CA2 neurons. Journal of Neuroscience *16*, 1982-1989.

Werner, H.B., Kuhlmann, K., Shen, S., Uecker, M., Schardt, A., Dimova, K., Orfaniotou, F., Dhaunchak, A., Brinkmann, B.G., Mobius, W.*, et al.* (2007). Proteolipid protein is required for transport of sirtuin 2 into CNS myelin. Journal of Neuroscience *27*, 7717-7730.

Wiesner, S., Ogunjimi, A.A., Wang, H.R., Rotin, D., Sicheri, F., Wrana, J.L., and Forman-Kay, J.D. (2007). Autoinhibition of the HECT-Type ubiquitin ligase smurf2 through its c2 domain. Cell *130*, 651-662.

Woo, N.H., Duffy, S.N., Abel, T., and Nguyen, P.V. (2003). Temporal spacing of synaptic stimulation critically modulates the dependence of LTP on cyclic AMP-dependent protein kinase. Hippocampus *13*, 293-300.

Wu, H.J., Nash, J.E., Zamorano, P., and Garner, C.C. (2002). Interaction of SAP97 with minus-end-directed actin motor myosin VI - Implications for AMPA receptor trafficking. Journal of Biological Chemistry *277*, 30928-30934.

Xu, J., Pang, Z.P.P., Shin, O.H., and Sudhof, T.C. (2009a). Synaptotagmin-1 functions as a Ca(2+) sensor for spontaneous release. Nat Neurosci *12*, 759-U111.

Xu, P., Duong, D.M., Seyfried, N.T., Cheng, D.M., Xie, Y., Robert, J., Rush, J., Hochstrasser, M., Finley, D., and Peng, J. (2009b). Quantitative Proteomics Reveals the Function of Unconventional Ubiquitin Chains in Proteasomal Degradation. Cell *137*, 133-145.

Yamashita, M., Ying, S.X., Zhang, G.M., Li, C.L., Cheng, S.Y., Deng, C.X., and Zhang, Y.E. (2005). Ubiquitin ligase Smurf1 controls osteoblast activity and bone homeostasis by targeting MEKK2 for degradation. Cell *121*, 101-113.

Yang, B., and Kumar, S. (2010). Nedd4 and Nedd4-2: closely related ubiquitin-protein ligases with distinct physiological functions. Cell Death Differ *17*, 68-77.

Yang, Y.L., Wang, X.B., Frerking, M., and Zhou, Q. (2008). Spine expansion and stabilization associated with long-term potentiation. Journal of Neuroscience *28*, 5740-5751.

Yao, I., Takagi, H., Ageta, H., Kahyo, T., Sato, S., Hatanaka, K., Fukuda, Y., Chiba, T., Morone, N., Yuasa, S.*, et al.* (2007). SCRAPPER-dependent ubiquitination of active zone protein RIM1 regulates synaptic vesicle release. Cell *130*, 943-957.

Ye, B., Zhang, Y., Song, W., Younger, S.H., Jan, L.Y., and Jan, Y.N. (2007). Growing dendrites and axons differ in their reliance on the secretory pathway. Cell *130*, 717-729.

Zhu, Y.H., Pak, D., Qin, Y., McCormack, S.G., Kim, M.J., Baumgart, J.P., Velamoor, V., Auberson, Y.P., Osten, P., van Aelst, L.*, et al.* (2005). Rap2-JNK removes synaptic AMPA receptors during depotentiation (vol 46, pg 905, 2005). Neuron *47*, 321-321.

Zucker, R.S. (1999). Calcium- and activity-dependent synaptic plasticity. Curr Opin Neurobiol *9*, 305-313.